Sensory coding in supragranular cells of the vibrissal cortex in anesthetized and awake mice

By Yadollah Ranjbar Slamloo

A thesis submitted for the degree of Doctor of Philosophy of The Australian National University

30/10/2017

Declaration

All the materials in this thesis, including literature review, original results and conclusions, are exclusively produced for the degree of Doctor of Philosophy at the Australian National University. All the text is either original results or interpretations of the candidate or reference to previous studies of others which is cited based on academic routines. All the figures in this thesis are originally generated by the candidate.

Name: Yadollah Ranjbar Slamloo

Date: 30/10/2017

Ethics statement

All the experiments were performed at the John Curtin School of Medical Research, under ARC and NHMRC codes of practice for animal care and use and ANU ethics committee.

Published materials

Ranjbar-Slamloo Y, Arabzadeh E. High-velocity stimulation evokes “dense” population response in layer 2/3 vibrissal cortex, Journal of Neurophysiology, 117: 1218-1228, 2017.

Manuscript pending

Ranjbar-Slamloo Y, Arabzadeh E. Diverse tuning underlies sparse activity in L2/3 vibrissal cortex of awake mice.

Conference presentations

- Ranjbar-Slamloo Y, Arabzadeh E. High-velocity whisker stimulation evokes “dense” population response in layer 2/3 vibrissal cortex, a *poster presented at Neuroscience (SfN), San Diego CAL; November 2016.*
- Ranjbar-Slamloo Y, Arabzadeh E. High-velocity whisker stimulation evokes “dense” population response in layer 2/3 vibrissal cortex, *oral presentation at Kioloa Neuroscience Colloquium, Kioloa NSW, Australia; April 2016.*
- Ranjbar-Slamloo Y, Arabzadeh E. Sub-threshold stimulus-response function in mice layer 2/3 barrel cortex, *a poster presented at ISN-APSN-ANS Joint Conference, Cairns QLD, Australia; August 2015*

Acknowledgments

First and foremost, I would like to thank my supervisor Associate Professor Ehsan Arabzadeh for his consistent support, insightful advice and encouragement throughout my PhD. He has inspired me to work hard, to think critical and to be confident and value my research. His passionate supervision and commitment to produce high quality, original knowledge have been always enlightening.

I would like to thank my advisors Professor Gregory Stuart and Professor John Bekkers for their valuable feedback and comments on my work. I should also thank Mr. Garry Rodda for his workshop assistance, Ms. Anastasia Seizemova and Dr. Minh-Son To, for their helpful instructions for calcium imaging and whole-cell recording. Finally, I should thank all of the past and present members of the Neural Coding lab for their comments and friendly assistance during my PhD.

This work was supported by the Australian Research Council (ARC) Discovery Project DP130101364 and the ARC Centre of Excellence for Integrative Brain Function CE140100007.

Ethics statement

All animals used in this study were provided by the Australian Phenomics Facility (ACTON, ACT, 2601). This work is implemented under two animal ethics protocols (A2015/74 and A2016/14) approved by the Animal Experimentation Ethics Committee of the Australian National University. Animal housing and experimental procedures were followed based on these protocols. Animals were kept in flow-regulated home cages (SmartFlow, Techniplast) with free access to the food and water and 12h/12h light/dark cycle.

Abstract

Sensory perception entails reliable representation of the external stimuli as impulse activity of individual neurons (i.e. spikes) and neuronal populations in the sensory area. An ongoing challenge in neuroscience is to identify and characterize the features of the stimuli which are relevant to a specific sensory modality and neuronal strategies to effectively and efficiently encode those features. It is widely hypothesized that the neuronal populations employ "sparse coding" strategies to optimize the stimulus representations with a low energetic cost (i.e. low impulse activity). In the past two decades, a wealth of experimental evidence has supported this hypothesis by showing spatiotemporally sparse activity in sensory area. Despite numerous studies, the extent of sparse coding and its underlying mechanisms are not fully understood, especially in primary vibrissal somatosensory cortex (vS1), which is a key model system in sensory neuroscience. Importantly, it is not clear yet whether sparse activation of supragranular vS1 is due to insufficient synaptic input to the majority of the cells or the absence of effective stimulus features.

In this thesis, first we asked how the choice of stimulus could affect the degree of sparseness and/or the overall fraction of the responsive vS1 neurons. We presented whisker deflections spanning a broad range of intensities, including "standard stimuli" and a high-velocity, "sharp" stimulus, which simulated the fast slip events that occur during whisker mediated object palpation. We used whole-cell and cell-attached recording and calcium imaging to characterize the neuronal responses to these stimuli. Consistent with previous literature, whole-cell recording revealed a sparse response to the standard range of velocities: although all recorded cells showed tuning to velocity in their postsynaptic potentials, only a small fraction produced stimulus-evoked spikes. In contrast, the sharp stimulus evoked reliable spiking in a large fraction of

regular spiking neurons in the supragranular vS1. Spiking responses to the sharp stimulus were binary and precisely timed, with minimum trial-to-trial variability. Interestingly, we also observed that the sharp stimulus produced a consistent and significant reduction in action potential threshold.

In the second step we asked whether the stimulus dependent sparse and dense activations we found in anesthetized condition would generalize to the awake condition. We employed cell-attached recordings in head-fixed awake mice to explore the degree of sparseness in awake cortex. Although, stimuli delivered by a piezo-electric actuator evoked significant response in a small fraction of regular spiking supragranular neurons (16%-29%), we observed that a majority of neurons (84%) were driven by manual probing of whiskers. Our results demonstrate that despite sparse activity, the majority of neurons in the superficial layers of vS1 contribute to coding by representing a specific feature of the tactile stimulus.

Thesis outline: *Chapter 1* provides a review of the current knowledge on sparse coding and an overview of the whisker-sensory pathway. *Chapter 2* represents our published results regarding sparse and dense coding in vS1 of anesthetized mice (Ranjbar-Slamloo and Arabzadeh 2017). *Chapter 3* represents our pending manuscript with results obtained with piezo and manual stimulation in awake mice. Finally, in *Chapter 4* we discuss and conclude our findings in the context of the literature. The appendix provides unpublished results related to *Chapter 2*. This section is referenced in the final chapter for further discussion.

Table of contents

List of figures

List of tables

List of abbreviations

- vS1: primary vibrissal somatosensory cortex
- V1: primary visual cortex
- V_m: membrane potential (membrane voltage)
- AP: action potential
- PSP: postsynaptic potential
- EPSP: excitatory postsynaptic potential
- IPSP: inhibitory postsynaptic potential
- GABA: gamma aminobutyric acid
- RS: regular spiking
- FS: fast spiking
- L1: layer 1
- L2/3: layer 2 and 3
- L4: layer 4
- L5: layer 5
- L6: layer 6

Chapter 1: Introduction

1.1. Prelude

The ability of animals to efficiently process ecologically relevant sensory information is crucial to their survival. Specialized sensory organs have evolved across the animal kingdom to extract relevant features of the outside world to guide behavior. Sensory organs transduce physical stimuli into electrical impulses, which travel through multiple pathways formed by brainstem and thalamic nuclei before arriving at the cerebral cortex. An example of a highly specialized sensory system is the rodent vibrissal system (Diamond and Arabzadeh 2013; Feldmeyer et al. 2013). Vibrissae (whiskers) are the long hair around the rodent's snout which project to a topographically organized area in the cortex, the vibrissal primary somatosensory cortex or vS1 (Woolsey and Van der Loos 1970). Like many other cortical areas, the vS1 is divided into 6 layers based on cellular size and morphology and the projection patterns. Layer 4, which is also called the granular layer, is the primary recipient of the sensory information. The input to layers 2 and 3, which are known as supragranular layers, is mainly from layer 4. Supragranular layers are strongly connected to layer 5 and also to the secondary somatosensory and the motor cortex while infragranular layers which comprise layers 5 and 6, predominantly project to the subcortical areas such as the striatum, superior colliculus, and the thalamus (Feldmeyer 2012).

Among cortical layers, layer 2/3 and 6 are the least active, with a small fraction of neurons in the supragranular layers being responsive to sensory stimulation, a phenomenon known as "sparse" coding. In most of studies on the vS1, a small fraction of highly responsive neurons (with a certain criterion for responsiveness) are found, which reflects a high degree of sparseness. Key questions remain unanswered regarding the sparse activity of layer 2/3. How does the choice of stimulus affect the sparseness? How do different experimental conditions such as anesthesia affect population sparseness? Do "silent" neurons contribute to sensory coding, and if so under

what conditions? In this thesis, we aim to approach these questions with a number of recording and imaging techniques using anesthetized and awake head-fixed preparations.

In this chapter, first we will introduce the experimental evidence for sparse coding across sensory areas (1.2). This will be followed by a review of the cellular and circuit mechanisms underlying sparse cortical firing (1.3), and theoretical basis of sparse coding (1.4). Finally, we will review the connectivity and functional organization of the rodent vibrissal system (1.5) and the current knowledge about response properties and sensory coding in the vS1 (1.6).

1.2. Evidence for sparse cortical representations

For decades neurophysiologists have widely utilized extracellular unit recordings to determine various aspects of spontaneous and stimulus driven activity of cortical cells. The classic study of Hubel and Wiesel (Hubel and Wiesel 1959) on cat visual cortex prompted subsequent studies on the neurophysiological mechanisms of perception (Wurtz 2009). This trend increasingly involved extracellular recordings form the primary sensory cortex in search of stimulus features which modulate the activity of single neurons. Across sensory modalities, neurons were found to represent variable degrees of "tuning" to the experimentally defined values of a sensory feature. For example, "simple cells" in primary visual cortex (V1) exclusively respond to a moving rectangular light with a certain orientation at a certain direction and do not respond to the same stimulus with other orientations or even same orientation with opposite direction of movement (Hubel and Wiesel 1959). Similar properties of single neuron responses were found in auditory and somatosensory cortices, such as tuning to tone frequency in the auditory cortex (DeWeese et al. 2003) and motion direction in the somatosensory cortex (Pei et al. 2010). The main focus of such studies has been to describe the receptive field and tuning properties of neurons.

Despite its common use, extracellular unit recording presents potential drawbacks for unbiased sampling of neurons. Towe and Harding proposed that extracellular unit electrodes may be biased to sample from large cells (Towe and Harding 1970). David Robinson in 1968 estimated that a standard metal electrode only records a tiny fraction of the neurons surrounding the tip (Robinson 1968) and that the extracellular spike currents from many neurons might be shielded by glia cells or compression of the tissue and hence undetected. Twenty years later, Dykes and colleagues established the presence of a large proportion of silent cortical neurons by explicitly keeping record of all neurons encountered by their recording probe (Dykes and Lamour 1988a). A key feature of their methodology was iontophoretic application of Glutamate or GABA antagonist bicuculline, which activated neurons regardless of their tonic discharge rate (Hicks and Dykes 1983; Dykes et al. 1984). Dykes and colleagues activated neurons as they advanced their recording electrodes and found that only a quarter of neurons recorded across layers of the somatosensory cortex were driven by sensory input (Dykes and Lamour 1988a, 1988b). They also detected a large fraction of spontaneously inactive neurons consistent with earlier reports (Baker et al. 1971). A critical finding of these studies was that the fraction of silent neurons was much higher in L2/3 and L6 compared to the middle layers 4 and 5 (Dykes and Lamour 1988a). Such laminar profile of sparseness was consistently replicated in a number of studies using modern techniques. Subsequent studies confirmed the prevalence of silent neurons across multiple sensorimotor cortical areas including recordings in cat somatosensory cortex (Tremblay et al. 1990; Warren and Dykes 1992) and rabbit motor (Swadlow 1994), primary somatosensory (Swadlow 1994) and secondary somatosensory cortex (Swadlow 1994). However, at least one study, using iontophoretic drug application, reported high proportion of spontaneously active neurons in awake rats (Bassant et al. 1990) that was in contrast to the results of other studies of

the time (Baker et al. 1971; Dykes and Lamour 1988a) and to modern experiments on mice (see the next paragraph).

In the late 1990s increasing popularity of in-vivo whole-cell recordings began to provide new insight into single cell activity in the cortex. In the rat vS1, this method has been used to characterize sub-threshold receptive fields (Moore and Nelson 1998): synaptic responses were found for 20 out of 24 recorded neurons but the spiking responses were driven only in 7 of these neurons (Moore and Nelson 1998). Subsequent whole-cell experiments in rat vibrissal pathway reported 0.74 spikes per stimulus in VPM (Brecht and Sakmann 2002a), 0.14 spikes per stimulus in L4 (Brecht and Sakmann 2002b) and 0.031 spikes per stimulus in L2/3 (Brecht et al. 2003). In a later study by Sakmann and colleagues the average evoked response was found to be layer-dependent and also cell-type specific in L5 (de Kock et al. 2007). This study showed however, somewhat higher average evoked responses of 0.41 spikes per stimulus in L4 and 0.11 in L2/3 (de Kock et al. 2007). In awake condition, low probability, temporally precise spiking was evident in L4 of vS1 (Jadhav et al. 2009). Svoboda and colleagues employed cell-attached recording in mice vS1 and found that during active sensation, a small fraction of neurons fired the majority of action potentials (O'Connor et al. 2010b). The average firing rate of L4 neurons was 11.9 and 3.0 and the median was 3.48 and 0.18 in L4 and L2/3 respectively (O'Connor et al. 2010b). Such high disparity of the mean and median firing rate indicates sparse distribution of neuronal activity. Overall, there is substantial evidence for sparse activity particularly in supragranular layers of the vS1 cortex.

Multiple factors may affect the responsiveness of cortical neurons including anesthesia (Haider et al. 2013), cortical state (Sakata and Harris 2012) and learning (Gdalyahu et al. 2012; Kato et al. 2015). The impact of anesthesia on neuronal activity and sensory response is noticeable

(Rinberg et al. 2006; Haider et al. 2013; Cazakoff et al. 2014; Durand et al. 2016). A comparison of the visually evoked spiking in L2/3 of mouse visual cortex in anesthetized and awake conditions revealed a marked reduction of spiking response in awake cortex which was associated with a substantially stronger inhibitory conductance and a reduced variability in PSP amplitudes (Haider et al. 2013). Notably, variability of inhibition/excitation ratio across neurons substantially increased in awake condition (Haider et al. 2013). This study encourages a systematic examination of the mechanisms underlying such strong inhibition in awake cortex (Arroyo et al. 2012; Haider et al. 2013). Spontaneous or behavior driven changes in cortical state is another factor which can considerably change the degree of cortical activity (Petersen and Crochet 2013). Laminar analysis of spontaneous and stimulus driven activity in auditory cortex showed that, "desynchronized" or "activated" state caused a marked decrease in spontaneous activity of the L2/3 pyramidal and fast spiking neurons, and an increase in the spontaneous firing of deep layer neurons (Sakata and Harris 2012). These layer-specific effects may also be mediated by various neuromodulatory inputs that arrive in the cortex (Petersen and Crochet 2013; Eggermann et al. 2014; Sabri and Arabzadeh 2018). Such layer-specific modulation of spontaneous activity is also observed in the visual cortex following the stimulation of the basal forebrain which induces desynchronized state (Goard and Dan 2009). A desynchronization induced by locomotion however, prominently increased the stimulus evoked response rather than changing spontaneous activity (Niell and Stryker 2010). It is hard to reconcile various reports on sensory response during activated states induced by various methods in different sensory systems. For example, a study in vS1 induced activated state by stimulation of brainstem reticular formation and reported a larger response to infrequent whisker stimulations in quiet state compared to activated state (Castro-Alamancos 2004).

Another factor which can largely affect neuronal responsiveness is learning. For example, Gdalyahu et al. trained mice in a Pavlovian fear conditioning paradigm with passive whisker deflections as the conditioning stimulus (Gdalyahu et al. 2012). Monitoring responses of population of vS1 neurons by calcium imaging showed that association of the whisker stimulus with a foot shock significantly reduced the fraction of responsive neurons. Interestingly, Gdalyahu and colleagues report a stronger stimulus representation by a subset of responsive neurons after learning (Gdalyahu et al. 2012). Thus, sparse coding of the circuits of the primary sensory cortex may reflect the ecological significance of a sensory stimulus. In primary auditory cortex, Isaacson and colleagues showed that the presentation of a tone with no behavioral significance reduced overall L2/3 activity by upregulating the activity of somatostatin expressing GABAergic neurons (Kato et al. 2015). Importantly, when the tone gained behavioral significance in reward collection, L2/3 neurons reversed this long-lasting habituation (Kato et al. 2015). These results indicate that learning about the behavioral significance of a stimulus can influence the degree of sparseness in a population of primary sensory cortical neurons. However, the direction of the changes in each task across sensory modalities, and the underlying mechanisms are not fully understood.

1.3. Cellular and circuit mechanisms underlying sparse cortical firing

The rate of spiking is considerably different among cortical neurons. The rate of spiking is mainly determined by the neuron's intrinsic molecular and biophysical properties and its specific synaptic inputs and network dynamics (Barth and Poulet, 2012, Harris and Mrsic-Flogel 2013, Petersen and Crochet 2013). Resting membrane potential in a typical neuron is about -65 mV (Kandel et al. 2000). In theory, spikes can be triggered in a neuron when the membrane potential exceeds a threshold level (often reported in a range between -55 and -35 mV). In physiological

conditions *in vivo*, membrane potential is controlled by postsynaptic potentials (PSPs). Excitatory postsynaptic potentials (EPSPs) cause a depolarization towards the reversal potential for the conducted cations (potassium and sodium) which is ~0 mV (Kandel et al. 2000). Inhibitory postsynaptic potentials (IPSPs) are generated by inputs from GABAergic neurons which cause a hyperpolarization towards chlorine reversal potential at -70 mV (Kandel et al. 2000). Unitary EPSPs to the cortical neurons are relatively weak (Barth and Poulet 2012, Lefort et al. 2009). Hence spike generation requires a number of presynaptic neurons to converge on a postsynaptic neuron to depolarize membrane potential up to the threshold. Cortical neurons have diverse shapes and sizes, which in turn affect their electrical properties and synaptic integration. An elaborated dendritic tree often integrates synaptic inputs from multiple presynaptic neurons (Chadderton et al. 2014). Due to the passive electrical properties of the membrane, synaptic potentials rapidly decay on the way to the soma (Williams and Stuart 2002). However, a substantial drop of AP threshold in axon initial segment (Coombs et al. 1957; Kole and Stuart 2008) can compensate for the EPSP attenuation. Therefore, an EPSP generated in the dendritic tree and attenuated by passive conduction may still trigger action potential in axon initial segment but not in the soma, due to its higher AP threshold. Furthermore, various active dendritic mechanisms can amplify dendritic depolarizations (Stuart and Spruston 2015; Manita et al. 2017). Local generation of both sodium and calcium spikes in the dendrites has been confirmed (Stuart et al. 1997; Larkum and Nevian 2008; Manita et al. 2017). It is shown that calcium spikes can enhance the spiking output of cortical neurons during sensory processing (Palmer et al. 2014). Such active mechanisms may have a significant effect on the spiking output of the cortical neurons. Active dendritic mechanisms may play significant role in sensory processing, since distant dendrites can be potentiated by various cellular and circuit mechanisms

such as disinhibition (Gentet et al. 2012), synaptic potentiation following learning and involvement of additional sensorimotor pathways.

Spatiotemporal synaptic integration is also determined by the circuit connectivity. In local cortical circuits, excitatory and inhibitory neurons are tightly connected to each other and receive a common input from presynaptic excitatory neurons (Helmstaedter et al. 2008; Lefort et al. 2009; Xu and Callaway 2009). This causes a proportional inhibitory input for any given excitatory input which is observed in both driven (Anderson et al. 2000a; Xue et al. 2014) and spontaneous cortical activity (Okun and Lampl 2008). Such proportionality or "balance" of the major synaptic components (GABAergic and glutamatergic inputs) is mostly maintained across various conditions such as neuronal adaptation (Higley and Contreras 2006) or deprivation-induced map plasticity (House et al. 2011). However, a close comparison of inhibitory and excitatory conductance has revealed that individual neurons may dynamically change the ratio of excitation and inhibition in response to sensory stimulation (Isaacson and Scanziani 2011). For example in the vS1 cortex, the precise timing of the excitatory and inhibitory inputs are highly dynamic and provide a mechanism for stimulus selectivity (Wilent and Contreras 2005a). A similar mechanism underlies non-monotonic intensity tuning in the auditory cortex (Wu et al. 2006). Furthermore, individual neurons may receive different excitation-inhibition ratios (Haider et al. 2013). In the superficial layers of the vS1, the excitation-inhibition ratio is higher for neurons which have a low response threshold for the feedforward input, compared to those which have a high threshold (Elstrott et al. 2014). Individual neurons may have a constant ratio of excitation-inhibition over a large range of stimulus intensities. This however does not remove all spiking activity because the cortical IPSPs are often delayed with one additional synapse, and this delay can provide a window of opportunity for spiking (Isaacson and Scanziani 2011).

Cortical neurons continually receive input from thalamus and other cortical neurons. Regardless of the sensory input, spontaneous activity in the thalamus and cortex causes fluctuations in the membrane potential of the cortical neurons. Recording of membrane potential *in-vivo* shows slow but high amplitude oscillations due to a variable synchrony in the synaptic inputs. This often results in a bimodal distribution of the membrane potential values indicating up-down states (Petersen et al. 2003; Constantinople and Bruno 2011). These fluctuations are influenced by various mechanisms which control the cortical state by diminishing this variability (Constantinople and Bruno 2011; Eggermann et al. 2014; Fazlali et al. 2016). As the membrane potential of cortical neurons fluctuates between up and down states, the spontaneous spikes often happen in the up state which is more than 10 mV more depolarized than down state (Constantinople and Bruno 2011). Although spontaneous spikes predominantly occur during up-state, it seems that these oscillations affect sensory evoked responses in different ways across sensory modalities. For example in the visual cortex, up-state is associated with stronger evoked responses (Haider et al. 2007) while in the vS1, down-state is associated with higher spiking probability in response to whisker stimulation (Petersen et al. 2003; Sachdev et al. 2004). A potential mechanism which may contribute to this state-dependent spiking is the variability of action potential threshold *in-vivo* (Azouz and Gray 1999, 2000; Henze and Buzsáki 2001); spike threshold is inversely correlated with the rate of increase in the membrane potential leading to the spike threshold (Anderson et al. 2000b; Azouz and Gray 2003; Poulet and Petersen 2008). Membrane potential of L2/3 pyramidal cortical neurons in up state is often more than 20 mV more depolarized than the down state *in-vivo* (Petersen et al. 2003). Driving force is given by the difference between membrane potential and the reversal potential of the excitatiory post-synaptic potentials which is ~0mV (Kandel et al. 2000). Hence the driving force in the down state is ~20

mV higher than the up state. Membrane time constant in a L2/3 pyramidal neuron is ~20 ms (time to charge the membrane capacitor, which is independent of the driving force). As a result, the slope of the membrane potential (i.e. slope of EPSP) can be on average 1 mV/ms faster in the down state compared to the up-state. Therefore, stimulus-evoked post-synaptic potentials in the down state can provide a higher rate of increase in membrane potential due to the higher excitatory driving force. This can decrease spike threshold and result in higher probability of spiking in down-state as observed in the vS1 (Petersen et al. 2003).

In many cortical neurons, the stimulus driven post-synaptic potentials (PSPs) often do not lead to a spiking response (Brecht et al. 2003; Crochet et al. 2011). Membrane potential in any moment is determined by a mixture of excitatory and inhibitory inputs (Isaacson and Scanziani 2011). Therefore, reversal potential of a synaptic current depends on the ratio of excitatory to inhibitory input. The reversal potential for the majority of neurons in the superficial layers is more hyperpolarized than action potential threshold, precluding any spiking response in these cells (Crochet et al. 2011). Strong feedforward and feedback inhibition underlies such hyperpolarized reversal potentials (Xu and Callaway 2009; Haider et al. 2013; Petersen and Crochet 2013). Consistently, *in-vitro* studies show that the biophysical and morphological properties of superficial cortical neurons do not predict their responsiveness whereas the amount of excitatory input they receive can be predictive of their responsiveness (Pouille et al. 2009; Elstrott et al. 2014). These studies suggest that the input normalization by feedforward inhibition allows the cortical circuits to operate in a wide dynamic range (Pouille et al. 2009). A question which remains to be addressed is to what extent these *in-vitro* results extend to sensory representations in superficial layers of the cortex (i.e. whether a wide range of stimulus intensities can be encoded by a gradual recruitment of the population).

In summary, experimental evidence suggests that the dominance of inhibitory inputs and/or insufficient excitatory inputs do not allow frequent spike firing in majority of the cortical neurons, which leads to the observations of sparse activity across cortical area. However, cortical neurons may overcome inhibition by increasing the ratio of excitation-inhibition, temporal modulation of input dynamics and/ or generation of action potential in a considerably more hyperpolarized state. These may involve the specific tuning of the upstream neurons, input synchrony, post- and pre-synaptic plasticity and voltage sensitivity of the cationic channels.

1.4. Theoretical support for sparse coding

The terms “sparse coding” and “sparseness” have been used in various context. Experimental studies often refer to sparseness as the degree of similarity in the response among neurons (population sparseness) or the degree of similarity of a neuron’s response to a set of stimuli (lifetime sparseness) (Rolls and Tovee 1995; Vinje and Gallant 2000). This approach is very useful when dealing with experimental data because it can be generalized to any data set and effectively quantify tuning properties of the neurons and population responses (Olshausen and Field 2004). However, in a theoretical framework elaborated by Foldiak and Enders, the activity of a neuron is reduced to a binary code of zero and one (Foldiak and Enders 2008). In this context, coding density for a population of neurons can lie in a spectrum from extreme cases of local codes involving only one or a few neurons selective to a given stimulus to dense codes where stimulus representation can involve the activity of a large fraction of the population (Foldiak 2002; Foldiak and Endres 2008). A “sparse” code may constitute an intermediate fraction of active neurons which offers a number of computational advantages over dense and local codes (Foldiak 2002; Foldiak and Endres 2008) and is consistent with the “efficient coding hypothesis” (Barlow 1972; Levy and Baxter 1996). A pivotal assumption of the efficient coding hypothesis is that neuronal systems minimize the number of spikes required to transmit a signal or to represent an ecologically relevant stimulus. Neuronal activity is a metabolically expensive function of the brain (Attwell and Laughlin 2001). Available energy in form of ATP molecules must support various metabolic functions of the cortical tissue other than spiking activity (Lennie 2003). The remaining pool of ATP is estimated to only support 0.16 spikes per second per neuron (Lennie 2003). However extracellular recordings report firing rates 10 times higher than this estimation (Shoham et al. 2006). As discussed earlier, more recent studies, using whole-cell

and cell-attached recordings have revealed that the average rate is indeed close to the estimations based on the energetic constrains of the brain tissue (Brecht et al. 2005; Shoham et al. 2006).

As the synaptic projections downstream to the sensory input expand and target a much larger population of neurons, the degree of sparseness is expected to depend on the stage of processing in the sensory pathway (Babadi and Sompolinsky 2014). It is hypothesized that a hierarchical processing underpins object recognition in the sensory pathways such as the ventral visual pathway (Riesenhuber and Poggio 1999; DiCarlo et al. 2012). Up the hierarchy, features being represented by individual neurons become gradually more complex, the receptive field expands and the number of neurons receiving input from up-stream stations increase. Based on efficient coding hypothesis, a hierarchical expansion of the neuronal populations requires gradual increase in representation sparseness (Barth and Poulet 2012; Babadi and Sompolinsky 2014). However, the sparseness at a given stage of processing may also depend on the stimulus; for example, naturalistic stimuli covering the whole visual field increase the level of sparseness in V1 (Vinje and Gallant 2000). Therefore, the stage of sensory processing and the interactions with the processing outside the receptive field may play an important role in the sparseness of a local population.

Consistent with the hierarchical view, neurophysiological studies have identified neurons responsive to very specific stimuli, the so called "grandmother" stimulus (Quian Quiroga et al. 2008, 2009) particularly at the final stages of visual pathway (e.g. human medial temporal lobe). However, even at this stage of processing it is not clear how many neurons are involved in the representation of a grandmother stimulus. In other words, it is not clear whether a high level of stimulus selectivity (also known as lifetime sparseness) results in a high level of population sparseness. A fundamental difficulty in estimation of sparseness is the limitations in sampling a

sufficiently large pool of neurons, ideally the whole population (Quian Quiroga et al. 2008). A precise measure of sparseness therefore requires an unbiased, large-scale single-cell resolution monitoring of spiking activity and inclusion of a large and diverse array of stimuli. An alternative hypothesis for coding density is that perception of complex stimuli does not require highly selective neurons and can be achieved by the collective activity of a large population which are broadly tuned to simpler features of the complex stimulus (Decharms and Zador 2000). Consistent with efficient coding hypothesis, at lower levels of the hierarchy (e.g. first order sensory neurons) a dense coding may be required because a small population of neurons has to carry all relevant information about the stimuli. Therefore, they may need to use their full spiking capacity to reliably encode the quality or the strength of the feature or features to which they are tuned to. An example of a dense coding in the first order neurons in rodent whisker pathway encode multiple features of whisker motion (Severson et al. 2017). Another example is the tuning of the neurons in the primary visual cortex to elementary features such as edge orientation (Hubel and Wiesel 1959) which can repeatedly occur in a natural scene and hence require a denser code than higher cortical area which encode more complex stimuli (Quian Quiroga et al. 2008). Altogether, dense coding appears to be a dominant strategy in the initial stages of sensory processing, where a small number of neurons must reliably encode spatiotemporal patterns of the stimulus, while increasing representation sparseness is necessary for the higher order neurons to efficiently encode complex stimuli.

A stable, invariant perception of stimuli requires repeatable patterns of spiking activity representing those stimuli. Trial-to-trial variability (Shadlen and Newsome 1998) can thus degrade the ability of ensembles to reliably repeat a certain pattern (Kerr et al. 2007). Such trial-to-trial variability may have multiple sources including random cellular/circuit processes (i.e.

noise) and instability in the internal states (Faisal et al. 2008). Trial-to-trial variability can be quantified in terms of spike count as well as spike time (Buračas et al. 1998). Spike count variability is often quantified as the spike count variance divided by mean which is known as "Fano factor" (Teich et al. 1990; Buračas et al. 1998; DeWeese et al. 2003; Hires et al. 2015). Fano factor can be markedly different between different stages of sensory processing and across modalities (DeWeese et al. 2003). Studies in the cat and primate visual cortex have typically reported Fano factors ≥1 (Dean 1981; Buračas et al. 1998; Oram et al. 1999) with a few exceptions (Gur et al. 1997; Kara et al. 2000). In the auditory and somatosensory cortex, cell-attached recordings have shown precisely timed spiking response with Fano factors close to or equal to the theoretical minimum (DeWeese et al. 2003; Hires et al. 2015).

It is not entirely clear how variability changes from lower to higher processing stages. In both cat visual system and rat whisker pathway, spike time and spike count variability increase from primary afferents to the cortex (Kara et al. 2000; Arabzadeh et al. 2005; Bale and Petersen 2009) whereas in the auditory system, spike count variability appears to be much lower in the cortex compared to the auditory nerve (Teich et al. 1990; DeWeese et al. 2003). Various experimental conditions may affect the apparent variability in each area; these include cortical state (Arieli et al. 1996; Fazlali et al. 2016), the choice of the spike count window, behavioral state, attention and the alignment of trials to a specific stimulus feature (Hires et al. 2015). Despite a large body of knowledge on the nature and extent of response variability in the neocortex, it is not yet clear how different sensory regions deal with variability. The specific role of each stage in processing of sensory information may also determine their tolerance to response variability. Consistent measures of both temporal and spike count variability across sensory regions and various

experimental conditions can provide a better picture of the sources of variability and the factors affecting response reliability.

In the cortex, trial-to-trial variability is often correlated among neurons which is called “noise correlation”. Noise correlations are known to limit or enhance information about the stimulus, depending on the signal and noise directions and also the readout mechanisms (Shadlen and Newsome 1998; Averbeck et al. 2006; Lin et al. 2015). Noise correlations often limit information processing capability of similarly tuned neuronal ensembles (Lin et al. 2015; Panzeri et al. 2015; Pitkow et al. 2015).Therefore, even a near-optimal readout mechanism can only extract a limited amount of information from a correlated population activity which may explain why behavioral performance in stimulus detection is not much better than single neuron performance (Pitkow et al. 2015). In the presence of noise, a sparse code with little overlap between contributing neurons can provide a more robust and invariant representation bearing in mind that this is also a highly energy efficient coding strategy (Lennie 2003).

1.5. Connectivity and functional organization of the vibrissal system

Whiskers, or vibrissae, are highly organized arrays of long hair which constitute a specialized sensory organ located around the snout of many mammalian species. Whiskers are highly developed in rodents and play a crucial role in their navigation and their interactions with the environment (Diamond and Arabzadeh 2013). Innervations of the whisker base at the follicle-sinus complex transduce whisker dynamics into neuronal impulses. Although the morphology of the follicle-sinus complex is fairly known (Ebara et al. 2002) the exact functional mapping of whisker movements and forces on the various nerve terminals in follicle is just beginning to be explored (Severson et al. 2017; Wallach et al. 2017). Nevertheless, the spiking activity in trigeminal ganglion (TG), where cell bodies of these innervations are located has been

extensively studied (Zucker and Welker 1969; Lichtenstein et al. 1990; Bale and Petersen 2009; Bale et al. 2015; Campagner et al. 2016). Primary afferents relay their information to the second-order neurons in the trigeminal nuclei of the brainstem.

Second-order neurons in the trigeminal nuclei are somatotopically organized into "barrelettes"; a one-to-one mapping of each whisker into the clusters of neurons encoding mainly the deflections of a principal whisker (Minnery and Simons 2003). The primary afferents to the brainstem bifurcate and terminate in anatomically distinct nuclei (Chiaia et al. 1991; Feldmeyer et al. 2013). Second-order neurons in the principal nucleus (PrV) which form the lemniscal pathways mainly project to the somatotopically organized nuclei in head and core of the ventral posterior medial (VPM) thalamus known as "barreloids" (Feldmeyer et al. 2013). In parallel, second-order neurons in spinal trigeminal complex (SpV) form para-lemniscal and extra-lemniscal pathways, which respectively target the posterior medial thalamus (POm) and the tail of VPM. These parallel pathways target distinct cortical regions and interact via several feedback loops (Furuta et al. 2010; Feldmeyer 2012; Feldmeyer et al. 2013). It is not entirely clear whether these parallel whisker-to-cortex pathways are functionally segregated and thus convey distinct information about the whisker variables (Yu et al. 2006; Moore et al. 2015).

As mentioned earlier, VPM is organized into somatotopic regions called barreloids. vS1 inherits somatotopic organization from VPM so that every single whisker maps into a single "barrel column" through the lemniscal pathway (Woolsey and Van der Loos 1970; Diamond and Arabzadeh 2013; Feldmeyer et al. 2013). Neuronal activity in a barrel column mainly represents its corresponding whisker (Simons 1978). The whisker barrel system has provided a unique model to study cortical sensory processing and neuronal circuitry devoted to an "expert" sensory system (Brecht 2007; Diamond and Arabzadeh 2013; Feldmeyer et al. 2013).

Like that of primate somatosensory and visual cortex, each cortical column in vS1 is vertically organized into 6 layers based on functional connectivity and cytoarchitectonics. Layer 1 (L1) of the vS1 contains sparsely distributed inhibitory neurons, distal dendritic branches and various axonal projections from cortical and subcortical neuromodulatory systems (Brombas et al. 2014; Muralidhar et al. 2014). This layer may have a role in learning through disinhibition of deeper layers (Letzkus et al. 2011). Layer 2 is the first layer where excitatory neurons appear sparsely and as the depth increase their density increase to a plateau which is sustained up to the border of layer 3 and 4 (Oberlaender et al. 2012). Layer 2 and 3 do not have a clear border and are thus often referred to together as L2/3. The inputs to L2/3 are mainly feedforward excitatory and inhibitory from layer 4 (Lefort et al. 2009; Xu and Callaway 2009). The VPM input to L2/3 is much sparser than that to L4 and does not provide significant input to upper layer 2 (Oberlaender et al. 2012). L4 contains a dense pack of neurons which are tightly connected with VPM (Oberlaender et al. 2012). L5 contains large pyramidal neurons with long apical dendrites which often expand in superficial layers 1 and 2. L5 can be further divided into L5A and L5B, based on cell morphology and the source of the synaptic input (Bureau et al. 2006; Oberlaender et al. 2012). L6 has neurons with diverse morphologies with a predominantly modulatory role in cortical and subcortical circuits (Briggs 2010).

The excitatory cortical neurons within a column are highly interconnected. This includes connections with neighboring cells and vertical projections between layers (Lefort et al. 2009). *In vitro* analysis of unitary excitatory post-synaptic potentials (uEPSP) showed that L4 receives little input from other layers but neighboring cells in this layer are strongly connected (Lefort et al. 2009). Likewise, within L5A and L3 neurons are strongly connected to each other (Lefort et al. 2009). Lefort and colleagues also showed that laminar connectivity is especially strong

between L4 and L2 and between L3 and L5B and provided further details of other ascending and descending connections; ascending connections are mainly from L4 to L2/3 and descending connections mainly from L2/3 and L4 to L5 and L6. This connectivity scheme is compatible with the idea of a canonical circuit within the cortical column: L4 → L2/3 → L5. However, *in vivo* studies have debated the functionality of this cortical loop; the direct projections from the VPM to the deep layers 5 and 6 appears to dominate and determine the activity of these layers (Bureau et al. 2006; Constantinople and Bruno 2013). Moreover, deep L2/3 is also targeted by VPM/LGN axons in vS1 and V1 and may represent a distinct stage of processing (Petersen and Crochet 2013; Morgenstern et al. 2016).

Long-range connectivity in vS1 is both cell-type and layer specific. Superficial layers (L2/3) project to other cortical regions. This includes a sensorimotor loop between vS1 and vM1, and a sensory feedback loop between vS1 and vS2 (Mao et al. 2011; Chen et al. 2013; Kwon et al. 2016). These circuits are mostly non-overlapping and are deemed critical in whisker mediated tasks; neuronal activity in vS1↔vS2 loop appears to be a key component in shaping the decision about a sensory input (Yang et al. 2015; Kwon et al. 2016), and vS1↔vM1 is shown to be critical in the initiation of whisking behavior (Sreenivasan et al. 2016). Furthermore, recruitment of these pathways is task dependent, suggesting that separate cortical channels may be utilized to solve a whisker-mediated perceptual task (Chen et al. 2013). L2/3 also sends projections to the contralateral vS1 (Wang et al. 2007). The laminar pattern of contralateral projections seems to be the same as the home column connectivity (Petreanu et al. 2007). Ipsilateral cortical projections of the L2/3 neurons is cell specific and non-overlapping (Chen et al. 2013). Other targets of L2/3 projections includes non-barrel S1, perirhinal cortex and striatum (Feldmeyer 2012). It is also known that both lemniscal and para-lemniscal pathways ascend to different cells in the L2/3

(Shepherd and Svoboda 2005). The mapping of lemniscal and para-lemniscal inputs to different cortical projecting neurons in L2/3 has not yet been addressed.

In vS1, L4 projections are limited to the cortical column, while deeper layers project to a range of distant, cortical and extra-cortical targets (Feldmeyer 2012). L5A neurons directly communicate para-lemniscal information with other cortical area, in parallel with L2/3 projections to these area (Mao et al. 2011; Feldmeyer 2012). On the other hand, axonal projections of thick-tufted L5B pyramidal neurons predominantly target distant sub-cortical targets such striatum, superior colliculus, pons and trigeminal nuclei (Feldmeyer 2012). The last cortical lamina, L6, can be divided into L6A and L6B based on developmental and morphological characteristics. Three distinct type of neurons based on projecting targets can be identified; VPM projecting, VPM&POm projecting and corticocortical projecting neurons (Feldmeyer 2012). L6 corticothalamic projecting neurons receive input from non-barrel S1, S2, M1 and even perirhinal cortex (Feldmeyer 2012). Hence, they may critically modulate both VPM and POm by a strong and highly integrated feedback. Notably, a more recent study in mouse visual cortex revealed a prominent role of L6 corticothalamic cells in recruiting "translaminar" fast-spiking inhibitory neurons in this layer (Bortone et al. 2014). Corticocortical projecting neurons in L6 project to distant cortical area such as vM1, vS2 and perirhinal cortex similar to L2/3 neurons (Mao et al. 2011; Feldmeyer 2012). The deeper subdivision of L6 contains heterogeneous excitatory neurons which project to L1 and POm (Feldmeyer 2012). Overall, long-range connectivity in vS1 suggests a key role of superficial layers in communication with other cortical area together with the deeper layers (other than L4) which also project to thalamic and other sub-cortical regions. A prominent interplay between multiple areas connected to the vibrissal columns is hence expected, during whisker-mediated behaviors.

Local inhibitory circuits in the vS1 cortex play a prominent role in cortical computations (Petersen and Crochet 2013; Tremblay et al. 2016). Cortical GABAergic inhibitory interneurons have been categorized into diverse classes based on morphological, molecular and physiological characteristics (Petilla et al. 2008; Tremblay et al. 2016). Three major classes of GABAergic neurons comprise nearly all inhibitory interneurons in the vS1: somatostatin-expressing (SOM), fast spiking interneurons which express parvalbumin (FS or PV) and serotonin receptor-expressing (5HT3AR) cells (Rudy et al. 2011). Laminar distribution of the major inhibitory classes is markedly diverse; FS cells are the most abundant category which are more densely located in L4-6 with a peak density in L4 (Xu et al. 2010; Tremblay et al. 2016). FS neurons mainly target proximal dendrites and the axon initial segment of other neurons and have a major role in silencing excitatory neurons (Rudy et al. 2011; Petersen and Crochet 2013; Yu et al. 2016)). SOM cells are abundant in deeper layers 5 and 6 and have diverse axonal projections which mainly target distal dendrites, especially in L1 (Tremblay et al. 2016; Muñoz et al. 2017). 5HT3AR neurons are mostly localized in superficial layers, L1 and L2/3 and mainly target SOM neurons (Xu et al. 2010; Tremblay et al. 2016). The abundance of all major types of inhibitory neurons in L2/3, suggests a prominent role of inhibitory connections in controlling spontaneous and sensory evoked activity in L2/3 (Gentet 2012).

1.6. Response properties and sensory features in the vibrissal system

In this section, we review stimulus related activity in different stages of processing and in different pathways in the vibrissal system. This provides a background on how a multistage processing in parallel pathways shapes cortical representation of elementary stimulus features and sets a potential for encoding more complex and diverse features. In vS1, we will focus on the differential encoding of the active and passive whisker movements by major neuronal subtypes

since the interneuron activity during natural behavior is crucial to sparsening of the cortical output.

In the vibrissal system, clusters of primary afferent neurons in TG lack somatotopic organization but individual neurons strictly respond to the deflections of a single whisker with a high trial-to-trial fidelity (Arabzadeh et al. 2005; Bale et al. 2015; Campagner et al. 2016). TG neurons display two major types of responses to simple stimuli; slowly adapting and rapidly adapting responses, both with strong directional selectivity (Zucker and Welker 1969; Lichtenstein et al. 1990; Bale and Petersen 2009). Multiple features of the stimulus can be encoded by the TG neurons such as whisking, contact, pressure and detachment from objects (Szwed et al. 2003). Second-order neurons in PrV inherit most of their response properties from the primary afferents (Minnery and Simons 2003). However, due to bifurcation and convergence of the afferents (Chiaia et al. 1991), the second-order neurons typically have larger receptive fields and a significantly decreased direction selectivity compared to the first-order neurons in TG (Minnery and Simons 2003). PrV neurons have variable spatial tuning depending on their projecting area; single-whisker (narrowly tuned) neurons are associated with the lemniscal pathway whereas multi-whisker neurons project to POm and other subcortical nuclei (Veinante and Deschênes 1999). The majority of neurons in SpV have multi-whisker receptive fields, often directionally tuned with a high sensitivity to whisker deflection (Gibson 1987; Veinante et al. 2000). Some of the most studied neurons in the pathway are those located in barreloids of VPM due to their somatotopic organization and dominant input to vS1 (Deschênes et al. 1998; Feldmeyer et al. 2013). Whisker evoked responses in VPM almost faithfully reflect those of projecting neurons in PrV with slightly more evident adaptation and surround-suppression mediated by thalamic reticular nucleus (Lee et al. 1994; Hartings and Simons 2000; Minnery et al. 2003). VPM

responses are quick, temporally precise and repeatable, while responses of POm neurons are weak, delayed, highly adaptable and temporally scattered (Diamond et al. 1992; Sosnik et al. 2001). This is due to a feedforward inhibitory input to POm which counterbalances excitatory input from SpV (Lavallee et al. 2005).

In a classic paper, Simons described key response properties of the vibrissal cortical neurons (Simons 1978) which were further reproduced in subsequent studies ; 1) the majority of units had only transient responses (58%) to ramp-and-hold stimuli while a smaller fraction (32%) represented a sustained response during steady-state of ramp-and-hold stimuli. 2) Most of the units had preferred direction with a high level of variability in their width of tuning. 3) More than half of the recorded neurons only responded to deflections of a single whisker while the rest responded to a variable number of whiskers. 4) The fraction of multi-whisker units was highly variable depending on the layer, with L4 having the highest fraction of single-whisker units (85%) and L5&6 representing the highest fraction of multi-whisker units. 5) The FS units were more prevalent in L4, more robustly driven by whisker deflections and broadly tuned to the whisker deflection angles compared to the RS units. 6) Various stimulus properties such as amplitude, velocity and direction were encoded by the vS1 neurons. Subsequent behavioral studies combined with spike recording from the cortex revealed various neural correlates of whisker-object interactions (Jadhav et al. 2009; O'Connor et al. 2010b; Chen et al. 2013; Hires et al. 2015) and importantly revealed a causal link between vS1 activity and the behavioral report of vibrissal stimuli (Miyashita and Feldman 2013; O'Connor et al. 2013; Sachidhanandam et al. 2013). Despite substantial progress in neuronal recording/imaging techniques coupled with various behavioral tasks, we still lack a full understanding of features that are encoded in the vS1

and how columnar processing shapes simple and complex feature representations, which form the building blocks of object perception.

To date, a number of studies have shown that first-order neurons reliably encode elementary mechanical variables of a single whisker, such as deflection amplitude, direction, phase, velocity/acceleration and curvature (Lichtenstein et al. 1990; Stüttgen et al. 2008; Bale et al. 2013, 2015; Campagner et al. 2016; Severson et al. 2017). These features are more or less preserved in the sensory pathway up to the level of vS1 (Simons 1978; Lichtenstein et al. 1990; Arabzadeh et al. 2005; Stüttgen et al. 2008). In anesthetized preparations the most prominent feature encoded by cortical neurons is velocity of the whisker deflection (Shoykhet et al. 2000). Studies on texture discrimination showed that high-velocity events caused by whisker stick and slip over the texture grains are reliably represented by vS1 neurons which provides a "kinetic signature" for texture discrimination (Arabzadeh et al. 2005; Diamond et al. 2008a; Wolfe et al. 2008; Jadhav et al. 2009). Reliable representation of certain features by individual neurons appears to degrade from primary afferents to the vS1. For example, directional selectivity of cortical neurons was shown to be pronouncedly lower than VPM (Simons and Carvell 1989) and ganglion neurons, with ganglion neurons having the sharpest tuning (Bale and Petersen 2009). Nevertheless, directional tuning maps are unique characteristics of the barrel columns and have specially stronger manifestation in L2/3 compared to the deeper layers (Andermann and Moore 2006; Kremer et al. 2011).

Rodent whiskers are under volitional motor control, enabling the system to operate in a receptive (passive) or generative (active) mode (Diamond and Arabzadeh 2013). In awake condition, rodents move their vibrissae forward and backward at frequencies ranging from 1-20 Hz (Cao et al. 2012). This exploratory behavior is highly variable depending on the nature of the behavior

and dimensions of the objects being explored (Mitchinson et al. 2007). In addition to adjusting the whisker movements (Mitchinson et al. 2007), motor cortex can also provide an efferent copy to the vS1 and vS2 and contribute to sensory perception (Diamond et al. 2008b). Alternatively, object location can already be encoded by the phase-locked activity of the primary afferent neurons which do not receive any motor feedback (Szwed et al. 2003; Knutsen and Ahissar 2009). Single whisker, phase-locked responses in TG, therefore, can provide localization signals to downstream stations (Curtis and Kleinfeld 2009; Kleinfeld and Deschênes 2011; Severson et al. 2017) in the absence of proprioceptive signals (Moore et al. 2015).

In the vS1, free whisking can weakly modulate the firing rate of neurons in a diverse manner; pyramidal neurons express a layer and cell-type specific activation by free whisking (de Kock and Sakmann 2009). It appears that whisking is mainly represented by slender-tufted pyramidal cells in L5A (de Kock and Sakmann 2009). These neurons increase their activity during whisking with a weak modulation by the phase of the whisking while the pyramidal neurons in other layers are mainly suppressed by the whisking (de Kock and Sakmann 2009). Whisking seems to have a diverse effect on the firing rate of FS cells depending on their location. Although L2/3 FS neurons are robustly driven by whisker deflections, free whisking can reduce their firing rate (Gentet et al. 2010). Free whisking however, activates L4 FS neurons which prevent excitatory neurons from being driven by the whisking (Yu et al. 2016). Although feedforward inhibition is also dominant in L2/3, studies have shown that L2/3 pyramidal neurons are able to encode either touch, whisking or both (Peron et al. 2015b). This might be due to the segregation/integration of parallel whisker pathways in the cortex. Indeed, targeted whole-cell recordings from fos-GFP positive, excitatory neurons in L2 vS1 showed that these neurons are more responsive to surround whiskers compared to their neighboring fos-GFP negative cells and

are preferentially evoked by POm photo-stimulation (Jouhanneau et al. 2014). Therefore, the para-lemniscal pathway may contribute to the representation of whisking (Yu et al. 2006) in a subset of excitatory neurons in L2/3 of vS1 (Peron et al. 2015b). Para-lemniscal pathway is also shown to be involved in long term potentiation of synaptic inputs in L2/3 of vS1 (Gambino et al. 2014). Such multi-whisker interactions in the cortex induced by free whisking can reset the network for additional, and potentially more complex features to be encoded during active behavior.

A given whisker may contact an object in different phases of the whisking cycle or different angles of the whisker relative to the face (Curtis and Kleinfeld 2009). Furthermore, an object may come in contact with a whisker at the same angle or phase but at a different position along the whisker axis (Bagdasarian et al. 2013; Pammer et al. 2013). In freely moving rodents, the head and body movements may further constrain encoding of the contact location. Algorithms used by the vS1 to encode objects and their locations have faced ongoing debate (Curtis and Kleinfeld 2009; O'Connor et al. 2013). Recent studies suggest that integration of multi-whisker contact information may be necessary to form a reliable map of the space in the cortex (Ramirez et al. 2014; Estebanez et al. 2016; Pluta et al. 2016) Multi-whisker tunings are particularly strong in L2/3 and this may facilitate the emergence of additional features in this layer (Jacob et al. 2008; Estebanez et al. 2012, 2016). Regarding feature coding in vS1, two questions require further investigation; 1) to what extent is the sparse coding in vS1 due to high selectivity of the neurons? 2) If this is the case, which additional features are presented by vS1 neurons?

Chapter 2: High-velocity stimulation evokes “dense” population response in layer 2/3 vibrissal cortex

2.1 Abstract [1]

Supra-granular layers of sensory cortex are known to exhibit sparse firing. In rodent vS1, a small fraction of neurons in layer 2 and 3 (L2/3) respond to whisker stimulation. Here, we combined whole-cell recording and two-photon imaging in anesthetized mice and quantified the synaptic response and spiking profile of L2/3 neurons. Previous literature has shown that neurons across layers of vS1 are tuned to the velocity of whisker movement. We therefore used a broad range of stimuli that included the standard range of velocities (0-1.2 degree/ms) and extended to a "sharp" high-velocity deflection (3.8 degree/ms). Consistent with previous literature, whole-cell recording revealed a sparse response to the standard range of velocities: although all recorded cells showed tuning to velocity in their postsynaptic potentials, only a small fraction produced stimulus-evoked spikes. In contrast, the sharp stimulus evoked reliable spiking in the majority of neurons. The action-potential threshold of spikes evoked by the sharp stimulus was significantly lower than that of the spontaneous spikes. Cell-attached recordings confirmed that application of sharp stimulus to single or multiple whiskers produced temporally precise spiking with minimal trial-to-trial spike-count variability (Fano factors equal or close to the theoretical minimum). Two-photon imaging further confirmed that most neurons that were not responsive to the standard deflections responded to the sharp stimulus. Altogether, our results indicate that sparseness in L2/3 cortex depends on the choice of stimulus: strong single- or multi-whisker stimulation can induce the transition from sparse to "dense" population response.

Keywords: sparse coding; post synaptic potentials; Fano factor; two-photon imaging, somatosensory; AP threshold; whisker velocity

[1] This chapter is maintained as it appeared in the Journal of Neurophysiology (Ranjbar-Slamloo and Arabzadeh, 2017), except minor changes for consistency with the rest of the thesis.

2.2 Introduction

The mammalian cerebral cortex contains a fine laminar organization for processing sensory information. In rodents, the whisker associated area of the somatosensory cortex, known as the vS1, provides an example of efficient functionality and a well-described circuitry (Ahissar and Kleinfeld 2003; Brecht 2007; Diamond and Arabzadeh 2013; Feldmeyer et al. 2013). Recent advances in functional imaging combined with conventional electrophysiological techniques have revealed that sensory processing within local circuits of neocortex is layer and cell type dependent (Gentet et al. 2010, 2012; O'Connor et al. 2010b; Harris and Mrsic-Flogel 2013; Petersen and Crochet 2013). Investigating the contribution of different cortical layers to sensory processing is thus a key step in understanding cortical computations.

It is well established that neurons in layer 2 and 3 (L2/3) of vS1 have low spontaneous rates of spiking and sparsely respond to sensory stimulation (Harris and Mrsic-Flogel 2013; Petersen and Crochet 2013). During object localization tasks, a small fraction (~10%) of L2/3 neurons discriminated object location (O'Connor et al. 2010b; Peron et al. 2015b). This is not limited to the active touch; passive whisker deflection in awake or anesthetized mice also evoked sparse activity in L2/3 of vS1 (Clancy et al. 2015; Peron et al. 2015b). However, the choice of stimulus may critically determine the degree of sparse coding (Barth and Poulet 2012; Spanne and Jörntell 2015).

The mechanisms underlying sparseness of L2/3 neurons are not well understood. Neurons with distinct degrees of responsiveness exhibit similar intrinsic biophysical properties and morphology (Elstrott et al. 2014). The interactions of inhibitory and excitatory synaptic inputs

determine the specific properties of whisker-evoked postsynaptic potentials or PSPs (Petersen and Crochet 2013). Intracellular recordings *in vivo* have revealed that amplitude of whisker-evoked PSPs is dependent on the state of membrane potential immediately preceding the stimulation (Petersen et al. 2003; Sachdev et al. 2004). In a majority of L2/3 neurons, whisker stimulation produces maximum reversal potentials that are more hyperpolarized than the action potential (AP) threshold, precluding spiking response (Crochet 2012; Sachidhanandam et al. 2013). Overall, these observations combined with evidence from connectivity studies (Xu and Callaway 2009; Avermann et al. 2012) suggest that strong inhibition through local GABAergic circuitry counterbalances the excitatory input to L2/3 pyramidal cells resulting in excess silence and sparse sensory response in this layer (Petersen and Crochet 2013).

A question that arises here is whether a majority of the neurons in L2/3 of vS1 are always silent or certain mechanisms allow them to contribute to the sensory processing despite their dominant inhibitory input. Strong inhibition may not always prevent spiking for two reasons: (i) The spike threshold can depend on the stimulus preference (Carandini and Ferster 2000; Wilent and Contreras 2005b). (ii) The temporal dynamics of inhibition and excitation can provide a "window of opportunity" for cortical neurons to fire action potentials in response to the preferred stimulus (Wilent and Contreras 2005a). Such mechanisms can modulate both the reversal potential and the spike threshold of the less active L2/3 pyramidal cells, allowing them to respond to certain sensory features (Barlow 1972; Andermann and Moore 2006; Harris and Mrsic-Flogel 2013; Petersen and Crochet 2013; Garion et al. 2014).

Previous literature has shown that neurons across layers of vS1 are tuned to the velocity of whisker movement (Simons 1978; Ito 1981, 1985; Pinto et al. 2000; Arabzadeh et al. 2003, 2004; Wilent and Contreras 2004; Boloori et al. 2010; Gerdjikov et al. 2010). However, a

relatively low range of velocities (typically up to 1.3 degree/ms) are used in controlled experimental settings to reveal the dynamic range of neuronal response. But a broader range of whisker velocities are reported in behaving mice (O'Connor et al. 2010a; Bale et al. 2015) and rats (Carvell and Simons 1990; Ritt et al. 2008; Wolfe et al. 2008; Jadhav et al. 2009) including velocities as high as 10 degree/ms (O'Connor et al. 2010a; Bale et al. 2015). It is not clear to what extent the sparse activation of L2/3 neurons may maintain over a wider range of velocities. Here, we hypothesize that the population of L2/3 neurons may be preserved for coding of such high-velocity events. We use whole-cell and cell-attached recording and two-photon calcium imaging in anesthetized mice to quantify the synaptic and spiking response of L2/3 neurons. Critically, the stimulus set includes a "sharp" deflection that falls in the range of high-velocity events that occur in object/texture palpation.

2.3 Methods

2.3.1 Surgery

Male ~6 week old C57BL6/J mice were used in this study. Light anesthesia was induced with a brief exposure to isoflurane (3.5% in oxygen) followed by intra-peritoneal injection of 5 mg/kg chlorprothixene and 500-mg/kg urethane in ringer solution. Corneal and paw reflexes were checked to be absent before mounting the animal on a custom built head fixation plate with ear bars and nose clamp. The skull was then exposed and the coordinates of the vS1 were marked. A head bar was attached onto the skull using a thin layer of tissue adhesive (Vetbond, 3M, St Paul, Minnesota), adhesive gel and dental acrylic cement. Tissue adhesive was used all around the skull (except for the top of vS1) to seal the area and to keep drops of ringer solution on top of the vS1. A cranial window of 1-3 mm diameter was drilled over the vS1 using vascular patterns and stereotaxic coordinates (center; 1-1.5 mm posterior to bregma and 3-4 mm lateral to the midline) or with intrinsic signal optical imaging (see below). Throughout the surgery, drops of artificial cerebrospinal fluid (ACSF) were applied to the exposed area. Dura mater was left intact.

2.3.2 Intrinsic signal optical imaging

Intrinsic signal optical imaging (Grinvald et al. 1986) was carried out through the intact skull to map the S1 area representing whisker C2 (Ferezou et al. 2006). Ringer solution was applied to make the skull translucent and a cover slip was used to trap the ringer solution and prevent it from drying. Surface blood vessels were visualized by green light (527 nm, Figure 2.3*B*, top). Images were captured under red light (626 nm) using a CMOS camera (Photonfocus, Lachen, Switzerland) mounted on a Leica M80 stereomicroscope. In each trial, a sequence of 100 frames was acquired at 10 Hz with 70 ms exposure time. A sharp deflection (Figure 2.1*B*, green) was applied to whisker C2 at the onset of each frame during the second half of the sequence (frames

51-100). This sequence was repeated 30 times, with 20 s intervals. In each sequence the first 50 frames (background signal) were averaged and subtracted from the second 50 frames (sensory stimulation). The difference matrix was averaged across trials to produce the localized intrinsic signal (Figure 2.3*B*, middle, dark spot) in the final image. This image was then adjusted, filtered and merged with the vasculature image (Figure 2.3*B*, bottom) to guide surgery and recording. This imaging protocol was repeated if the vasculature pattern was obscured after craniotomy.

2.3.3 Calcium Imaging

The animal was transferred to a two-photon microscope system with a Chameleon (Coherent) Ti:Sapphire laser tuned at 810 nm and focused by a water immersion Nikon objective (16x, 0.8NA). Calcium florescent dye, Cal5-20 AM (AAT Bioquest) was dissolved in 20% Pluronic acid in DMSO and diluted in ACSF. Sulforhodamine (0.5µl) was added to the solution such that the final concentrations of Cal-520 and Sulforhodamine were 1.0 and 0.06 mM respectively. This solution was pressure-injected (100-200 mmHg) at 100-300 µm depth using micropipettes with 4-6 µm tip diameter. The injection was monitored with the two-photon microscope. Whisker evoked local field potentials (LFPs, Figure 2.1*D*) were monitored with a MultiClamp 700B amplifier (Molecular Devices) and Axograph software, while the pipette was injecting the dye. Image acquisition began 30-60 min after the dye injection with recording 100 frames of background activity in two channels; red for Sulforhodamine which labels astroglia (Nimmerjahn et al. 2004) and green for Cal-520. During whisker stimulation protocol, only the green channel was recorded at 30 frames per second. Image stacks were corrected for drifts in x-y plane using TurboReg in ImageJ (Thévenaz et al. 1998). Average images were then merged (Figure 2.5*A*) to differentiate neurons from glia. Simultaneous cell-attached spike recording and

calcium imaging was attempted for a few cells to confirm action potential generation during whisker stimulation by the sharp stimulus (Figure 2.5*A*&*B*).

2.3.4 Electrophysiology

Whole-cell recordings were performed using 4-6 mΩ pipettes loaded with intracellular solution containing (in mM): 10 KCl, 130 K-Gluconate, 10 HEPES, 4 MgATP, 0.3 Na_2GTP, 10 Na_2 Phosphocreatine, 0.047 Alexa594 (pH ~ 7.25, Osmolality ~280 mOsm). The electrode passed the dura with ~200 mmHg positive pressure. The pressure was then dropped to ~45 mmHg at a depth of ~100 µm and pipette offset was corrected. When a gigaseal was established, membrane rupture was made with brief suctions applied to the pipette and then pipette capacitance and resistance were corrected. The whole-cell configuration was confirmed with a stable membrane potential in the range of -50 to -70 mV, the firing of overshooting action potentials and responsivity to a current-steps protocol (100 pA steps from -300 to 1000 pA, 500 ms duration).Voltage was low-pass filtered at 10 kHz using Bessel filter prior to being digitized at 20 kHz sampling rate either with an ITC-18 (Instrutech) or a PCIe-6321 data acquisition board (National Instruments). Cell-attached recordings were made by patch pipettes filled with ACSF. Sulforhodamine (0.06mM) was added to ACSF to visualize the pipette and allow targeting of cal-520 loaded cells for cell-attached recording combined with functional imaging (Figure 2.5*A*&*B*).

2.3.5 Whisker stimulation

To stimulate a single whisker, a small pipette was attached to a piezoelectric ceramic (piezo). The pipette was positioned ~4 mm away from the base of the whisker. For the whole-whisker pad stimulation, a rigid aluminum mesh was glued to the piezo and was positioned ~4 mm away from the base of the whiskers and tilted to engage as many whiskers as possible. Deflection

commands were generated in MATLAB (MathWorks) and sent to the analogue output of the National Instruments board (20 kHz sampling rate) via a piezo amplifier (PiezoDrive, amplification gain of 20) to the piezo. The voltage signal had a Gaussian waveform, which produced a brief deflection (4-ms rise, 5-ms drop). Deflections were generated at 11 different amplitudes (0-2.8 degrees; peak velocities of 0-1.21 degrees/ms; Figure 3.1*B*). The Gaussian function resulted in a smooth rise and drop in piezo's movement trajectory with minimal ringing (~10%, second peak/first peak). In addition, a step voltage command to the piezo generated a sharp deflection with ~2 ms rise time, 3.6 degrees amplitude, 3.82 degrees/ms peak velocity and ~40% ringing (Figure 2.1*C*). We used a calibrated infrared optical sensor and obtained the actual movement trajectory of the vibrating mesh (Figure 2.1*B*, average of 100 trials). Partial blockade of the infrared beam by the piezo deflections generated proportional changes in the sensor's output voltage, which was then converted to actual position (in μm) by matching the voltage values to a voltage-position curve obtained from sensor calibration. The linear position was then converted to angular position to yield angular velocities in degree/ms. Moment-by-moment velocity was calculated as the first derivative of the position profile and the peak velocity was used to represent stimulus intensity. The movements were highly reproducible across trials: movement profiles were visually identical with a negligible variation at the peak velocity (across 100 trials, standard deviation = 0.0097 degree/ms for the sharp stimulus which had the highest variability). The 12 stimuli were repeated 25 times each with a pseudorandom order and with 1.5-2.5 s inter-stimulus intervals. One minute of spontaneous activity was recorded at the beginning and end of each recording session.

2.3.6 Data analysis

We applied two procedures to isolate synaptic responses (PSPs) from action potentials: (i) Action potentials were truncated from the membrane potential (V_m) and substituted with a linear interpolation (Figure 2.2*A*&*B*). (ii) As an alternative, we excluded trials that contained action potentials within 75 ms from the stimulus onset (Figure 2.2*C*) which allowed direct quantification of the peak PSPs. Peak value of PSPs was measured at the interval of 10-75 ms after stimulus onset and was averaged over trials and over cells for each stimulus (Figure 2.2*C*). To quantify spiking response, recordings were high-pass filtered (at 200 Hz) in MATLAB using Butterworth filter to magnify APs which were then reliably isolated from artifacts. Spiking response was defined as the number of APs within 75 ms from the stimulus onset, averaged across 25 repetitions of each stimulus (Figure 2.2*D*). AP waveforms were filtered using a 10 sample moving average implemented by smooth function in MATLAB. AP threshold was then calculated as the positive peak of the second derivative of the AP waveform (Figure 2.2*E*&*F*). AP latency was calculated at 50 µs resolution within 35 ms from the stimulus onset (only two neurons fired a few outlier spikes beyond 35 ms). Response jitter was defined as the standard deviation of spike latency across trials. Fast spiking (FS) neurons were identified based on their characteristic narrow spike waveform and excluded form analyses (except Figure 2.4*C*). Spike width was measured at 10% of the normalized spike peak (Figure 2.4*E*). Initial analysis on calcium imaging data was performed using ImageJ software. After averaging all recorded frames, and merging that with the red channel, free-hand regions of interest were drawn around each soma. Average fluorescence was then calculated across frames and converted into $\Delta F/F$ and further analyzed in MATLAB (Figure 2.4*B*). Potential neuropil contamination was not corrected in our data. For ROC analysis, the average $\Delta F/F$ of ~200 ms (6 frames) before stimulus onset

was used as the noise distribution and 6 frames after stimulus (including the stimulus frame) as the signal distribution. These distributions were used to calculate ROC curves and the area under these curves (AUROCs). A random permutation test was performed to determine statistical significance of detection performance ($p < 0.05$).

2.4 Results

To determine the response profile of L2/3 neurons to sensory stimulation, we performed whole-cell recording (n = 20), cell-attached recording (n = 20) and two-photon calcium imaging (n=44 sessions; n=1640 cells) in vS1 cortex of urethane-anesthetized mice. We quantified the synaptic response and spiking profile of L2/3 neurons to 11 "standard" deflections (amplitudes; 0-2.8 degrees, peak velocities; 0-1.2 degree/ms) as well as a "sharp" deflection (amplitude; 3.6 degrees, peak velocity; 3.8 degree/ms) that falls in the range of high-velocity events that occur when whiskers interact with objects and textures. Figure 2.1*A* illustrates the experimental set-up, the stimulus parameters and the corresponding local field potentials (LFPs) measured on a dye injecting pipette. The peak velocity of the standard stimuli linearly increased with the peak amplitude (Figure 2.1*B*, black). The sharp stimulus had a peak velocity more than 3 times higher than that of the fastest standard stimulus (Figure 2.1*B*, green; Figure 2.1*C*). The amplitude of the evoked LFPs increased systematically with deflection amplitude. The sharp stimulus produced a prominent LFP with an average amplitude that was ~2.5 times larger than that evoked by the fastest standard stimulus (25 trials, Figure 2.1*D*).

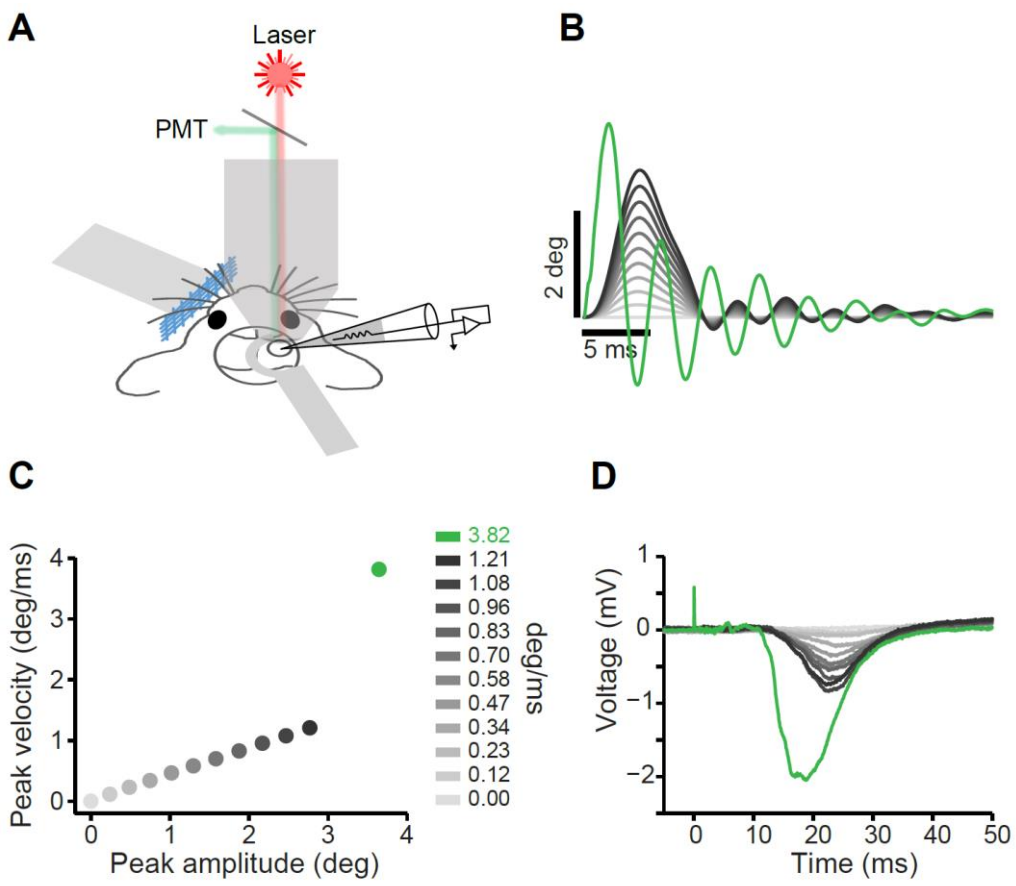

Figure 2.1*: Experimental set-up and stimulus properties.*

A*: Schematic illustration of the experimental set-up.* ***B****: Average position profile of the piezo movement (100 trials per each stimulus). This color convention (grayscale for the standard and green for the sharp stimulus) is used in all figures.* ***C****: Peak velocity of the piezo movement is plotted against peak amplitude. Every dot represents one stimulus* ***D****: Example evoked LFPs averaged across 25 trials per stimulus.*

2.4.1 Synaptic response in L2/3 cells

We recorded membrane potential (V_m) of 20 neurons in L2/3 of vS1 cortex (104-256 μm below dura, 4 mice) along with multi-whisker stimulation. The standard stimuli evoked a quick depolarization followed by a longer hyperpolarization and a second delayed depolarization (Figure 2.2*A*&*B*). The sharp stimulus evoked a considerably larger depolarization compared to the standard stimuli. We quantified maximum depolarization by the peak value of the evoked PSPs. Figure 2.2*C* plots the average peak-PSP over trials and then over neurons. As the lowest stimulus amplitude was set to zero, peak-PSP for this stimulus represents the magnitude of spontaneous PSPs (3.8 mV above average V_m; Figure 2.2*C*; lightest gray). The peak-PSP increased with stimulus amplitude and reached an average 9.1 mV above the spontaneous peaks for the fastest standard stimulus (Figure 2.2*C*). The peak-PSP for the sharp stimulus was 4.6 mV more depolarized than that of the fastest standard stimulus (Figure 2.2*C*, green, $p = 0.036$, Wilcoxon rank sum test). The latency of the peak-PSP systematically decreased as the stimulus velocity increased (Figure 2.2*D*, gray): on average, the peak-PSP evoked by the sharp stimulus (Figure 2.2*D*, green) occurred 7.3 ms earlier than that of the fastest standard stimulus ($p < 0.001$, Wilcoxon rank sum test).

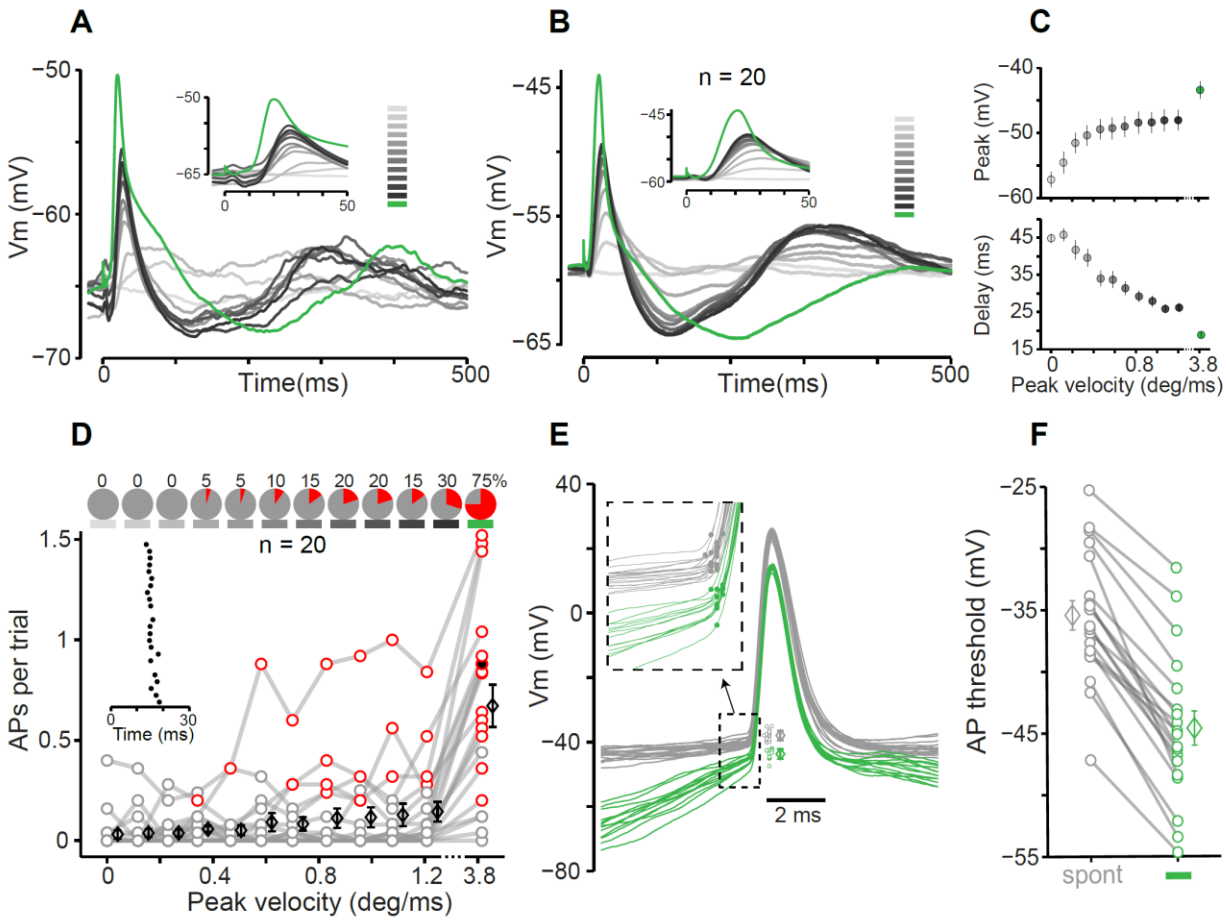

Figure 2.2*: Synaptic responses in L2/3 neurons.*

A*: Average PSPs of an example neuron is plotted versus time from the stimulus onset (25 trials per stimulus). The inset shows an expanded view of the first 50 ms.* ***B****: Average PSPs across 20 neurons.* ***C****: Top, peak of PSP is averaged over trials and then over neurons (Mean ± SEM over neurons). Bottom; delay of the peak PSP averaged over trials and then over neurons (Mean ± SEM over neurons). Note that in both panels (and subsequent figures), x-axis is broken beyond 1.2.* ***D****: AP per trial versus stimulus peak velocity for whole-cell recordings (circles). Red circles represent significant response based on ROC analysis. Average AP per trial across 20 cells is slightly shifted rightward and plotted as black diamonds (Mean ± SEM). The inset raster plot*

represents spikes in response to the sharp stimulus for an example neuron-stimulus pair (25 trials, filled circle). Pie charts represent fraction of significantly responsive neurons for each stimulus. ***E****: Spontaneous (grey) and sharp stimulus evoked APs of an example neuron. Individual AP thresholds are shifted to the right for better visibility and are plotted along with their mean and standard deviation. The inset represents an expanded view of the initial segment of the AP waveforms (box). The dots on each expanded waveform represent the position of the peak of the second derivative, representing the AP threshold.* ***F****: AP thresholds across 20 neurons for sharp stimulus evoked (green) and spontaneous (grey) spikes. Each line represents a neuron and diamonds are Mean ± SEM.*

2.4.2 Spiking response in L2/3 cells

The whole-cell recordings revealed that the probability of spiking in response to the sharp stimulus was 0.67 AP per trial which was ~5 times higher than that of the fastest standard stimulus (0.14 AP per trial). The sharp stimulus was reliably encoded in the spiking activity of 15 out of 20 patched neurons (Figure 2.2*D*, $p < 0.05$, ROC analysis random permutation test). APs exhibited a precise timing relative to the onset of the sharp stimulus: mean AP latency was 15.6 ms with 1.3 ms jitter (standard deviation across trials) for the example neuron (Figure 2.2*D*, inset). We also observed a consistently lower action potential threshold for the spikes evoked by the sharp stimulus compared to the spontaneous spikes. Figure 2.2*E* shows an example recording where the threshold of the spikes evoked by the sharp stimulus was on average 5.7 mV more hyperpolarized than that of the spontaneous spikes ($p < 0.001$; Wilcoxon rank sum test). Across 20 neurons, the threshold of the spikes evoked by the sharp stimulus was on average 9.2 mV more hyperpolarized than that of the spontaneous APs (Figure 2.2*F*, $p < 0.001$; Wilcoxon rank sum test). Despite applying an inclusion criterion for whole cell recording based on resting

membrane potential and overshooting APs (see Methods), a small number of neurons showed action potential thresholds above -30 mV (Figure 2.2 *F*), that were higher than what is typically reported (Crochet et al. 2011). Excluding those cells did not affect the main finding: the sharp stimulus showed a lower AP threshold compared to the spontaneous spikes ($p < 0.001$; Wilcoxon rank sum test, n = 15). We also calculated the threshold for rare spikes generated by the standard stimuli. Although a full quantification was not possible due to low number of evoked spikes, the threshold in the case of standard stimuli was higher than that of spikes evoked by the sharp stimulus. Figure 2.2*E* also revealed a systematic difference in the membrane potential preceding the APs, which was higher for the spontaneous spikes compared to those evoked by the sharp stimulus. To verify whether this finding generalized across neurons, we calculated the average membrane potential value during the 5-10 -ms window preceding the AP threshold. This analysis revealed an average 19.4 mV difference which was statistically significant across neurons ($p < 0.001$, Wilcoxon rank sum test, n = 20). This observation is consistent with state-dependent spiking previously reported in vS1 (Petersen et al. 2003; Sachdev et al. 2004).

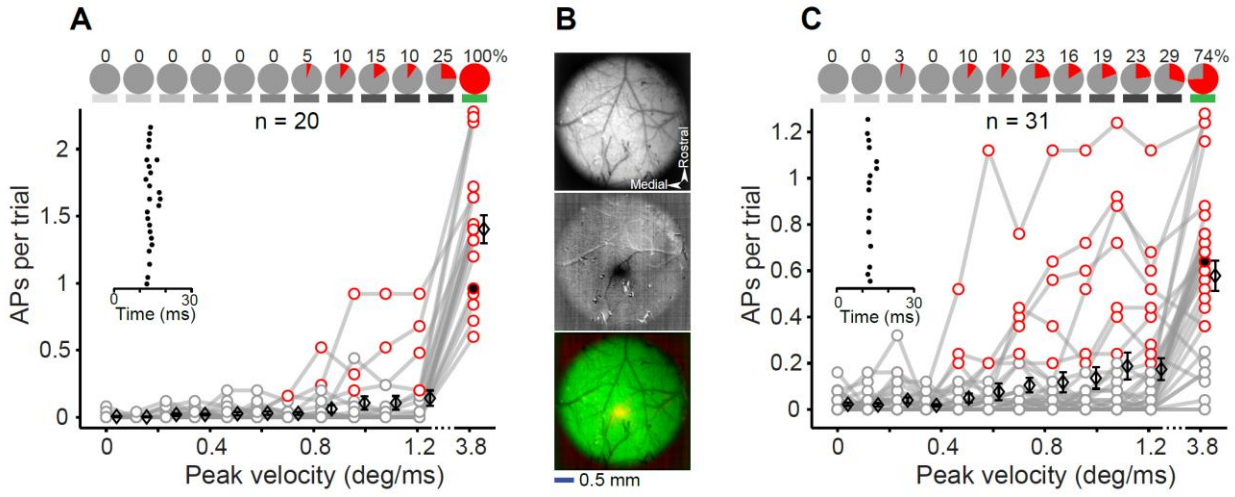

***Figure 2.3**: Spiking responses for cell-attached recordings*

***A**: Spiking responses evoked by multi-whisker deflections (details as in Figure 2.2D).* ***B**: Intrinsic signal optical imaging through intact skull. Top: vasculature pattern imaged using 527 nm light. Middle: intrinsic signal (dark spot) captured by whisker deflections under 626 nm light. Bottom: merge of top (green) and middle (red) panels.* ***C**: Spiking responses evoked by C2 whisker deflections (details as in Figure 2.2D).*

In the next step, we recorded spiking activity of 20 L2/3 neurons (142-400 µm, 5 mice) without breaking into the cell (cell-attached method). These recordings replicated the transition from a low to a high probability of spiking observed in the whole-cell experiments; the average AP per trial was more than 10 times higher for the sharp stimulus compared to the fastest standard stimulus (1.5 versus 0.14 AP per trial) and all of the recorded neurons were significantly responsive to the sharp stimulus (Figure 2.3*A*). To test whether such high spiking probability was due to the simultaneous stimulation of multiple whiskers, we repeated the experiments with single whisker deflections. Barrel C2 was localized using intrinsic signal optical imaging (Figure 2.3*B*) and cell-attached recordings were targeted to the center of the activated area. Here, the average response to the sharp stimulus was 0.58 AP per trial, 3.4 times higher than that of the fastest standard stimulus (0.17 AP per trial) and the majority of neurons (74%) were significantly responsive to the sharp stimulus (n = 31, 152-400 µm below dura, 4 mice, Figure 2.3*C*).

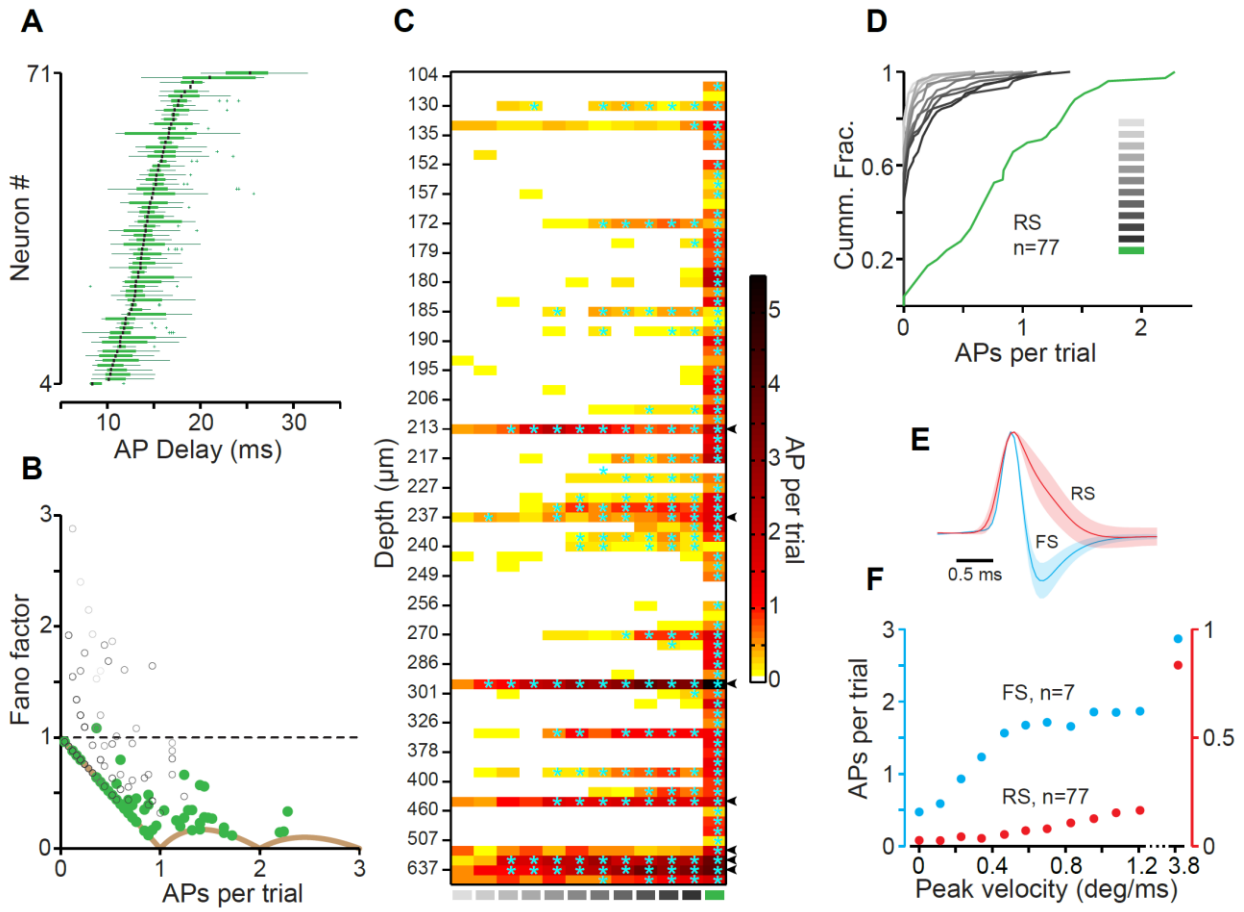

***Figure 2.4**: Properties of the spiking responses across all neurons*

***A**: Box and whisker plot representing spike time variation about median (black lines) in response to the sharp stimulus. **B**: Fano factor versus APs per trial (75ms). Colour-code of the circles is retained from Figure 2.1B. Solid brown curve represents the theoretical minimum Fano factor. **C**: color plot representing APs per trial (color-coded) versus stimulus intensity (x-axis) versus depth (y-axis) across 84 neurons including all previous neurons from figures 2.2 and 2.3 (71), 7 fast spiking neurons and 6 deep neurons (> 400 µm). Significant responses are marked with cyan asterisks and arrowheads on the right indicate fast spiking (FS) neurons. **D**: Cumulative distribution of response across all 77 regular spiking (RS) neurons color-coded for different*

stimuli as in Figure 2.1B. ***E****: cell-attached spike waveforms of RS (red, n = 19) and FS (blue) neurons (Mean ± SD).* ***F****: Average response of FS (blue, left y-axis) and RS (red, right y-axis, n = 77) neurons versus stimulus intensity.*

Next we pooled the whole-cell and cell-attached recordings to characterize trial-to-trial variability of the spike times (box and whisker plots in Figure 2.4*A*). For neurons that fired a minimum of 2 spikes (n = 66) the average interquartile range of spike times (boxes in Figure 2.4*A*) was 2.6 ± 1.5 ms (mean ± SD). For the fastest standard stimulus the interquartile range was 4.2 ± 3.1 ms (n = 28). Average spike latency was 14.6 ± 2.4 ms (mean ± SD, median = 14.1 ms) ranging from 9.0 to 20.3 ms (Figure 2.4*A*; n = 68). The standard deviation of spike times across trials provides another measure of spike time variability or jitter: for the sharp stimulus this measure was 1.7 ± 0.7 ms (mean ± SD, median = 1.7 ms, n = 66) ranging from 0.6 to 5.6 ms. In order to quantify variability in neuronal response across trials, we calculated the spike count Fano factors (Figure 2.4*B*). The evoked response to the sharp stimulus produced Fano factors close to the theoretical minimum (brown curve in Figure 2.4*B*; for the sharp stimulus, 58% of neurons were on this curve).

The preceding analyses only included regular spiking (RS) neurons recorded from L2/3 cortex. Figure 2.4*C* plots the spontaneous and evoked spike rates for all L2/3 neurons (regular and fast spiking) as well as those recorded from deeper layers (>400 μm) after sorting the neurons based on their depth (n = 83). Figure 2.4*D* plots a cumulative distribution of the response of the regular spiking neurons revealing reliable spiking to the sharp stimulus (green) at the population level. A total of 7 fast spiking neurons were identified by their narrow spikes in cell-attached recordings (FS: 0.46 ± 0.032 ms, n = 7, RS: 1.23 ± 0.39 ms, n = 19, Mean ± SD, Figure 2.4*E*). FS neurons exhibited higher spontaneous (FS: 0.47 ± 0.16 AP per trial, RS: 0.026 ± 0.085, $p < 0.001$) and

evoked spike rates (Figure 2.4*F*, sharp stimulus; FS: 2.87 ± 1.42 AP per trial, RS: 0.83 ± 0.55, $p < 0.001$, Wilcoxon rank sum). FS neurons were also highly responsive to the standard stimuli (Figure 2.4*F*): e.g. a stimulus with peak velocity as low as 0.47 degree/ms evoked significant spiking response in 6 out of 7 neurons ($p < 0.05$, ROC analysis followed by permutation test).

Finally, we employed two-photon calcium imaging to further establish the response profile of L2/3 neurons at the population level (Figure 2.5*A*&*B*). Consistent with the electrophysiological data, we found that across 44 imaging sessions from 8 mice, 1574 out of 1640 neurons (96%) produced a significant response to the sharp stimulus (i.e. AUROC values that were significantly above 0.5; permutation test, $p < 0.05$). The fastest standard stimulus, on the other hand, induced a statistically significant evoked activity in 647 out of 1640 neurons (39%, Figure 2.5*D*). Figure 2.5*E* provides a criterion-free illustration of changes in sparseness by plotting the cumulative distribution of AUROC values generated in response to the sharp stimulus (green) and to all other stimuli (gray). Across sessions, average $\Delta F/F$ evoked by the sharp stimulus was more than three times higher than that of the fastest standard stimulus (0.1745 versus 0.0553, $p < 0.001$, Wilcoxon rank sum test, Figure 2.5*F*). Altogether, our electrophysiological and imaging data demonstrate a transition from sparse to "dense" L2/3 population activity with sharp, high-velocity vibrissal stimulation.

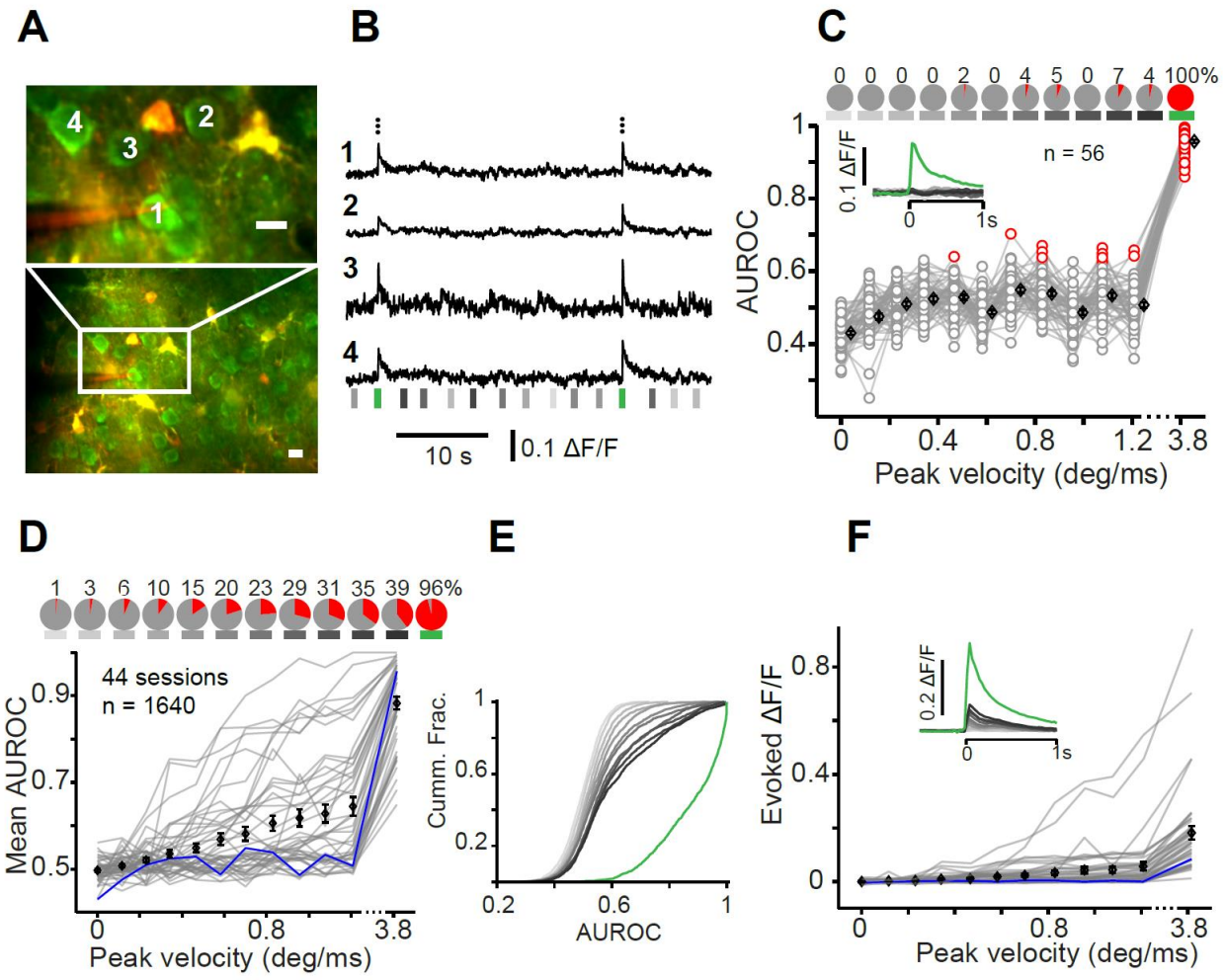

***Figure 2.5**: Calcium imaging from L2/3 of vS1*

***A**: Imaging field with green and red channels overlaid. Top panel is the outlined area at the bottom, recorded with higher magnification (scale bars are 10 µm). Neuron #1 is targeted for simultaneous cell-attached recording. **B**: Example ΔF/F of four neurons labelled in panel **A**. Black dots on top represent cell-attached spikes of neuron #1. Subsequent spikes occurring in the same frame are shown above the previous. Vertical lines represent stimuli, colour-coded as of convention. **C**: An example session where area under ROC curve (AUROC) is plotted versus stimulus velocity (n = 56). Red dots represent significant detection performance ($p < 0.05$). Pie*

charts on the top, represents fraction of neurons (in percent, n = 56) with significant response. The inset shows average peri-stimulus (at zero) ΔF/F over trials, over neurons. ***D****: Average AUROC for each session (grey plots, 44 sessions). The average AUROC of the example session in C is plotted in blue. Pie charts on top shows the fraction of all imaged neurons with significant response.* ***E****: Cumulative distribution of AUROCs across 1640 imaged cells color-coded for different stimuli as in Figure 2.1B.* ***F****: Average of the evoked ΔF/F (baseline subtracted) for each session (grey plots). The inset is peri-stimulus ΔF/F averaged over all sessions. Black diamonds in all panels represent mean ± SEM.*

2.5 Discussion

Sparse, distributed coding is a well-known property of the rodent sensory cortex (Shoham et al. 2006; Barth and Poulet 2012; Harris and Mrsic-Flogel 2013; Petersen and Crochet 2013). The sparse neuronal activation is well-documented in the supra-granular layers (L2/3) of the vS1 cortex during both active and passive stimulation of the vibrissae in awake or anesthetized preparations (Brecht et al. 2003; de Kock et al. 2007; Kerr et al. 2007; O'Connor et al. 2010b; Petersen and Crochet 2013; Ramirez et al. 2014; Clancy et al. 2015; Peron et al. 2015b). However, the functional relevance of sparse activity remains unknown (Barth and Poulet 2012; Spanne and Jörntell 2015). Here, we found that the choice of stimulus affects the extent of sparseness in L2/3 neurons and a dense population response is evoked by high-velocity micro-motions applied to whiskers.

We measured synaptic and spiking responses in L2/3 of vS1 cortex of urethane anaesthetized mice. All recorded neurons received the sensory signal: standard deflections evoked a PSP with an early, brief depolarization followed by a prolonged hyperpolarization and a delayed slow depolarization as observed previously (Carvell and Simons 1988; Zhu and Connors 1999; Sachdev et al. 2004). As reported previously, synaptic responses increased with the peak angular velocity of the stimulus (Wilent and Contreras 2004). However, we found that synaptic responses tended to plateau at around 0.4 degree/ms for the standard range of stimulation and often did not evoke spiking activity (Figure 2.2*C*). The sharp stimulus, on the other hand, evoked reliable spiking in the majority of neurons. These spikes had a significantly lower action potential threshold compared to those generated during the spontaneous activity (Figure 2.2*E*&*F*). The transition from sparse activation to high-probability spiking response was further confirmed in the cell-attached recordings, as well as in calcium imaging, despite its limitation in

single spike detection (Sato et al. 2007; Clancy et al. 2015) and potential neuropil contamination (Kerr et al. 2005) which can cause false detection of spiking activity in the imaging data. Finally, we demonstrated that deflection of a single whisker with the sharp stimulus was sufficient to evoke reliable spiking in a majority of L2/3 neurons in the corresponding barrel (Figure 2.3*C*).

Sparse coding might be due to the energy constraints over spiking activity (Lennie 2003) and is known to present several advantages for cortical computation (Olshausen and Field 2004; Barth and Poulet 2012; Harris and Mrsic-Flogel 2013). The term "sparseness" may refer to a number of different scenarios: (i) the overall rate of spiking (Shoham et al. 2006), (ii) the number of spikes a single neuron fires in response to a stimulus (DeWeese et al. 2003; Jadhav et al. 2009; Ramirez et al. 2014), (iii) the fraction of active cells in a neuronal population (Rolls and Tovee 1995; Wolfe et al. 2010; Barth and Poulet 2012) or (iv) the selectivity of neurons to the stimulus space – being responsive only to the "grandmother" stimulus (Barlow 1972; Quian Quiroga et al. 2008). Here, we quantified sparseness as the fraction of neurons that produced a statistically significant response to a certain stimulus based on an ROC analysis. Furthermore, the cumulative distributions of evoked responses provided a criterion-free demonstration of sparseness both for the electrophysiological (Figure 2.4*D*) and the imaging data (Figure 2.5*E*) which were comparable with those reported earlier (O'Connor et al. 2010b; Clancy et al. 2015).

Previous literature identified velocity as the effective stimulus feature in driving vS1 neurons (Simons 1978; Ito 1981, 1985; Pinto et al. 2000; Arabzadeh et al. 2003, 2004; Boloori et al. 2010; Gerdjikov et al. 2010). Our hypothesis was that most L2/3 neurons may be preserved for coding of high-velocity events that occur in object/texture palpation but remain silent for the standard range of velocities. This scenario would increase the capacity to encode distinct high-velocity events at the population level and enhance the overall perceptual capacity by expanding

the dynamic range of population responses (Pouille et al. 2009; Elstrott et al. 2014; Spanne and Jörntell 2015). Sparseness may also arise from selectivity of neurons to specific features of the stimulus space such as directional tuning (Simons 1985; Lee and Simons 2004; Andermann and Moore 2006). As another example, in behaving animals whisking and touch can be represented by distinct and spatially intermixed populations of neurons (Peron et al. 2015b). It is therefore possible that strong selectivity of L2/3 neurons preserves them for encoding additional stimulus features or task variables in awake animals (Chen et al. 2013).

Behavioral studies show that whisker velocities can reach as high as 10 degree/ms (O'Connor et al. 2010a; Bale et al. 2015). However, neuronal and behavioral detection thresholds reveal that rats can detect stimuli with velocities much slower than the fastest standard stimulus used here (Adibi et al. 2012; Ollerenshaw et al. 2012, 2014; Lee et al. 2016). Such low detection thresholds are compatible with the motor strategy of the animals to gently palpate obstacles during exploration (Mitchinson et al. 2007). On the other hand, animals might use different whisking strategies depending on the behavioral task. For example, high velocity micro-motions are widely reported in texture discrimination tasks (Ritt et al. 2008; Wolfe et al. 2008; Jadhav and Feldman 2010) and object palpation (O'Connor et al. 2010a; Bale et al. 2015). Although mice use a broad range of whisker velocities in object localization and palpation (O'Connor et al. 2010a; Bale et al. 2015), it is not clear whether the high-velocity slip events contribute to neuronal and behavioral performances in such tasks (O'Connor et al. 2010a, 2010b). In texture discrimination tasks, slip events with fast kinetics provide a neuronal signature to distinguish between various textures (Diamond et al. 2008b; Ritt et al. 2008; Wolfe et al. 2008; Jadhav et al. 2009; Jadhav and Feldman 2010). The high-velocity events evoke precisely timed spikes in the first-order neurons in the trigeminal ganglion (Lichtenstein et al. 1990; Arabzadeh et al. 2005;

Bale et al. 2015) and in the vS1 (Arabzadeh et al. 2006; Jadhav et al. 2009). Our data suggests that dense activation of L2/3 may contribute to coding of object surface properties by highlighting the slip events critical for such discriminations (Wolfe et al. 2008; Jadhav et al. 2009; Jadhav and Feldman 2010).

High-velocity whisker stimulations such as that of the sharp stimulus employed here are not commonly used in anesthetized preparations (but see Arabzadeh et al. 2005 and Bale et al. 2015). However, a broad range of angular movements and velocities are found in behaving mice (O'Connor et al. 2010a; Bale et al. 2015) and rats (Carvell and Simons 1990; Ritt et al. 2008; Wolfe et al. 2008; Jadhav et al. 2009). Bale and colleagues found that during object palpation the high-velocity events had a median of 6.6 degree/ms (Bale et al. 2015). They therefore delivered a high-velocity "ping stimulus" by a piezoelectric actuator in order to explore temporal precision of the spikes in trigeminal ganglion (Bale et al. 2015). Intense ringing is a characteristic of such ultrafast deflections (Bale et al. 2015) as it is the case for our sharp, high-velocity deflection (Figure 2.1*B*). The contribution of the resonation of the sharp stimulus to generation of the dense response of L2/3 cannot be ruled out in our study. However, whisker resonations following high-velocity events are observed in behaving mice (see supplementary figure 6 in O'Connor et al. 2010a) and rats (Ritt et al. 2008; Jadhav et al. 2009; Lottem and Azouz 2009). Although, the velocity of the sharp stimulus presented in our study falls in the range of the salient high-velocity events observed in natural whisker object interactions, the mechanical properties are not necessarily the same. Future experiments could quantify the response of L2/3 neurons to the high-velocity slip events in behaving animals.

In our whole-cell recordings, the action potential threshold was significantly decreased by the sharp stimulus (Figure 2.2*E*&*F*). This is consistent with earlier studies reporting highly variable

AP thresholds *in vivo* (Azouz and Gray 1999, 2000; Henze and Buzsáki 2001). This variability can provide a mechanism for stimulus selectivity (Anderson et al. 2000b; Azouz and Gray 2003; Sachdev et al. 2004; Wilent and Contreras 2005b). In particular, the action potential threshold correlates with the rate of rise in the membrane potential immediately before the threshold (Anderson et al. 2000b; Azouz and Gray 2003; Poulet and Petersen 2008). VS1 neurons are found to have a higher probability of spiking during the down state (Petersen et al. 2003; Sachdev et al. 2004). The effect of state on spiking was also present in our data, where action potentials evoked by the sharp stimulus tended to occur in the down state (Figure 2.2*E*). On the other, the spontaneous spikes were less likely to occur during the down state; hence they are preceded by a higher membrane potential corresponding to the up state (Figure 2.2*E*). In the down state, the highly synchronous excitatory input (Azouz and Gray 2000) from L4 that is evoked by the sharp stimulus can raise the membrane potential at a high rate and thus produce spiking at the observed lower AP threshold. Although, the contribution of the action potential threshold modulation to cortical computation is not entirely clear (Yu et al. 2008), our results indicate that regulation of spike threshold along with the modulation of excitatory and inhibitory currents (Wilent and Contreras 2005a; Cohen-Kashi Malina et al. 2013) may play a role in selective spiking of L2/3 neurons. To confirm, this requires measurement and comparison of the membrane potential and synaptic currents in anesthetized, awake and actively behaving animals since the balance of the synaptic currents can vary with the brain state (Haider et al. 2013; Taub et al. 2013).

Previous studies have established that the balance between excitation and inhibition sets the synaptic reversal potential below the action potential threshold for the majority of L2/3 pyramidal neurons (Crochet et al. 2011). To generate evoked spikes, the synaptic reversal

potential must exceed the action potential threshold. Our results suggest that following a high-velocity stimulation, a synchronous input drives a fast increase in the neurons' membrane potential, which may be sufficient to reach a supra-threshold potential before di-synaptic inhibition arrives. Our whole-cell experiment suggests that synchronous input also reduces the action potential threshold by a fast rise in membrane potential, which guarantees the firing of action potential before overwhelming inhibitory input arrives. In summary, following the sharp stimulus, a brief window of opportunity is opened by a "synchrony filter" which promotes action potential at a lower threshold.

Another advantage of the synchronous excitatory input to a sparsely active network is reliability of response across trials. Accumulating evidence suggests that cortical neurons can process the sensory input with high trial-to-trial fidelity both in terms of spike count and spike timing (DeWeese et al. 2003; Baudot et al. 2013; Hires et al. 2015). The trial-to-trial variability can be stimulus dependent: in response to the sharp stimulus, we observed lower temporal variability compared to earlier recordings in the supra-granular layers (L2/3) of the vS1 (Brumberg et al. 1999; Ahissar et al. 2001; Glazewski and Barth 2015). Furthermore, the high-velocity whisker stimulus excited L2/3 neurons with minimal spike count variability, suggesting a binary process as observed in L4 barrel (Hires et al. 2015), auditory (DeWeese et al. 2003) and visual cortex (Baudot et al. 2013). These findings indicate that the supra-granular coding of the whisker stimuli can be robust and highly reliable. Strong inhibition in L2/3 of the vS1 (Xu and Callaway 2009; Crochet et al. 2011) seems to contribute to such reliable coding. The inhibition dampens the spontaneous fluctuations and the evoked response to the weak inputs (Pinto et al. 2003) to preserve the precisely timed spiking of silent neurons for the more prominent events during whisker-object interactions. On such a low background activity, a flash of driven response in a

population of neurons is a salient signal that can reliably encode the time, frequency and magnitude of events during sweeps of whiskers across surfaces.

The laminar organization of the vS1 suggests distinct information processing across cortical layers (Petersen and Crochet 2013). Unlike infragranular layers which mainly project to the subcortical targets, L2/3 neurons make prominent connections with higher cortical areas such as the secondary vibrissal cortex (vS2) and the primary motor cortex (Chen et al. 2013). This positions the L2/3 neurons at the core of the whisker mediated decision process (Kwon et al. 2016). It is therefore surprising that the majority of neurons in this layer remain silent during sensory processing (O'Connor et al. 2010b; Petersen and Crochet 2013; Clancy et al. 2015; Peron et al. 2015b). Consistently (Crochet et al. 2011; Sachidhanandam et al. 2013), we found that L2/3 neurons elicit synaptic responses with a high sensitivity, reflecting a strong connection with L4 which is the primary recepient of the sensory signal in vS1. The overall profile of the PSPs (Figure 2.4*C*, top, gray) also reflects the nonlinearities observed in stimulus-response funcions in L4 vS1 (Adibi and Arabzadeh 2011) and may reflect a probabilistic nature of cortical activation (Gollnick et al. 2016). Despite a prominent functional connection with L4 (Lefort et al. 2009), rapid recruitement of inhibitory neurons precludes spiking response in a majority of excitatory L2/3 neurons (Petersen and Crochet 2013). In our data, we were able to distinguish a fraction of neurons as fast-spiking cells. Unlike regular-spiking neurons, these cells were highly responsive to the standard stimuli (Figure 2.4*F*) suggesting that they may have a role in blocking action potential in L2/3 regular-spiking neurons (Xu and Callaway 2009; Crochet et al. 2011). The sharp stimulus on the other hand revealed a transition from sparse to dense activity in the population of L2/3 neurons. This transition could be attributed to a number of cellular and cuircuit mechanisms such as (1) the modulation of AP thershold, (2) the increased synchrony of

the excitatory input from thalamus to L4 (Wang et al. 2010) which can propagate from L4 to the L2/3 (Jadhav et al. 2009; Bruno 2011) due to the sharp event and (3) the temporal modulation of inhibition/excitation. The interplay of these mechanisms may provide additional coding capabilities for L2/3 circuits involved in perception of ecologically relevant stimuli. It is also possible that the sharp stimulus recruits additional pathways, such as POm-paralemniscal pathway. This pathway is known to potentiate L2/3 neuronal responses (Gambino et al. 2014). However we did not observe long-latency spikes as predicted by plateau potentials in L2/3 neurons following repetitive, 8 Hz whisker stimulation (Gambino et al. 2014). This could be due to the low frequency of our stimuli (0.5 Hz).

In summary, we found that sparse spiking response in L2/3 of vS1 critically depends on sensory input and a "dense" population response can be evoked by a sharp high-velocity whisker deflection. Given the low trial-to-trial variability, this strong signal can effectively convey sensory information to downstream targets of L2/3 such as the secondary somatosensory cortex or the motor and pre-motor areas. Moreover, the transition from sparse to dense spiking implies a high capacity in population of L2/3 neurons for encoding a broad range of stimuli and may serve as an intrinsic mechanism to enhance stimulus discrimination rather than detection (Ollerenshaw et al. 2014; Waiblinger et al. 2015). These results motivate further investigation of sparse and dense coding in awake and behaving animals as well as an investigation of the cellular and circuit mechanisms involved in stimulus dependent spike generation in L2/3 neurons.

Chapter 3: Diverse tuning underlies sparse activity in L2/3 vibrissal cortex of awake mice

3.1 Abstract

Reliable perception of objects requires efficient representation of the elementary and complex features in the sensory cortex. Despite a large body of knowledge regarding sensory coding in the rodent somatosensory cortex, it is not clear how elementary and combined features are represented in this area. It is known that superficial layers of the somatosensory cortex represent stimuli in a sparse manner, whereby a large fraction of neurons are insufficiently driven by the feedforward sensory inputs to evoke action potentials and therefore cannot contribute to sensory coding. However, sparseness might simply reflect these neurons' tuning to unknown or higher-level complex features which are not sufficiently explored in the stimulus space. Here, we apply a range of vibrotactile and manual vibrissal stimuli in awake, head-fixed mice while performing loose-seal cell-attached recordings from the vibrissal primary somatosensory (vS1) cortex. Consistent with sparse coding, stimuli delivered by a piezo-electric actuator evoked significant response in a small fraction of regular spiking supragranular neurons (16%-29%). However, we observed that a majority of the supragranular regular spiking neurons (84%) were driven by at least one specific feature, manually delivered to the whiskers. Our results suggest that the majority of neurons in the superficial layers of sensory cortex contribute to coding by representing a specific feature of the tactile stimulus.

3.2 Introduction

The rodent vibrissal system provides a well-described sensory pathway (Brecht 2007; Diamond and Arabzadeh 2013; Feldmeyer et al. 2013) and a suitable setting in which to study the extraction of ecologically relevant sensory information and its transfer from one stage of processing to the next. It is known that vS1 neurons encode a number of kinematic features of the whisker movement including velocity/acceleration, phase and direction (Shoykhet et al. 2000; Arabzadeh et al. 2005; Andermann and Moore 2006; Jadhav et al. 2009). Moreover, behavioral studies have found a great capacity of the rodent vibrissal system in discriminating textures, objects and object locations (Brecht et al. 1997; Jadhav and Feldman 2010; O'Connor et al. 2010a; Morita et al. 2011).

Spiking activity of single cortical neurons is key to understanding sensory perception (Barlow 1972). In a classic single unit recording experiment, Dykes and Lamour found a surprisingly high number of silent neurons in the somatosensory cortex, such that only a quarter of neurons across layers were responsive to sensory input (Dykes and Lamour 1988a, 1988b). A number of recent studies confirmed that neuronal activity is sparse, especially in the supragranular layers of vS1 such that only a small fraction (~10%) of neurons evoke action potentials in response to whisker stimulation in various experimental conditions (O'Connor et al. 2010b; Barth and Poulet 2012; Clancy et al. 2015; Peron et al. 2015b). Supragranular vS1 is highly connected to other cortical areas (Chen et al. 2015), and the reciprocal connections of vS1 with higher sensory areas seem crucial for whisker-mediated perceptual decision (Yang et al. 2015; Kwon et al. 2016). Given the key role of supragranular vS1 in cortical connectivity, it is necessary to explore functional relevance of the sparse activity in these layers.

A number of factors may lead to the observation of an apparently sparse activity in vS1 (Barth and Poulet 2012; Petersen and Crochet 2013). These include anesthesia (Greenberg et al. 2008; Vincis et al. 2012; Haider et al. 2013), cortical state (Sakata and Harris 2012), learning and habituation (Gdalyahu et al. 2012; Kato et al. 2015). Moreover, small fraction of activated neurons may be the result of using systematically weak or simplified stimuli for precise control of the stimulation parameters (Barth and Poulet 2012; Spanne and Jörntell 2015; Ranjbar-Slamloo and Arabzadeh 2017). A number of recent studies showed that a large fraction of neurons in supragranular vS1 remain silent in both anesthetized and awake conditions or with multi-whisker, spatiotemporally complex stimuli under the light anesthesia (O'Connor et al. 2010b; Crochet et al. 2011; Ramirez et al. 2014; Peron et al. 2015b; Estebanez et al. 2016). Furthermore, *in vitro* studies show that strong translaminar (L4-to-L2/3) excitatory-excitatory connections are rare (Lefort et al. 2009) and weaker than excitatory-inhibitory connections (Helmstaedter et al. 2008). Therefore only those neurons which receive stronger excitatory input or weaker inhibition can be driven by the sensory input (Crochet et al. 2011; Petersen and Crochet 2013; Elstrott et al. 2014). These observations strengthen the hypothesis that in L2/3 of vS1 a small and stable fraction of neurons represent whisker movements while the remaining majority do not directly contribute to sensory coding (Barth and Poulet 2012; Ramirez et al. 2014). On the other hand, the presence of high-amplitude post-synaptic potentials in most L2/3 neurons (Moore and Nelson 1998; Crochet and Petersen 2006; Poulet and Petersen 2008; Crochet et al. 2011; Ranjbar-Slamloo and Arabzadeh 2017) and their selectivity of tuning properties (Andermann and Moore 2006; Kremer et al. 2011; Estebanez et al. 2016) imply that strong feature selectivity may underlie the sparse coding in vS1, similar to other sensory areas such as the visual and auditory cortex (Petersen and Crochet 2013).

Certain gating mechanisms may still allow the silent vS1 neurons to fire in special circumstances. For example, “propagation of synchrony” from L4 to L2/3 (Bruno 2011) may evoke a large fraction of neurons which would in turn effectively communicate strong, salient stimuli to downstream targets. Our previous work showed that under anesthesia, the majority of neurons (>70%) in the supragranular vS1 evoke action potentials in response to a high-velocity “sharp” stimulus (Ranjbar-Slamloo and Arabzadeh 2017). Here, we quantify the extent of sparse coding in the vS1 cortex of awake head-fixed mice, with loose-seal cell-attached recordings in the presence of piezo controlled and manual whisker stimulation.

3.3 Methods

3.3.1 Animals and surgery

All procedures were approved by the institutional animal ethics committee. C57BL6/J were kept in individual cages and provided with ad-libitum food and water. Anesthesia was initially induced by placing the mouse in a 3% of isoflurane chamber before moving the animal to a custom made head-restraining apparatus with a face mask delivering isoflurane at a constant rate in order to maintain a stable breathing rate at ~1.5 Hz. Hind-paw and corneal reflexes were also checked to be absent. A drop of local anesthetic was injected under the scalp before the operation. A circular piece of the scalp was cut and the skull was exposed. Aseptic tools were used throughout the surgery. The connective tissue was removed from the skull. When the skull was dry, shallow, crisscrossed patterns were made on the skull by the tip of a scalpel. The skull was covered with tissue adhesive (Vetbond; 3M, St Paul, MN) except for the area above the vS1. The edges of the scalp were also glued and sealed with the tissue adhesive. A custom-made aluminum head implant was then glued to the skull and secured by dental cement. After ~40 minutes the skull was imaged using intrinsic optical imaging to map the center of the C2 barrel

(Ranjbar-Slamloo and Arabzadeh 2017). A shallow well was made around the location of the C2 barrel. Cement was applied all over the skull, except the bottom of the well (~3 mm). The animal was injected by 5mg/kg of carprofen and 0.86ml/kg of penicillin. The well was covered with silicon sealant (Kwik-Kast). The animal was then returned to its home cage for recovery. After 3 days of recovery, the habituation started. The head of the animal was fixed to a custom-made fixation bar, where the body rested in a stainless steel tube (inner diameter of 29 mm) and the head implant was secured to the fixation bar with a #3 screw. The animal was left in the apparatus for 10 min at the first day, 30 min second and 1 hour for the two last days of habituation. At fifth day, the animal was deeply anesthetized with 3% of isoflurane circulation through the face mask and the Kwik-Kast was removed. In order to reduce brain pulsations during the recording, the skull was drilled circularly (Crochet 2012) over the location of C2 intrinsic signal which was marked with a shallow drill hole during the first surgery. The center of drilling (~300 µm) was thinned to the level of the dura matter, avoiding the blood vessels. Then the cranial window was covered with Ringer's solution and Kwik-Kast. The animal was returned to the home cage for recovery.

3.3.2 Electrophysiology

After recovery from the second surgery, the head was fixed to the apparatus while the mouse rested in the tube. The Kwik-Kast was carefully removed and a drop of saline was applied to the craniotomy and covered the bottom of the well. The ground wire was anchored on the head-bar using plasticine and the exposed tip was placed in the well in contact with the saline. Before the pipette penetration, the dura was nicked with the tip of a 25-G needle. The pipette was filled with ACSF and advance into the brain diagonally. The angle and alignment of the pipette was set to target the center of C2 barrel. Placement of pipette on the brain was monitored by the stereo-

microscope. In order to identify neurons, we used two criteria; (1) the interaction of the membrane with the tip of the pipette and the subsequent increase in pipette impedance and (2) spontaneous spiking or evoked spikes by an extracellular nano-current (1-10 nA).

3.3.3 Whisker tracking and whisker stimulation

For whisker tracking, all of the whiskers were trimmed to the level of the face hairs except the C row. Whiskers were illuminated form bellow by visible light. In piezo stimulation paradigm, the principle whisker was inserted in a 30-G cannula which was attached to the piezo and was advanced to reach ~4 mm from the base of the whisker. High speed videos were captured during 1-s period around the deflection onset (0.5 s before and 0.5 s after), at 400 frames per second with a PhotonFocus camera mounted on a Leica stereomicroscope. Frame acquisition was triggered by a National Instrument board (PCIe-6321). Stimuli were generated and delivered as in (Ranjbar-Slamloo and Arabzadeh 2017). Two stimulus intensities were presented: the standard stimulus (2.8-degree amplitude and 1.2 degree/ms peak velocity) along with the sharp stimulus (3.6-degree amplitude and 3.8 degree/ms peak velocity, Figure 3.1*B*). Each stimulus was presented 25 times with a pseudorandom order and with 1.5-2.5 s inter-stimulus interval. During manual stimulations, whiskers were imaged for 60 seconds along with the electrophysiological recording. The probes which were used for manual stimulation consist of two standard hex keys of size 2.0 and 5.0 and a hex screw (A2-70, M5) to engage one or more whiskers in various directions and combinations. The direction and strength of the stimulus application was adjusted to the most recent stimulation which resulted in a spiking activity of the same or previously recorded neuron. Responsiveness was defined as repeatable spike generation aligned to at least half of the repetitions of a stimulus feature. If a specific whisker-object contact did not produce a spike within a contact epoch (>5 repetitions), a different configuration was tested. This was

repeated for all individual whiskers and then a combination of multiple whiskers where deflected together and different orientations where tested. Axial tuning was defined when the object was moving towards the base of the whisker and the face of the animal, deflecting the whisker by a contact with the tip of the whisker. Lateral motions were applied by contacting the whisker shaft and moving it in four major directions (up, down, left and right). A "push" response was assigned to a neuron when the whisker contact or slip did not generate any spikes but the spikes were fired only during large amplitude movement of the whisker. "Slip" response was assigned to a neuron when spiking occurred upon the release of the whisker after a push with the object. This often generated high-velocity events (Figure 3.6C_2). A "tap" response was defined when a large amplitude deflection or mere contact was not able to drive a response but the object had to hit the whisker with a high negative acceleration similar to a tap on a heavy object. At the end of manual probing, an air puff was applied to the whole whisker pad in rostro-caudal direction with a rubber bulb.

3.3.4 Data analysis

The electrophysiological data were analyzed as in our previous study (Ranjbar-Slamloo and Arabzadeh 2017). Briefly, the spikes were reliably isolated from artefacts using principal component analysis in MATLAB and spike counts per trial were calculated. We observed a fast whisker reflex (>20 ms delay) after piezo stimulus (Figure 3.1), which is consistent with a recently described trigeminal-facial reflexive mechanism (Bellavance et al. 2017). To isolate the piezo responses, we therefore limited the window for spike counts to 30-ms (instead of 75-ms as used previously). Average APs per trial were used to calculate sparseness. The measure of population sparseness was based on the statistical methods developed by Rolls and Tovee and

improved by Vinje and Gallant (Rolls and Tovee 1995; Vinje and Gallant 2000): $S = (1 - A)/(1 - 1/n)$ where n is the number of neurons, S is the measure of sparseness and $A = (\sum_i^n r_i/n)^2 / \sum_i^n (r_i{}^2/n)$, where r_i is the ith neuron's response and n is the number of neurons (Rolls and Tovee 1995; Vinje and Gallant 2000). Receiver Operating Characteristic, ROC, analysis followed by a permutation test was used to quantify significance of the responses to the piezo stimuli at P <0.05 (Ranjbar-Slamloo and Arabzadeh 2017).

Fast spiking (FS) neurons were identified based on their characteristic waveform as in our previous report (Ranjbar-Slamloo and Arabzadeh 2017). Because the spike waveform of FS neurons has a negative deflection following the falling edge, we calculated the peak to trough interval of spike waveforms and plotted that versus spontaneous firing rate to verify the accuracy of spike waveform classification (Figure 3.2). In cases where the negative deflection was not present in the spike waveform, the interval was measured between the peak (maximum of the spike waveform) and the last value of the waveform on the time axis. The spontaneous firing rate of each neuron was calculated in a 500-ms interval before the stimulus onset.

For whisker tracking we used an automated software (Clack et al. 2012) to calculate whisker angle and curvature. Whisker measurements were imported to MATLAB for further analysis. Average spike triggered curvature was calculated within ±85 ms from the spike time (Figure 3.9).

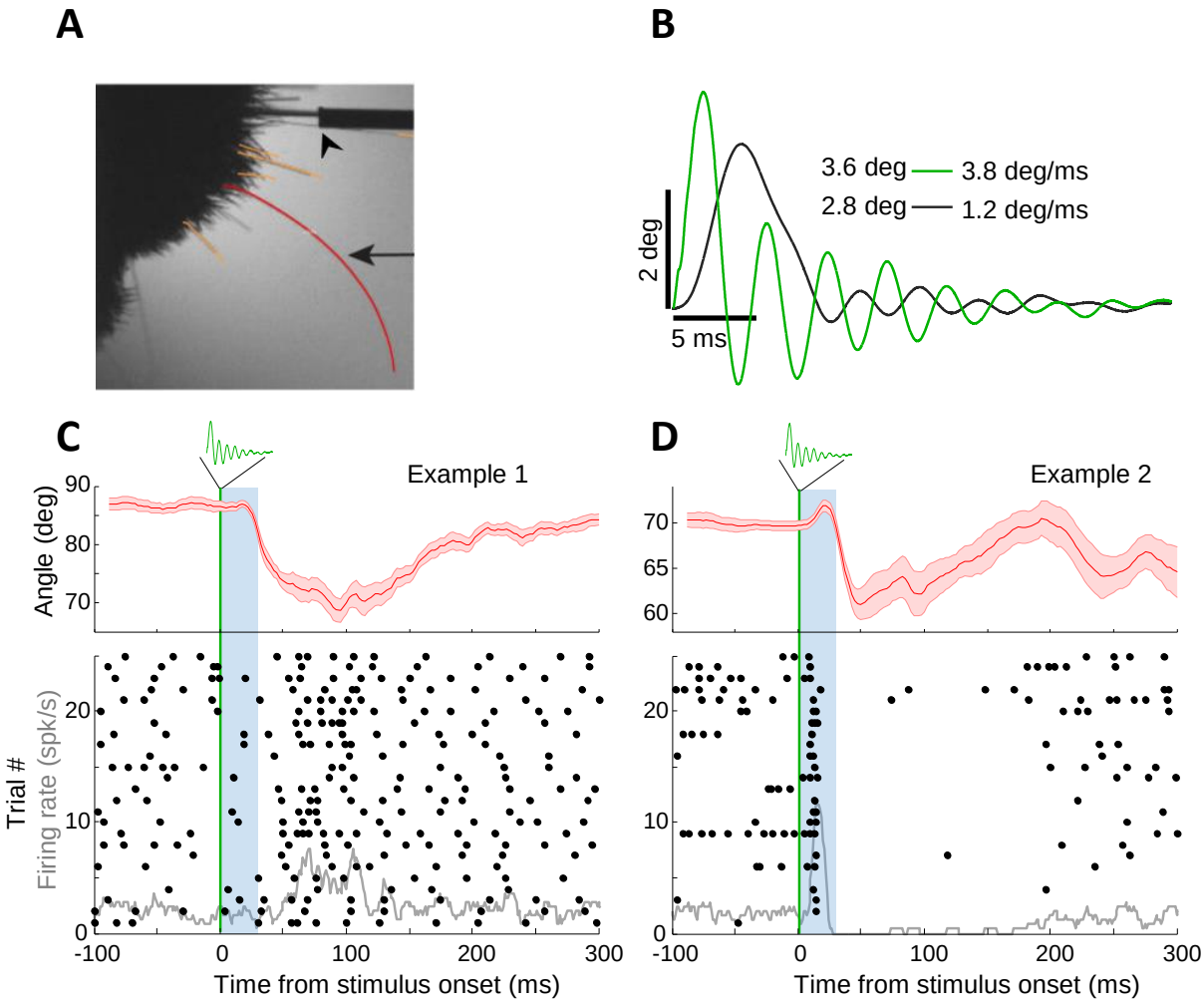

Figure 3.1*: Awake recordings with piezo stimulation*

A*: Top view of the snout showing the position of the stimulated whisker in the cannula (arrowhead). The arrow points to the tracked whisker (red).* ***B****: The profile of the piezo movement for the sharp (green) and standard (black) stimuli as measured by the optical sensor. Peak amplitude in degree (deg) and peak velocity in degree/ms (deg/ms) are reported for each stimulus.* ***C****: Top; average angle of the tracked whisker (mean ± SE) across 25 trials, aligned to the sharp stimulus onset (the vertical green line). Blue shading represents the 30-ms interval following the stimulus onset in which piezo-driven response is quantified. The inset numbers*

represent the identification numbers of the recorded neuron (neuron number: depth). Bottom; the raster plot (dots) and the overlaid peri-stimulus time histogram (PSTH, gray trace) for the recorded neuron. ***D****: Whisker angle (top) along with raster/PSTH (bottom) of a responsive neuron. Details are the same as in panel* ***C****.*

3.4 Results

3.4.1 Spiking response to piezo stimulation

We performed loose-seal cell-attached recordings in awake mice while presenting a range of whisker stimuli either applied through a piezo or by manual stimulation under high-speed whisker imaging. We first begin by characterizing the response of vS1 neurons to piezo stimulation, which included a sharp, high-velocity stimulus, (with a peak velocity of 3.8 degree/ms) and a standard single deflection stimulus (at 1.2 degree/ms) presented to the neuron's principal whisker. In the absence of anesthesia, the sharp stimulus often resulted in a bilateral reflexive movement of the whiskers (Figure 3.1*C*&*D*). We therefore limited our analysis to a 30-ms post-stimulus window to quantify the response evoked by the piezo movement eliminating any potential contamination by the reflex. The 30-ms choice of window was based on the observation that the reflex exhibited a >20 ms delay which could in turn influence the cortical activity after an additional 10 ms delay due to typical latencies (Figure 3.1*C*). The choice of window also matches our previous findings showing that the timing of the piezo-evoked spikes was mostly limited to this interval (Figure 2.4*A*).

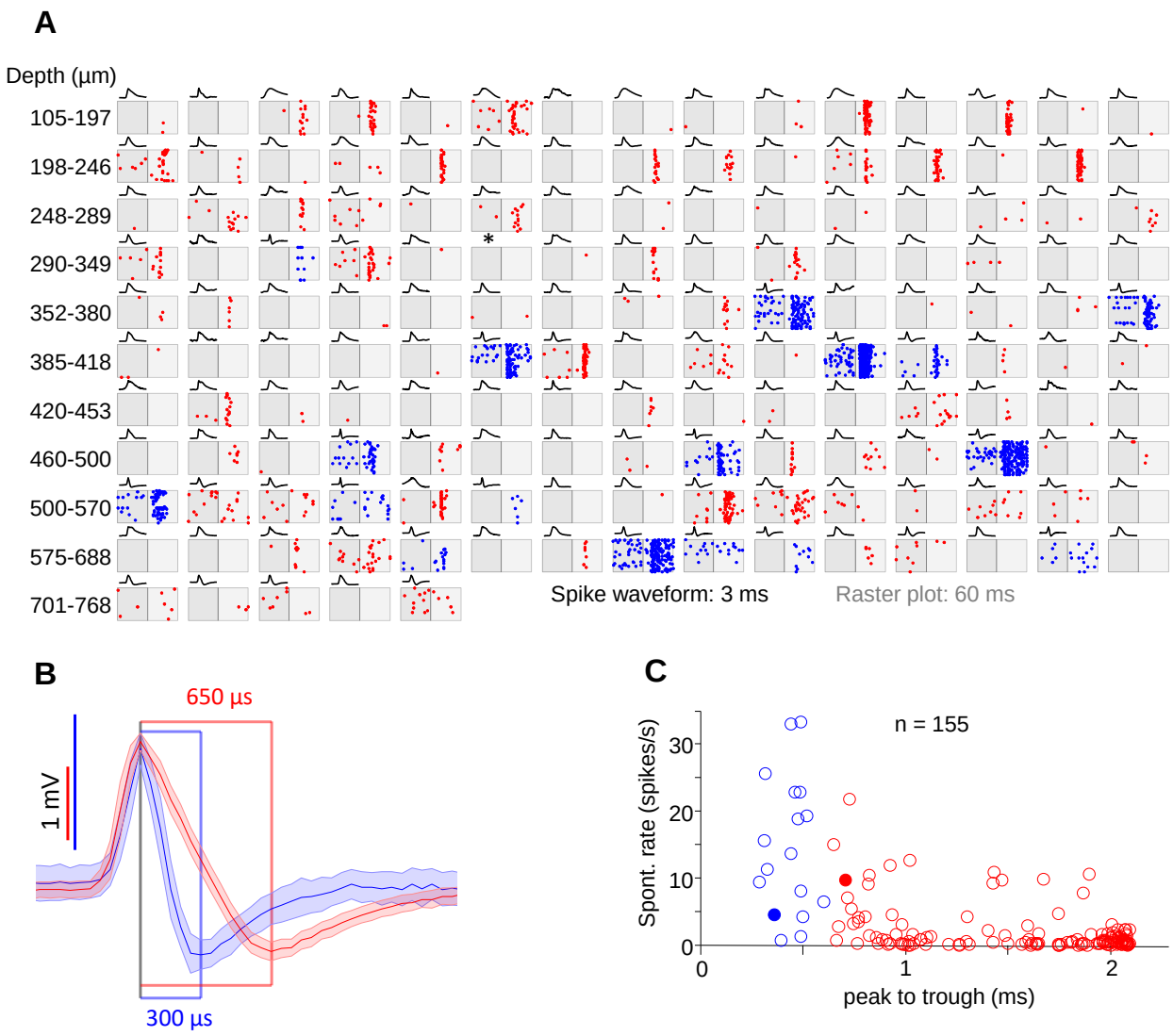

***Figure 3.2**: Response profile of 155 neurons recorded from 5 awake mice*

***A**: Subplots of raster plots sorted by the recording depth (from top-left to the bottom-right). Darker and lighter gray shades represent 30 ms before and 30 ms after the stimulus onset, respectively. Each dot represents the timing of a single spike relative to the stimulus onset (boundary between the two gray shades). Blue and red colored dots represent fast spiking (FS) and regular spiking (RS) neurons respectively. For each neuron the average spike waveform (normalized) is plotted on top of the spontaneous raster. For the neuron marked with an asterisk*

no spike occurred during the recording protocol. ***B****: Average spike waveform for two example neurons: FS (blue) and RS (red). The shaded error bands represent standard deviations.* ***C****: Scatter plot of spontaneous activity (y-axis) versus peak to trough (x-axis) of the average spike waveform for FS (blue) and RS (red) neurons. Filled circles represent example neurons in panel* ***B****.*

For the piezo-electric stimulation protocol, a total of 155 neurons were recorded from 5 mice at various depths of the vS1 cortex. Figure 3.2*A* illustrates the spike waveforms and the raster plots of these neurons. We separated fast spiking (FS) neurons from regular spiking (RS) neurons based on their spike waveforms. Figure 3.2*B&C* show that peak to trough value is consistently lower for those neurons identified as FS. Across all 155 neurons the average evoked response was 0.28 APs per trial for the standard stimulus and 0.44 APs per trial for the sharp stimulus (Figure 3.3*A*). After excluding 17 FS neurons, the average evoked response dropped to 0.13 and 0.24 APs per trial for the standard and the sharp stimuli respectively (Figure 3.3*B*). For FS neurons the corresponding average responses were 1.46 and 2.04 APs per trial (Figure 3.3*C*).

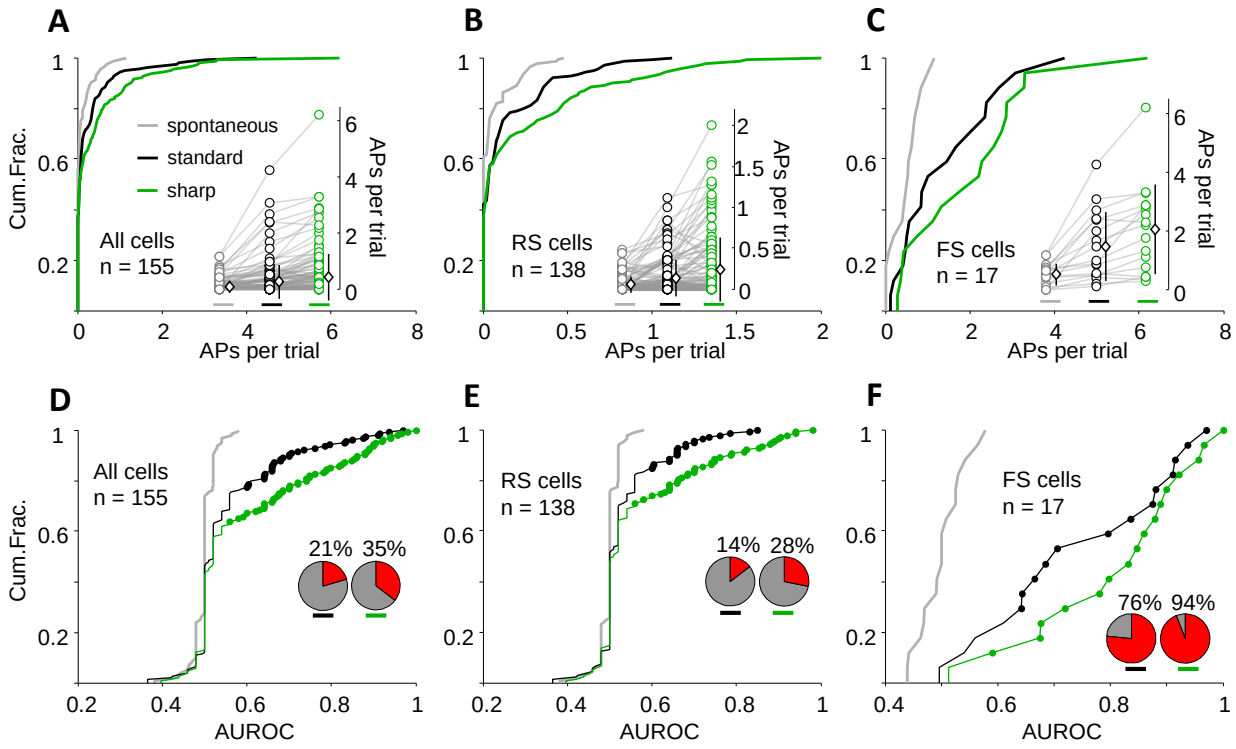

Figure 3.3*: Evoked spiking activity in response to the standard and the sharp stimulus* ***A-C****: Cumulative distribution of response for all cells (****A****), and separately for RS cells (****B****) and FS cells (****C****). The cumulative distributions are plotted for the spontaneous activity (gray), and for the evoked response to the standard stimulus (black) and the sharp stimulus (green). Inset plots represent spontaneous (gray) and evoked (black and green) activities where each circle is a stimulus-neuron pair. Diamond symbols represent average (± SD) spike count across neurons.* ***D-F****: Cumulative distribution of the area under ROC curves (AUROC) are plotted with the same color convention as above. Filled circles indicate neurons with significant responses ($p < 0.05$) based on a bootstrap permutation test on the ROC analysis. Inset pie charts represent the fraction of significant AUROCs for the standard (left chart) and sharp (right chart) stimulus.*

Overall, the standard stimulus resulted in significant response in 21% of neurons while the sharp stimulus evoked significant response in 35% of neurons (Figure 3.3*D*, ROC analysis followed by

permutation test, $p < 0.05$). Among 138 RS neurons, 14% produced a statistically significant response to the standard stimulus and this fraction increased to 28% for the sharp stimulus (Figure 3.3*E*). The majority of fast spiking neurons were responsive to both stimuli (76% to the standard and 94% to the sharp stimulus; Figure 3.3*F*).

Cumulative plots in Figure 3.3*B* (black and green) depict heavy-tailed distributions of responses, a signature of sparseness (Olshausen and Field 2004). To better quantify the degree of sparseness, we calculated population sparseness during spontaneous activity and for the standard and the sharp stimuli presented in both anesthetized and awake conditions (see Methods). Figure 3.4*A* illustrates population sparseness values calculated separately for the RS and FS neurons. For the RS cells recorded under anesthesia, sparseness dropped from 0.93 for stimulus zero to 0.75 for the standard stimulus and then to 0.31 for the sharp stimulus, indicating a dense activation as reported earlier (Ranjbar-Slamloo and Arabzadeh 2017). In awake condition however, sparseness remained highly stable and did not change with stimulation (0.78, 0.73 and 0.73 for the zero, the standard and the sharp stimulus respectively). Fast spiking neurons exhibited consistently low degrees of sparseness (≤ 0.40) both under anesthesia and in awake condition (Figure 3.4*A*). There was also a negative correlation between the sparseness and the fraction of the responsive neurons (Figure 3.4*B*, Spearman's correlation $r_s = -0.88$, $p = 0.007$). However, we did not find a proportional change in sparseness as the fraction of the responsive neurons increased; although in awake condition the fraction of responsive RS neurons increased from 14% to 28%, this increase did not result in any detectable change in the sparseness (filled red circles in Figure 3.4*B*).

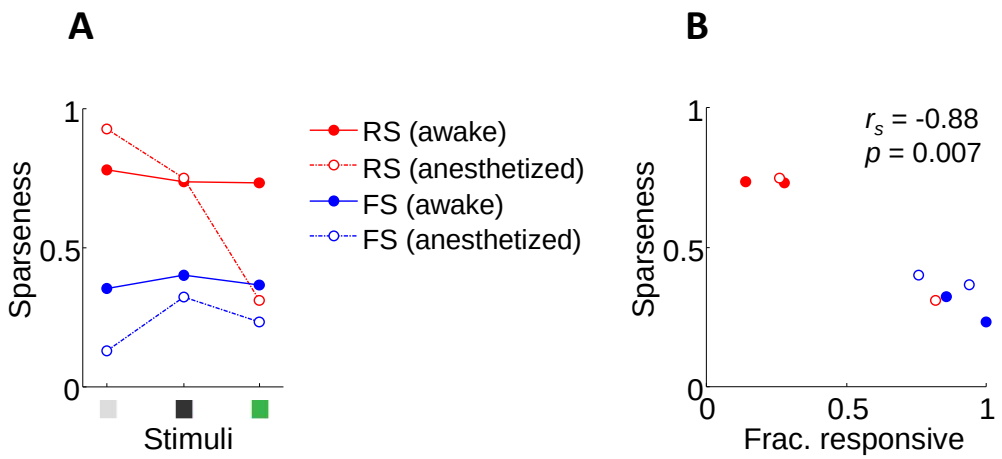

***Figure 3.4**: Quantification of sparseness across different states and levels of stimulation* ***A**: The gray, black and green stimulus conditions indicate spontaneous (stimulus zero), the standard and the sharp stimuli respectively. Filled circles with solid lines plot values for awake condition and open circles with dash-dotted line represent values for anesthetized condition.* ***B**: Scatter plot of sparseness versus fraction of responsive neurons (Frac. responsive) for the standard and the sharp stimuli. Colors and symbols are preserved from panel* ***A**. Inset represents the Spearman's correlation coefficient (r_s) and its p value.*

Next, we plotted the neuronal response as a function of depth. Panels *A* and *B* in Figure 3.5 represent the neuronal response sorted by the depth at which the pipette contacted the neuron (y-axis). The percentage of responsive RS neurons was similar in the two depth ranges (Figure 3.5*A*). Across 79 RS neurons recorded between 105-400 µm depths, 16% were responsive to the standard stimulus and 29% were responsive to the sharp stimulus (Figure 3.5*C*). Across 59 RS neurons recorded between 403-768 µm depths, 12% and 27% were responsive to the standard and the sharp stimulus respectively.

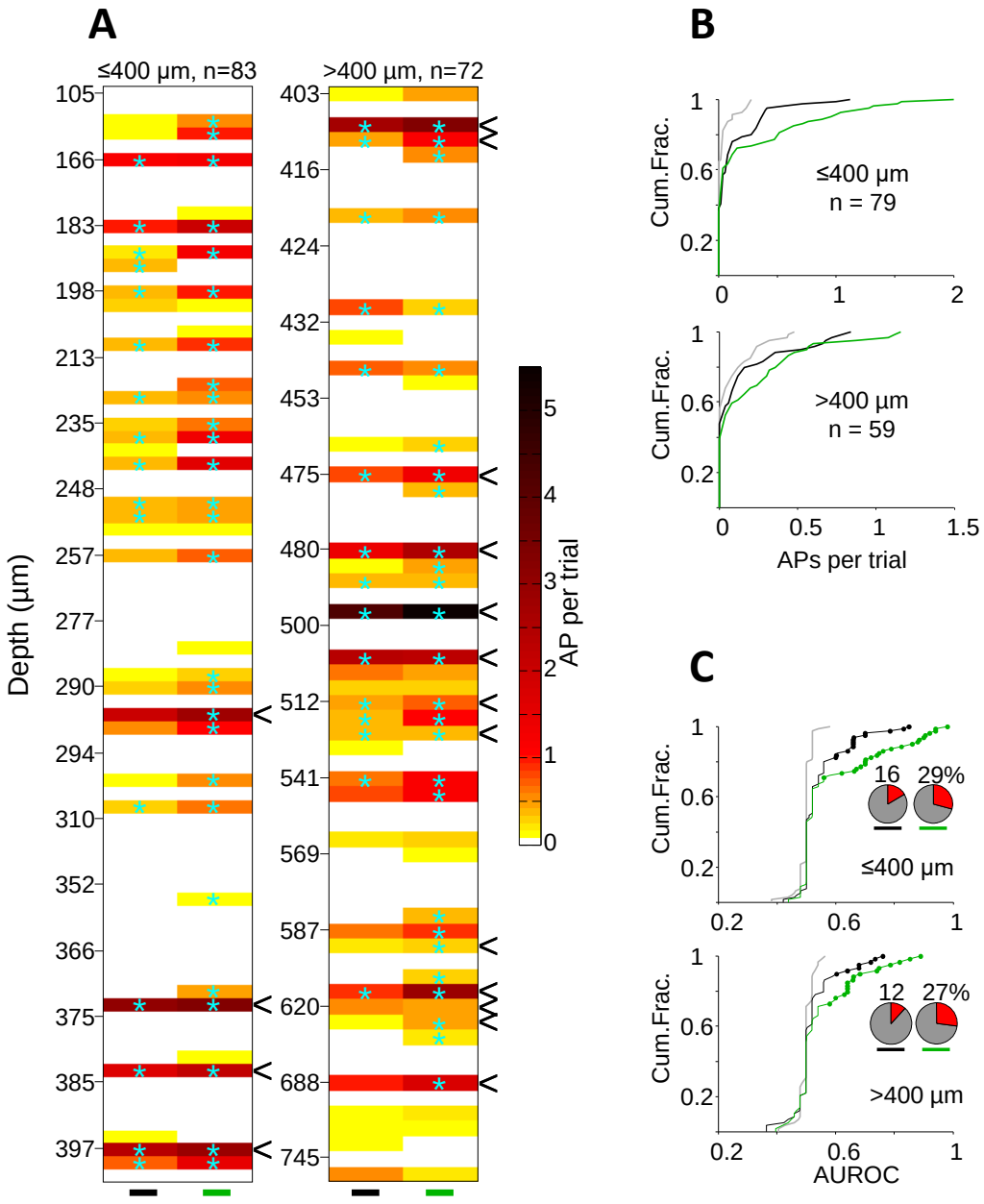

Figure 3.5*: Distribution of responsive neurons across cortical depth.*

A*: The average number of evoked APs for neurons recorded at various cortical depths (n = 155). Number of APs is calculated in the 0-30 ms post stimulus onset, for both the standard (black) and the sharp (green) stimulus. "<" symbols on the right edge of each plot mark fast spiking neurons. Cyan asterisks indicate significant responses based on ROC analysis (permutation test, p < 0.05).* ***B****: Cumulative distribution of responses in RS neurons by zero*

(gray), standard (black) and sharp (green) stimuli for the two depth ranges in panel ***A*** *(≤400 μm, top; >400 μm, bottom).* ***C****: Cumulative distribution of the area under ROC curves (AUROCs) for the two depth ranges in panel* ***A****. Filled circles mark neurons with statistically significant AUROCs (permutation test, p < 0.05). Inset pie charts visualize the fraction of responsive neurons at each depth range.*

3.4.2 Spiking response to manual stimulation

To examine whether the observed sparseness is due to the choice of stimulus, we expanded the dimensionality of the stimulation features by employing manual stimulation. For 18 neurons, we maintained the stable recording after the termination of piezo stimulation protocol, which allowed subsequent testing with manual stimulation. For these neurons, the piezo was removed and the whisker was manually deflected. Out of 18 neurons tested for both piezo and manual stimulation, 14 were RS and 4 FS. Out of the 14 RS neurons, 64% (9 neurons) were only responsive to the manual stimulation and not to the piezo (neither standard nor sharp stimulus). The rest of the RS neurons (36%, 5 out of 14) were responsive to both piezo and manual stimulation. No neuron was responsive to piezo stimulation only. As expected, all FS neurons were responsive to both piezo and manual stimulation (n = 4).

This finding encouraged us to undertake more manual stimulation experiments and characterize the feature selectivity in a bigger population of neurons (n = 118). For manual stimulation, we explored multiple ways of whisker-object contact to find the effective stimulus. This was facilitated by flexibility of the manual probing and an audio feedback, which helped identify and repeat touch incidents that elicited spiking activity. In order to quantify mechanical variables underlying the neuronal response during manual stimulation, here we plot the spiking activity of a number of example neurons along with high-speed tracking of the neuron's principal whisker.

Figure 3.6 illustrates an example neuron for which the spiking activity is overlaid on whisker angle, velocity and curvature. This neuron was responsive to tapping on whisker C2 (Figure 3.6C_1) and was silent otherwise, even when the whisker was pushed and released, producing high-speed events (Figure 3.6C_2).

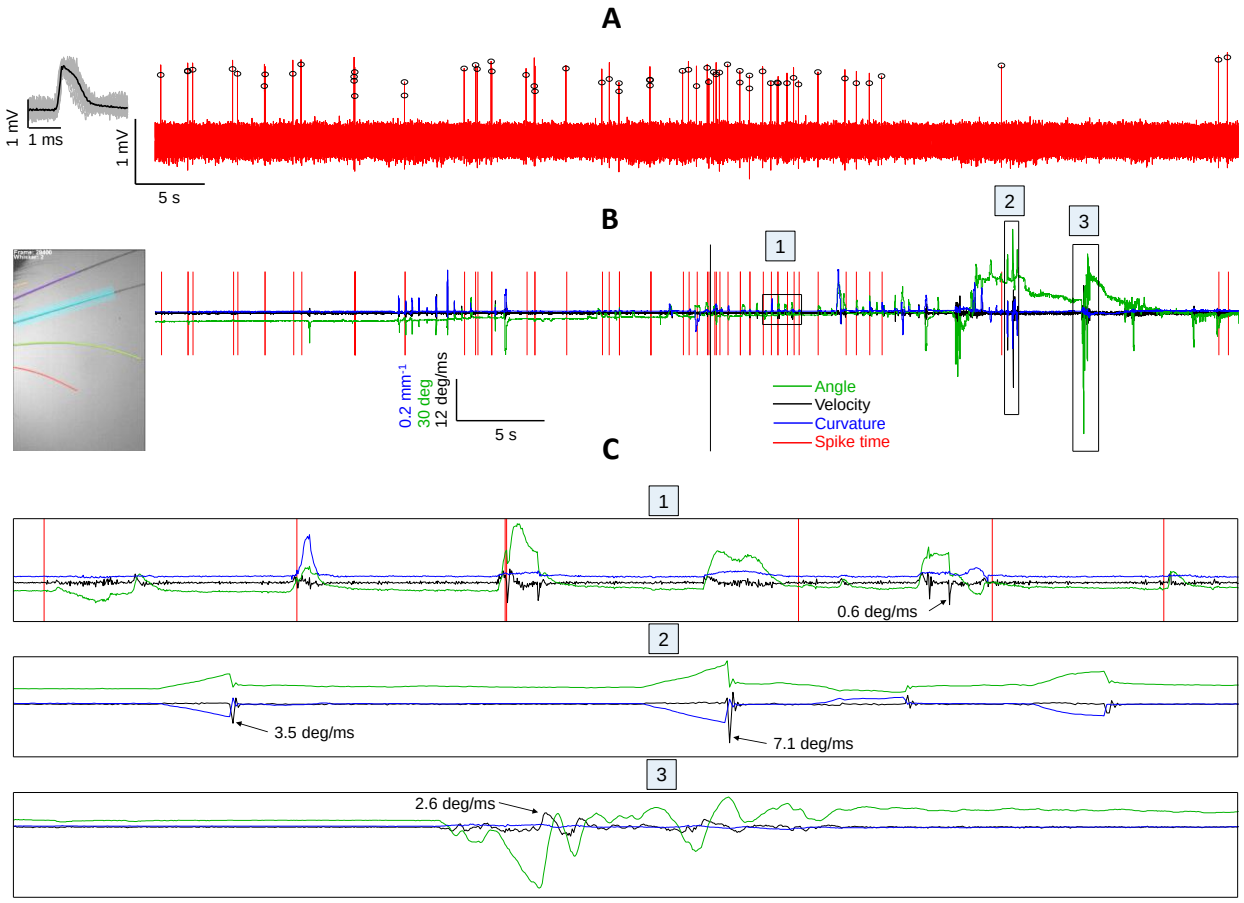

***Figure 3.6**: An example neuron driven by manual touch*

***A**: Trace of cell-attached recording (red) and sorted spikes (black circles). The inset on the left shows the spike waveforms (gray) and their average (black). **B**: Left; top view of the whiskers which were continuously filmed during the cell-attached recording. The cyan highlighted whisker is C2 for which the mechanical variables are plotted on the right. Right; three whisker variables (angle, velocity and curvature) are overlaid along with red, vertical lines which*

represent spike times. Blue boxes with numbers highlight the selected x-y limits (framed in rectangles), which are expanded in the subsequent panels 1, 2 and 3 maintaining their x-y limits. ***C****: Box* ***1*** *shows repeatable spiking activity upon tapping on the tracked whisker. Box* ***2*** *shows three rostro-caudal push and release and their associated curvature changes. Inset numbers indicate maximum velocity of the slip events. The slip events evoked no spikes in the recorded neuron. Box* ***3*** *shows expansion of a free whisking epoch. The inset number represents the peak velocity associated with this free whisking epoch.*

We recorded three neurons with exclusive response to touch during whisking. An object was introduced to the whisker field and the whiskers were engaged with the object upon whisking. Figure 3.7 shows an example neuron with exclusive response to contact during active touch. The expanded view in panel *B* part 1 shows that the animal started whisking and within a second brought the tip of the whisker into contact with the object. Whisker-object contact produced an increase in the curvature (Figure 3.7$B_{1\&2}$). Whisker protractions are marked by brief troughs within the elevated curvature event where trains of spikes occurred (Figure 3.7B_2). Panel B_3 in Figure 3.7 represents the expansion of a passive touch epoch marked with prominent changes in the curvature and high-velocity events. This example shows no response to curvature events when a number of kinetics were applied passively to the whiskers. This is despite the fact that the curvature events appear similar to those elicited by the active touch. The occurrence of spikes in the trough of the elevated curvature is better quantified in the spike triggered average curvature (Figure 3.7*D*).

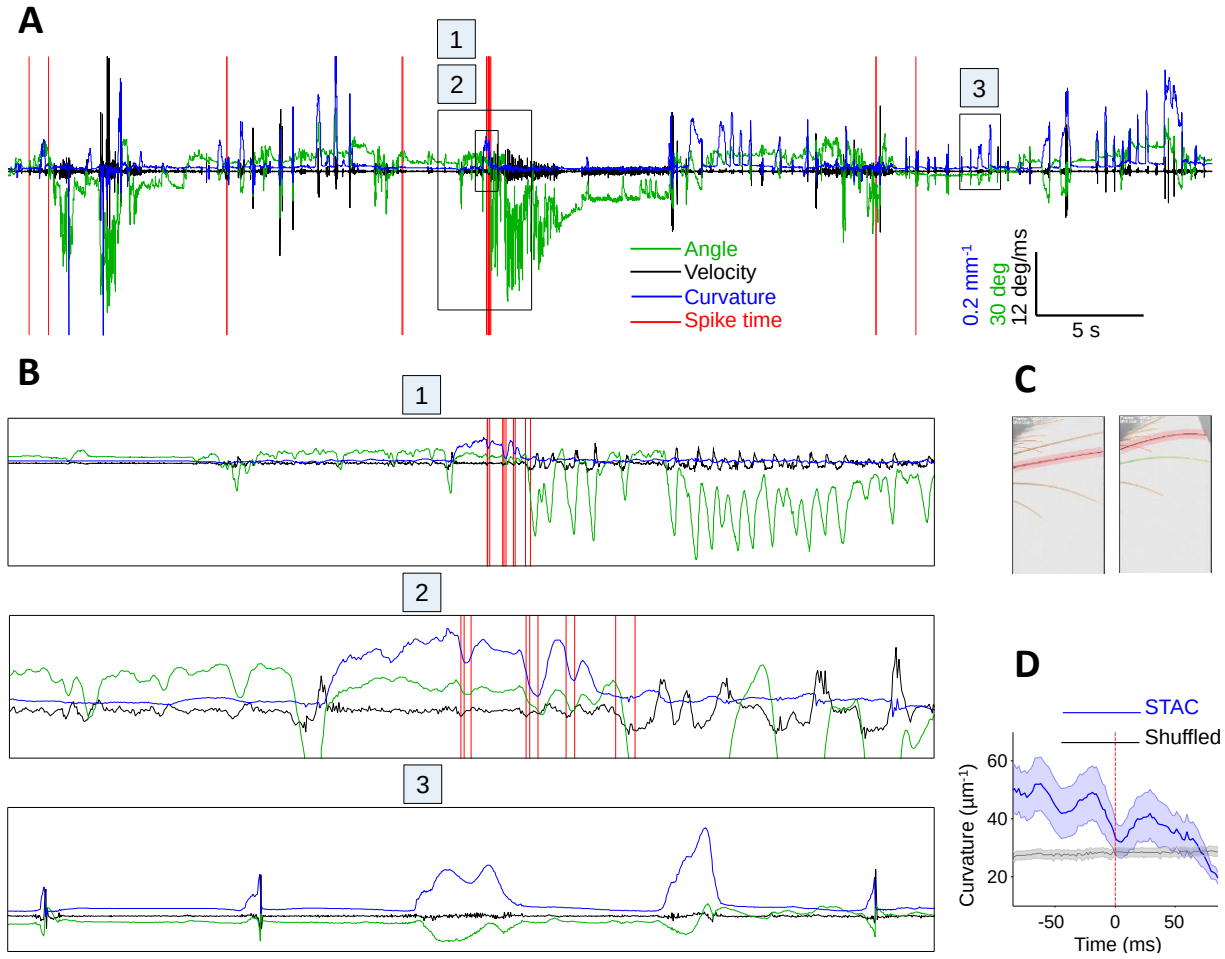

***Figure 3.7**: An example neuron with exclusive response to active touch*

***A**: Color conventions are as in the previous figure. **B**: Box **1** shows the expanded view of an active touch epoch. Box **2** shows the same active touch epoch further expanded in time for better visibility. Box **3** shows epochs of various passive contacts. **C**: Left; top view of the whiskers just before the contact onset. Right; same view during whisker-object contact. Note that the object contact (top right corner) increased the curvature of the whisker (red highlight). **D**: Spike triggered average (± SE) curvature (STAC, blue). Black curve shows the control average curvature (± SE) triggered by 1000 randomly selected times.*

Figure 3.8 shows another example neuron which was exclusively responsive to tapping on whisker C1. This neuron has a low spontaneous activity and produces highly reliable responses to whisker-object contacts. The expanded view (Figure 3.8*B*) shows that the spikes predominantly occur at a specific low-amplitude curvature event.

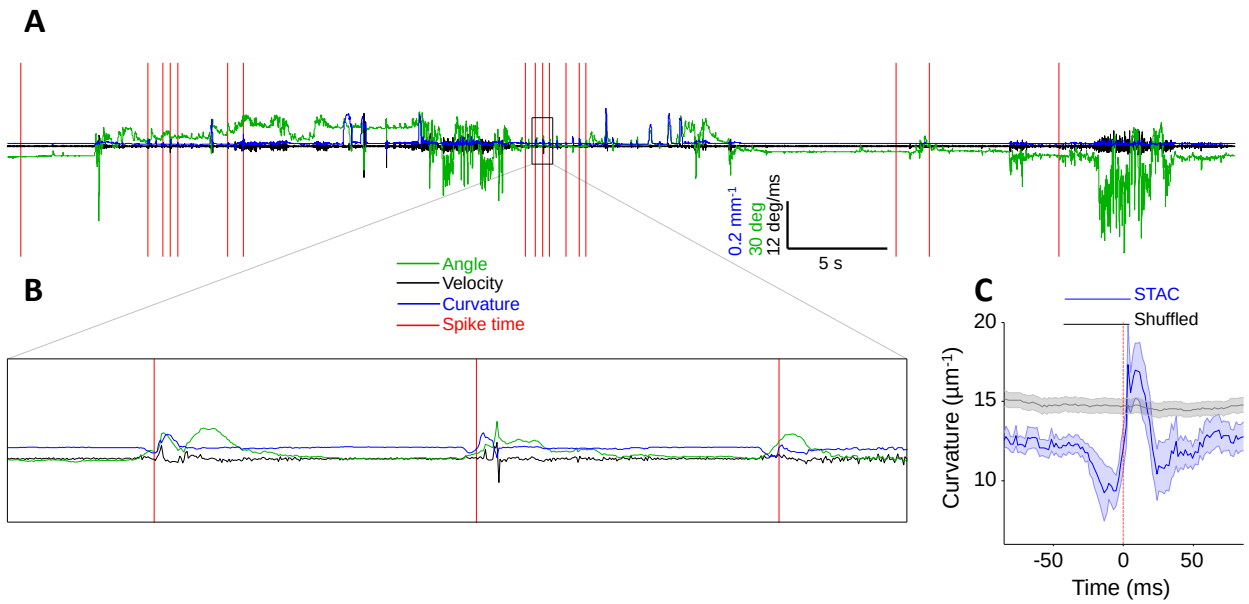

Figure 3.8*: An example neuron with exclusive response to tapping on whisker C1*

A*: Color convention as in previous figures.* ***B****: Expanded view of the response epoch.* ***C****: Spike triggered average (± SE) curvature (STAC, blue) along with the shuffled data in black.*

Spike triggered average curvature (STAC) for this example neuron shows a trough preceding the spike which is followed by a sharp increase in curvature at the spike time (Figure 3.8*C*). Figure 3.9 illustrates for 9 example neurons tuning to a particular stimulus category as captured by their STAC profile. These include neurons with tuning to both tapping and axial pressure on whisker C1 (Figure 3.9*A*), neurons with "tap/whisking" (Figure 3.9*E*) and "tap only" tuning (Figure 3.9*F*). These examples show that the tap response is associated with a sudden change in curvature just before the spike generation (~15ms), indicating that the initial force on the whisker

is effective in driving the neuron. Such tuning to a fast change in curvature was also observed for a number of slip-tuned neurons (see Figure 3.9*G as an example*). Post-hoc analysis of STAC shows that the neuron spiked on average ~9 ms after a slip event (Figure 3.9*G*). Some neurons were not temporally aligned to a specific phase of the curvature events (such as those in Figure 3.9*C*&*D*). This is despite the fact that the neuron corresponding to Figure 3.9*C* was clearly responsive to multiple types of touch during the experiment. Overall, these observations indicate that the curvature events can only partially capture the specific tuning of a neuron.

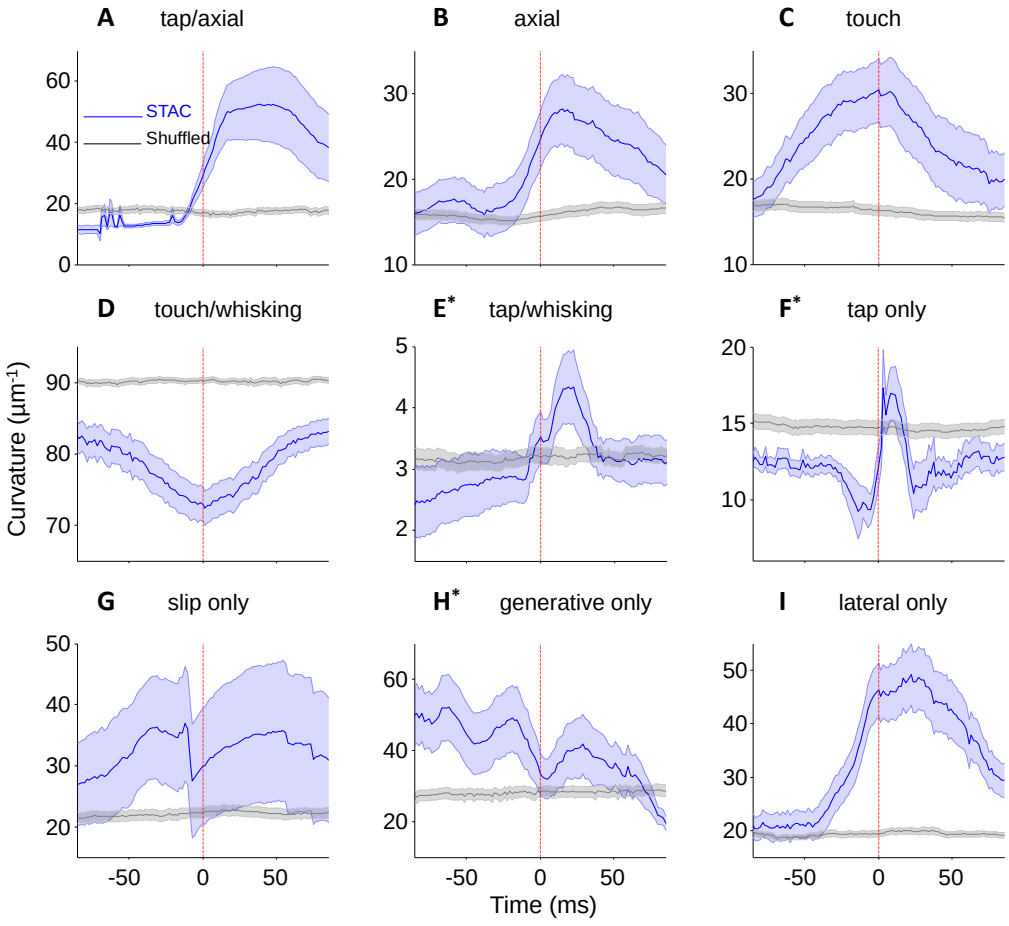

Figure 3.9: *Spike triggered average curvatures*

*Title of each panel shows the tuning of the neuron examined by manual stimulation. * Panels **E**, **F** and **H** correspond to example neurons in Figures 3.6, 3.8 & 3.7 respectively.*

From the whole population of neurons recorded during manual stimulation (n = 118), we identified 11 FS and 107 RS cells (Table 3.1). Regardless of the tuning characteristics, 78% of the RS neurons were categorized as responsive (i.e. they reliably produced a repeatable evoked response during whisking, touch or application of air puff).

		All depths	Shallow (≤400)
All types	# of cells	118	65
	# responsive	92	54
	% responsive	**78**	**83**
RS	# of cells	107	61
	# responsive	83	51
	% responsive	**78**	**84**

Table 3.1*: Neurons tested for a response to the manual stimulation*

Figure 3.10 shows that the RS neurons were almost evenly sampled from all depths and likewise responsive/nonresponsive neurons were not clustered at any specific depth range. Additionally, when we only considered neurons recorded at a depth shallower than 400 µm, 84% of the regular spiking neurons were responsive (Table 3.1). Further limiting the recording depth to <250 µm resulted in a similar fraction of responsive neurons (85%). Therefor the majority of neurons, regardless of their depth, could be activated by at least one type of whisker stimulation.

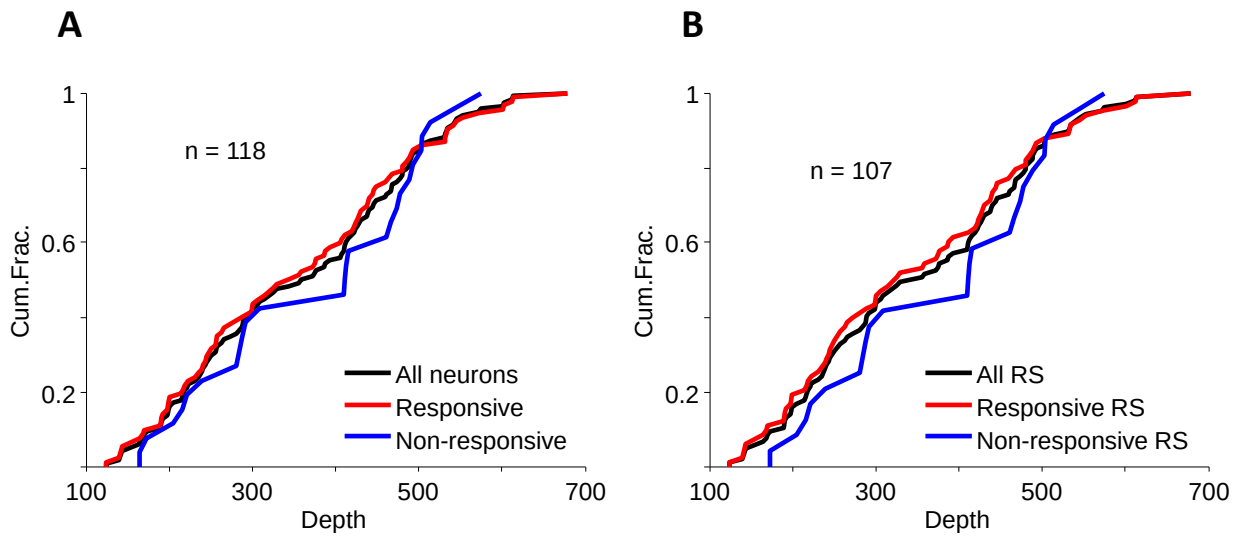

Figure 3.10*: Depth distribution of the recorded neurons*

A*: The cumulative distribution of all recorded neurons as a function of depth (black) and separately for the responsive (red) and non-responsive (blue) neurons.* ***B.*** *Same as* ***A*** *but only for the RS neurons.*

During manual stimulation and recording, we also classified neurons based on their "input category" and "tuning". In our definition, input category identifies a broad feature, which includes the size of the receptive field, movement source (touch or whisking), movement direction etc. (Table 3.2). However, tuning identifies more specific features branching from input categories; for example for the receptive field the neuronal response may be limited to a single whisker or multiple whiskers. Table 3.2 shows a classification of the response type based on input category and specific tuning within each category. Overall regarding movement source, we found 8 neurons with distinguishable response to both whisking and touch, 1 neuron with exclusive response to whisking and 81 neurons that were responsive to touch. For a large number of the touch responsive neurons, we further identified a specific tuning. These include neurons responsive to lateral push but not to release or slip movement (n = 6) and neurons exclusively

responsive to slip movement but not to any other type of movement (n = 5; Table 3.2). Notably, we found that a number of neurons only reliably responded to gentle touch but not to strong deflections of the whiskers (n = 11). Such movement specific responses indicate the diverse range of stimulus parameters captured by the vS1 neurons.

Input category	tuning	All	RS	RS (≤400)	FS
Receptive field	multi-whisker	30	27	15	3
	single-whisker	42	40	27	2
Movement source	touch only	81	74	46	7
	touch/whisking	8	6	4	2
Movement direction	axial only	8	8	8	0
	lateral only	7	7	4	0
	axial/lateral	1	1	0	0
Movement type	push only	6	6	3	0
	slip only	5	5	4	0
	tap only	4	4	4	0
	air puff only	2	2	0	0
Intensity	gentle only	11	11	6	0
	strong only	1	1	0	0
Location	distal (tip) only	2	2	1	0
Generative vs. receptive	generative only	3	3	1	0
	generative/receptive	9	8	5	1

***Table 3.2**: Various tunings of responsive neurons to each class of stimulus features*

3.5 Discussion

It is widely reported that a vast majority of vS1 neurons especially in the superficial layers are silent under various experimental conditions (Dykes and Lamour 1988a; Barth and Poulet 2012; Petersen and Crochet 2013; Ramirez et al. 2014; Peron et al. 2015b). An unresolved question is whether the large fraction of silent neurons contributes to sensory coding in rodent vS1, as is the case in the visual cortex, or whether they are not wired strongly enough with bottom-up excitatory input to do so. We aimed to directly answer this question in a number of experimental conditions. Previously, we found that a high-velocity stimulus can evoke reliable activity in a majority of L2/3 of vS1 neurons of anesthetized mice (Ranjbar-Slamloo and Arabzadeh 2017). Here, we tested the feature selectivity of vS1 neurons in awake mice using (i) simple well-controlled piezo stimulation and (ii) manual probing of whiskers, which was less controlled but more representative of complex natural interactions between whiskers and objects. We found that a majority of vS1 neurons, which did not produce spiking activity in response to simple vibrations of high intensity, were nevertheless responsive to a specific feature or a combination of features of manual stimulation.

To determine the extent of neuronal activation by a high-velocity stimulus in awake condition, we presented a standard (1.2 degree/ms) and a sharp (3.8 degree/ms) stimulus to the principal whisker as in our previous study (Ranjbar-Slamloo and Arabzadeh 2017). In contrast to the anesthetized recordings where the sharp stimulus evoked spiking activity in 74% of neurons (single whisker experiment), under awake condition, the sharp stimulus was only effective in 28% of neurons (n = 138). To further investigate responsiveness, in a subset of neurons we tested both piezo and manual stimulation and observed that manual stimulation of the same whisker effectively drove all of the tested neurons including the fraction which did not respond to the

piezo (9 out of 14). Next, we employed whisker tracking along with cell-attached recording in another subset of neurons to quantify mechanical variables of the whisker-object contact during manual stimulation. We found that the neuronal tunings were only partially reflected in the spike-triggered whisker curvature (Figure 3.9). Overall, we found that unlike piezo stimulation, the majority of neurons (84%) were driven by manually optimized whisker contacts. Using this approach, we also found a large fraction of neurons to be highly selective for a certain stimulus feature and condition (e.g. generative contacts or light taps on the whisker).

For response categorization, specific tunings such as “tap only” and “slip only” were assigned to a neuron only when it was rigorously tested for all possible ways of stimulation including all other types of stimuli in all input categories. Although we did not systematically present the stimuli (i.e. a fixed number of highly repeatable trials), sharply tuned neurons were highly reliable and resilient to variations within a feature. Nevertheless, all the classifications used in the table 3.2 are descriptive. In order to obtain a quantitative criterion, 3-dimentional dynamics of the whiskers has to be recorded. We were not able to measure whisker dynamics when all whiskers were kept intact (for most of the neurons). In the case of example neurons, only a row of whiskers was imaged, and we do not know how many additional whiskers/features could be coded by these neurons. Hence, due to technical limitations, a quantitative criterion to classify feature tuning could not be obtained.

It is widely reported that the stimulus representation in L2/3 of vS1 is sparse, engaging only a small fraction of the principal neurons (Shoham et al. 2006; Barth and Poulet 2012; Petersen and Crochet 2013). Multiple scenarios which can result in the apparent sparseness of cortical area were outlined by Barth and Poulet (Barth and Poulet 2012). These include uncorrelated trial-to-trial response variability, dominance of activity in a stable population, state dependent

excitability and high stimulus selectivity (Barth and Poulet 2012). Additionally, the behavioral relevance of a stimulus can influence the sparseness of the sensory representations, as does behavioral training (Gdalyahu et al. 2012; Kato et al. 2015). All of these scenarios can to some extent affect the apparent sparseness in various cortical areas. For example in the visual cortex, the apparent sparseness is due to the high degree of selectivity of neurons such as to stimulus orientation (Ohki et al. 2005).

In rodent vS1, it is not entirely clear how the diversity of feature selectivity contributes to the widely reported sparseness. Most previous studies confined the stimulus to a single whisker with simple stimulation parameters (such as velocity or amplitude). However, a few studies have explored the neuronal tuning to a complex, multi-whisker stimulation through independent piezo-electric actuators under light anesthesia (Estebanez et al. 2012, 2016; Ramirez et al. 2014). Using whole-cell recording, Ramirez et al. found that spatiotemporally complex stimuli delivered to an array of 8 whiskers failed to drive spiking activity in a majority of vS1 L2/3 neurons with the average spiking responses remaining below 0.1 spikes/s for the optimized stimulus (Ramirez et al. 2014). The authors thus concluded that widely reported sparseness in L2/3 is unlikely to be due to impoverished stimulation. However, in a recent study, Estebnez et al. showed that a complex multi-whisker stimulation paradigm (24 whiskers) markedly increased the fraction of responsive neurons in L2/3 such that the overall fraction of responsive neurons reached 41% (Estebanez et al. 2016). This is still much lower than the fraction of contributing neurons in an analogous study in rat visual cortex, where 75% of the L2/3 neurons significantly responded to at least one stimulus (Ohki et al. 2005). Nevertheless, the former study showed that complex feature representation prevails in populations of L2/3 neurons in vS1 (Estebanez et al. 2016). Such stimuli are difficult to deliver in a controlled manner in awake condition. Here,

using manual stimulation, the flexible presentation of three-dimensional movements, suggests that a high fraction of vS1 neurons respond to one or multiple naturalistic stimuli.

Controlled whisker stimulation and whisker imaging during behavior has revealed that the vS1 neurons are sensitive to a number of variables upon whisker movement such as velocity/acceleration, phase, direction and whisker curvature (Simons 1978; Shoykhet et al. 2000; Arabzadeh et al. 2003, 2004; Bale and Petersen 2009; Hires et al. 2015). These features are preserved from the activity of the primary sensory afferents (Arabzadeh et al. 2005; Bale and Petersen 2009; Campagner et al. 2016; Severson et al. 2017), therefore, comprise the elementary or low-level features that cortical neurons receive. The convergence of these simple features via sensory integration across multiple whiskers (Jacob et al. 2008), and possibly multiple sensorimotor pathways (Xu et al. 2012) in L2/3 of vS1 may underlie the synthesis of higher-level features which drive some neurons (Estebanez et al. 2012, 2016; Ramirez et al. 2014). Notably, such multi-whisker integrations can form emergent features such as “apparent motion” in a certain direction (Jacob et al. 2008) or contours of the objects (Kremer et al. 2011).

Rodents can map the object surfaces by a combination of body, head and whisker movements in either generative or receptive modes (Diamond and Arabzadeh 2013). In freely moving animals, interactions of whiskers with objects occur in three dimensions. Thus spatiotemporal patterns of whisker deflections must be able to tell the animal whether for example, the head/body approaches an object or moves away from it. Although our experiment was done in a head-fixed condition, three-dimensional movement of the objects in whisker field allowed us to identify the feature of interest for a number of neurons that would have otherwise been deemed unresponsive. For example, we found a number of neurons which were only driven by axial pressure at the tip of a specific whisker and therefore might encode the approach to an

object/obstacle at a certain orientation (table 2). Tap neurons may encode the location of contact point in the receptive mode while push and slip neurons (table 2) can provide information about object properties such as surface texture (Von Heimendahl et al. 2007; Diamond et al. 2008a; Wolfe et al. 2008; Jadhav and Feldman 2010). In our experiment, objects were manually introduced to the whiskers (mostly in the receptive mode) and therefore the features relating to the generative mode (such as slip events) could not be fully assessed. Nevertheless, we were able to identify 12 neurons with a generative mode response. In mice trained in an object localization task two different sets of L2/3 neurons were found to be activated in the generative and the receptive modes (Peron et al. 2015b). Based on this, we expected to observe several neurons with pure generative response. However, we observed a high degree of overlap such that 9 out of 12 neurons also responded to receptive contacts while only 3 neurons had pure generative response. Such discrepancy might be due to the use of anesthesia for receptive mode stimulation and/or training in the earlier report (Peron et al. 2015b).

In the awake condition, a number of factors can influence the mode of operation of the cortical circuit (Sabri and Arabzadeh 2018) and in turn affect responsiveness of cortical neurons; whisker position is under motor control and occasional whisking gives rise to rich whisker kinematics even in the absence of touch. Furthermore, anesthesia can damp down inhibition (Rinberg et al. 2006; Haider et al. 2013; Cazakoff et al. 2014) and alter the tuning properties of cortical neurons (Peron et al. 2015b; Durand et al. 2016). In contrast to our anesthetized results, we found that in awake condition, only a quarter of the recorded neurons responded significantly to the sharp stimulus delivered by piezo. However, when we further tested the responsiveness by removing the piezo and manually deflecting the whiskers, a majority of these neurons were clearly tuned to a non-classical stimulus feature such as light tap, axial pressure, and generative contact. This can

be attributed to a high degree of freedom in the stimulus space and/or state dependent modulation of responsiveness and tuning properties in awake condition.

Overall, our results reflect a marked difference in sparseness of vS1 regular spiking neurons between anesthetized and awake conditions. The diversity of conditions upon which vS1 neurons responded to the sensory input implies that various simple and complex features are encoded in vS1 by recruiting highly selective neurons especially in the supragranular layers.

Chapter 4: General discussions and conclusion

4.1 Main findings of this work

In this thesis, we employed multiple strategies to systematically quantify the neuronal response in vS1. First, we used whole-cell recording in anesthetized animals to quantify synaptic responses as well as evoked spikes in L2/3 neurons. Loose-seal cell-attached recording enabled us to measure spiking activity with a high fidelity, little interruption of the cell function and an unbiased sampling of active and silent neurons. We also used calcium imaging to verify our findings with simultaneous imaging of a population of L2/3 neurons. For a detailed quantification of the data we employed Receiver Operating Characteristic (ROC) analysis, Fano factor and statistical evaluation of sparseness to characterize spiking activity in L2/3. Overall, we found that under anesthesia, L2/3 neurons are sensitive to a high-velocity stimulus and the majority of these neurons are driven by this stimulus. We further explored the sparse representations in head-fixed, awake mice to determine the role of silent neurons in sensory processing in the awake state.

We first presented a high-velocity stimulus (the sharp stimulus) along with a standard stimulus to determine the extent of sparseness. Interestingly, under awake condition, only 29% of the regular spiking neurons in L2/3 responded to the sharp stimulus, which contrasts our earlier anesthetized findings where this proportion was 74% (single whisker experiment). We further calculated the population sparseness, which captures the structure of response distribution and does not necessarily reflect the fraction of responsive neurons. We found that in the anesthetized condition, a large increase in the fraction of responsive neurons was associated with a large drop in population sparseness. However, in the awake condition, the small increase in the fraction of responsive neurons did not translate to a proportional decrease of sparseness. Therefore, population sparseness of excitatory neurons in awake condition seems robust and invariant to

both stimulus intensity and the fraction of responsive neurons. This may reflect a subnetwork of neurons, which are highly tuned to a feature that is best presented by our method of piezo stimulation, such as velocity/acceleration in a particular direction. It is also possible that piezo responsive neurons represent a population of broadly tuned neurons in the L2/3. Other neurons may require their specific stimulus conditions and features to fire action potentials. To test this latter hypothesis, we explored the effectiveness of manual stimuli to drive the large subset of neurons, which were not responsive to the sharp stimulus. We found that these neurons were consistently driven by certain manual whisker stimulations. Our manual stimulation protocol revealed that the piezo stimulus did not effectively sample the whole stimulus space, and ignored certain features that could drive silent neurons. In order to have a better understanding of the responsiveness in vS1, we recorded 118 neurons with manual stimulation and found that 84% of L2/3 RS neurons (and all of the FS neurons) were responsive to at least one stimulus type. We frequently encountered neurons with narrow tunings to a very specific way of whisker-object interaction such as axial pressure, push, tap, and slip (Table 3.2). Surprisingly we found that a number of neurons did not respond to a strong deflection and only responded to a gentle contact in a specific direction. We also encountered neurons, which were drivable by any type of whisker contact (Figure 3.9*C*&*D*), implying the existence of a broadly tuned subset of RS neurons in L2/3 of vS1. Overall, we concluded that the sparse firing in L2/3 of vS1 is mostly due to high stimulus selectivity (i.e. high level of lifetime sparseness), which results in a high level of population sparseness. Thus a majority of vS1 neurons are directly involved in representation of various features in the case of naturalistic and complex stimuli.

4.2 Significance of the findings

Our results are in line with most of the literature regarding sparse coding; first of all, we confirmed that a set of "standard" deflections, which was in the range of most commonly used deflection velocities, evoked spikes only in a small fraction of the cells in L2/3 of vS1. Most of the studies on the vibrissal system have been carried out using air puff or piezoelectric deflectors. Based on a review across many studies, Moore and colleagues found that whisker stimuli which were used to drive cortical neurons in reduced preparations were often far below 2.5 degree/ms (Ritt et al. 2008) while the behavioral studies showed that a substantial fraction of whisker micro-motion have much higher velocities than this (Ritt et al. 2008; Wolfe et al. 2008; Jadhav et al. 2009; O'Connor et al. 2010a; Bale et al. 2015). Therefore, we added a sharp stimulus, in the range of high-velocity events, which were found during naturalistic whisker-object interactions, and found that this stimulus is effective in driving a high fraction of the L2/3 of vS1 neurons. This surprising finding provokes a number of questions regarding behavioral relevance, computational implications and cellular/circuit mechanisms involved in such dense recruitment of L2/3 neurons.

What cellular/circuit mechanisms may underlie a transition from sparse to dense coding as observed here? *In vitro* studies often take advantage of a stable local circuitry and the ability to dissect the synaptic components. A standard paradigm is to use electrical or optogenetic stimulation of the inputs to a given circuit and employ functional imaging and/or whole cell recording to measure spiking and synaptic activity in the target population. Using this approach, Elstrott and colleagues stimulated L4 barrels and recorded the population activity in L2/3 which is known to receive strong excitatory input from L4 (Elstrott et al. 2014). They showed that L2/3 neurons were gradually recruited by increasing the intensity of the electrical stimulation

delivered to L4 vS1, but 22% of the cells still did not respond reliably even to the strongest stimulus which caused LFP saturation in L2/3 (Elstrott et al. 2014). Such gradual recruitment of excitatory neurons is also reported in hippocampal slices (Pouille et al. 2009). Importantly Erstrott and colleagues also showed that the biophysical and morphological properties of the neurons did not predict their responsiveness but their synaptic inputs did; neurons which were activated with weaker stimuli were those which received stronger excitatory input (Elstrott et al. 2014). This study also showed a weak ($R^2 = 0.44$) but significant correlation between the response to the *in vivo* electrical stimulation of L4 and the response to a fixed intensity stimulus delivered to the principal whisker. In our study, we further tested the recruitment of L2/3 neurons by whisker stimuli with different intensities.

In our initial whisker stimulation paradigm (Chapter 2), standard stimuli covered a range of intensities that is typically explored in the literature (Wilent and Contreras 2004). In this range, post-synaptic potentials tended to plateau and spiking activity gradually increased on average. However, the percentage of activated neurons did not show a clear gradual trend and was highly variable across sessions (Figure 2.5*C&D*). Furthermore, we were not able to determine whether a gradual recruitment of the neurons occur in the range between 1.2-3.8 degree/ms. In an attempt to cover this range, we performed parallel experiments with modified paradigms (Appendix). In a variable duration paradigm, we systematically changed the duration of piezo deflection (Figure A.1&2). Compared to the previous paradigm (Chapter 2), here we were able to generate a more gradual increase of the peak velocity (Figure A.2*B*&*D*). We also calculated a corresponding value for peak acceleration (Figure A.2*C*&*E*). Importantly, the relation between peak velocity and peak acceleration was not monotonic; the sharp stimulus in this paradigm had a lower velocity but substantially higher acceleration than the fastest stimulus (Figure A.2*E*). This

paradigm shows that a decoupling of velocity and acceleration (Bush et al. 2016) is also achievable by adjusting piezo-stimulation parameters. Spike recordings showed that L2/3 neurons were at least two times more sensitive to the sharp stimulus that had the highest acceleration than the fastest stimulus which had the highest velocity (Figure A.3) and this was consistent in anesthetized and awake conditions (Figure A.3*A*&*B*). Plotting the spiking response versus either of the parameters showed that unlike the peak velocity, the peak acceleration was monotonically represented by L2/3 neurons (Figure A.3*C*&*D*). The stimulus with intermediate acceleration (and highest velocity) was able to recruit 40% of the neurons while the stimulus with the highest acceleration activated 80% of the neurons (Figure A.3*A*). This represents a possibly gradual recruitment of the L2/3 neurons into the active pool *in vivo*. This paradigm also addresses a potential mechanism which may contribute to the spiking of L2/3 neurons; piezo ringing. Figure *A.2* shows that the stimulus with intermediate acceleration (and highest peak velocity) also generates an intense ringing which is slightly higher than that of the sharp, high-acceleration stimulus. If the ringing is to play a significant role in the activation of the L2/3 neurons (e.g. via circuit-level summations or amplification of whisker resonance) response to the intermediate acceleration stimulus must be comparable to response to the sharp stimulus. However, we observed much higher response to the sharp, high-acceleration stimulus compared to the response to the other stimulus with intermediate acceleration which possessed the highest velocity and an intense ringing. The effectiveness of the sharp stimulus, therefore, is likely due to the initial acceleration that takes place within 2ms from the stimulus onset.

In the final paradigm that we tested in anesthetized mice (Figure A.4), we filled the intensity gaps by systematically increasing the amplitude of the sharp stimulus, which was used in the first paradigm (Chapter 2). This enabled us to explore the operational range and input-output function

of a small sample of L2/3 neurons. Spike recordings showed that the fraction of active neurons and the probability of spiking per neuron monotonically increased with the stimulus intensity and that this increase showed a sigmoidal trend (Figure A.5). This suggests that the stimulus-response functions in L2/3 might be similar to those obtained in L4 (Adibi et al. 2012; Ollerenshaw et al. 2012, 2014), with a dynamic range which spans a broad range of intensities. The top asymptote of the fitted sigmoidal functions was close to unity, implying that a dense recruitment of the L2/3 neurons is associated with a unit spike per trial per neuron. This indicates that in response to stimuli with submaximal intensities, most individual neurons did not generate more than one spike (detection) and hence would not discriminate stimuli based on their spike count per stimulus. However, if noise correlation is small enough, population spike count may carry a robust discerning signal, which can inform the presence, intensity and other properties of a stimulus, depending on the tuning characteristics of the population. In future studies, it is important to determine the dynamic range of the individual neurons across layers of vS1 and ideally thalamus, to determine response transformations and coding capacities in this area of the cortex.

Our results further highlight the role of synchrony in driving cortical neurons (Theunissen 2003; Bruno 2011). A fast changing stimulus, such as the sharp stimulus can effectively drive barrel neurons in L4, since they are most sensitive to rapid velocity events such as stick-slip events during whisker-object interactions (Arabzadeh et al. 2005; Wolfe et al. 2008; Jadhav et al. 2009; Jadhav and Feldman 2010; Maravall and Diamond 2014; Schwarz 2016). Individual synaptic connections in the cortex are weak (Lefort et al. 2009; Barth and Poulet 2012), therefore, a synchronous input from multiple presynaptic neurons is required to drive cortical neurons (Bruno and Sakmann 2006). A high level of input synchrony to L4 would result in highly synchronous

output, which can effectively drive L2/3 neurons before the arrival of the inhibitory inputs to these cells. In order to determine the role of synchrony in sensory processing, a systematic change in the vibrissal stimulation parameters may be required. For example, in our study we were not able to precisely induce fixed amplitude for the variable duration stimuli. More importantly the absolute peak and integrated values of the first and second derivatives (velocity and acceleration) need to be kept constant. Precise control of these parameters requires alternative stimulator devices as described in recent studies (Chagas et al. 2013; Waiblinger et al. 2015).

A challenge in sensory systems research is to extend the results obtained in controlled experimental conditions, often under anesthesia, to awake and ideally to naturalistic conditions. Often inevitable experimental constraints such as anesthesia and the choice of stimulus limit our understanding of the sensory processing. For example, studies have shown that the brain operation during awake condition is, to a great extent, different from anesthesia (Rinberg et al. 2006; Haider et al. 2013; Cazakoff et al. 2014; Durand et al. 2016). In this line, we set out to extend our results to awake condition and found that overall 35% of neurons responded to the sharp stimulus which had a velocity of 3.8 degree/ms. In their recent studies, O'Connor and colleagues has developed a piezo stimulus detection task to study stimulus and decision related activity in L2/3 of vS1 and vS2 (Yang et al. 2015; Kwon et al. 2016). They presented a 500ms sinusoidal deflection with peak velocity of 0.8 degree/ms and observed sparse task related activity in both vS1 and vS2 (Kwon et al. 2016). In the vS1, 37% of the neurons on average were responsive during this task and about half of the responsive neurons correctly encoded the stimulus (Kwon et al. 2016).

O'Connor and colleagues also showed that the whisker stimulus encoding neurons in L2/3 are somewhat clustered in the center of the barrel column (Kwon et al. 2016). Other studies have also found that the stimulus selectivity maps in adult rodents tend to cluster neurons with similar tuning (Andermann and Moore 2006; Kremer et al. 2011; Garion et al. 2014; Estebanez et al. 2016) which can affect the interpretation of population sparseness depending on the scale of population recording. Nevertheless, these studies are debated with more recent ones, which did not find a spatial clustering of similarly tuned neurons (Martini et al. 2017; Kwon et al. 2018). More sophisticated imaging studies are required to determine the structure of feature tuning in vS1 of awake, and behaving animals.

Regardless of the tuning map structure, we investigated which additional features are encoded by vS1 individual neurons. Previous studies have found that a rich spatiotemporal input can reveal higher-order features in vS1 which possibly emerge from the convergence of inputs from multiple whiskers (Jacob et al. 2008; Estebanez et al. 2012). These studies showed that the activity of the supragranular vS1 remained sparse despite high-dimensionality of the stimulus (Estebanez et al. 2012; Ramirez et al. 2014) and multi-whisker stimulation patterns activated up to 41% of the neurons in L2/3 of vS1 (Estebanez et al. 2016). This study revealed that 15% of the neurons in L2/3 were only responsive to correlated or "anti-correlated" movements of the whole whisker pad (Estebanez et al. 2016). Our experimental paradigm did not allow us to reveal such multi-whisker correlation preferring neurons. Nevertheless, we found that 84% of the L2/3 neurons were responsive to at least one type of manual stimulation. It is likely that the silent neurons in our experiment (16%) encode such multi-whisker features, which could not be produced in our manual stimulation paradigm. Alternatively, the silent population may reflect weakly connected neurons, which could not be driven by any sensory input.

Overall, our results are well aligned with the preceding research and address some of the implications of sparse coding in the vS1. We showed that the sparse coding can be modulated by stimulus kinetics (synchrony), a variable action potential threshold and the state of cortex (anesthesia versus wakefulness). Importantly, our awake experiments revealed that sparse coding in vS1 may result from strong selectivity of individual neurons – once the whole stimulus space is explored a majority of neurons evoke action potentials and hence contribute to sensory processing.

4.3 The relevance to sensory coding and perception

A principal function of the brain is to extract ecologically relevant information from the sensory environment. When the animal interacts with the external world, peripheral sensory organs continuously transduce physical features of the objects into bioelectric signals. These signals represent rich spatiotemporal patterns of activity, which impose three main challenge to the sensory system; 1) filtering of irrelevant information, 2) extraction and transfer of useful information and 3) integration of elementary features into more complex features and ultimately, a coherent percept of the environment. A hierarchical cortical processing is thus theoretically expected to result in progressively divergent and sparse representations in higher-order sensory areas (Barlow 1972; Lennie 2003; Olshausen and Field 2004; Babadi and Sompolinsky 2014). This divergence can ultimately produce an "explicit, selective and invariant" (Quian Quiroga et al. 2009) representation of complex stimuli in a small ensemble of neurons as the end-product of sensory processing.

In the case of the tactile sense, information about the shape, size and texture is obtained by communications between primary and secondary somatosensory cortical areas (Bodegård et al. 2001). Further identification of objects may require processing in multimodal sensory areas (Hernández-Pérez et al. 2017). The sense of touch can also evoke an explicit, invariant and Gestalt-like perception in small mammals with clear ecological benefit (Anjum et al. 2006; Brecht et al. 2011). Neuronal substrates and coding strategies underlying tactile object recognition is not yet well explored in the somatosensory cortex of both primates and non-primates. A systematic study of hierarchical feature representation in rodent tactile systems is therefore necessary to understand the mechanisms of whisker-mediated perception.

In order to understand feature representation in cortex we first need to know how neurons with similar tunings are spatially arranged. In rodents, the visual cortex lacks a fine columnar organization (Ohki et al. 2005) while the somatosensory cortex, especially in L4 barrel field is highly organized into columns receiving input primarily from a single vibrissa (Woolsey and Van der Loos 1970; Simons 1978). However, in the supragranular layers, columnar organization is substantially degraded so that a single whisker deflection activates a distributed population of neurons (Clancy et al. 2015). Sub-columnar tuning organizations are described in a number of studies (Andermann and Moore 2006; Kremer et al. 2011; Garion et al. 2014; Estebanez et al. 2016), yet other studies have shown highly distributed tunings (Martini et al. 2017; Kwon et al. 2018). Estimation of the fraction and number of activated neurons therefore is highly influenced with the method of sampling. However, an important question that could be addressed by our experimental approach was the broadness of tuning of a single neuron. Our results, along with the unique and well-known cellular and circuit properties of the L2/3 neurons (Barth and Poulet 2012; Petersen and Crochet 2013) suggest that this cortical layer may have an important role in feature representation towards formation of an explicit percept of external objects.

This study was an attempt to discover implications of sparse coding in the L2/3 of vS1. We found that a high-velocity stimulus can densely activate L2/3 neurons in anesthetized condition. However, the same stimulus only sparsely activated L2/3 neurons in awake condition. The effect of anesthesia on the responsiveness of the cortical neurons is not yet fully explored. A better replication of our anesthetized experiments is to immobilize the whiskers in awake condition and ideally use the same animal in both conditions. This would address whether synaptic adaptations due to the voluntary movements of the whisker inside the cannula, resulted in sparseness of the response. Another possibility is that the stimulus-response curve in the awake condition is shifted

to cover a higher range of stimulus velocities before saturation. We partially addressed this question by manual stimulation where high-speed slip events failed to produce any spiking activity in a majority of the cells. This indicates that other mechanisms may be involved in differential tuning of the cells in the two conditions. A candidate mechanism is a higher selectivity of the inhibitory interneurons to various stimulus features. More specifically, in awake condition, SOM interneurons are dynamically controlled by the active behavior (Crochet et al. 2012) and possibly by more variable cortical states. This can potentially enhance the tuning diversity of the neurons in the awake condition.

We further tested the implications of the consistent sparseness in awake condition by employing a flexible approach to present a vast number of the stimulus features in a relatively short period of time. This enabled us to quickly find the optimal stimulus which drove a certain L2/3 neuron. Therefore, we were able to estimate the overall fraction of responsive neurons which is much higher than what is reported in other studies. We also found that various non-classical and conditional features were encoded by L2/3 neurons. Here, we hypothesize that the L2/3 of vS1 in mice encodes a substantially high number of simple and complex stimulus features by engaging most of the excitatory neurons. A more systematic and complete quantification therefore should aim to reveal; 1) the number of features that can be encoded in L2/3 of vS1, 2) the breadth of neuronal tunings and 3) the spatial organization of the tuning maps. Moreover, the mechanical, circuit and cellular mechanisms underlying feature selectivity in L2/3 would be revealed by testing neuronal responsiveness to non-classical stimulus features.

Overall, our findings suggest a model of sparse coding for L2/3 of vS1, where the sharp tuning of neurons to non-classic features underlies the sparse coding of stimuli in awake condition. We found that the sparse activity is not due to the broad tuning of a minor population of vS1 neurons

and overall silence of many neurons, but rather a result of the sharp tunings which has been neglected due to limitations in effective stimulus presentation. Our finding that the majority of the neurons receive sufficient synaptic input to fire when their preferred stimulus is presented, clarifies the implications of sparse coding in vS1 and encourages further investigations to identify and fully characterize relevant features and underlying mechanisms of stimulus selectivity in vS1.

4.4 Limitations of this study

A challenge in neuroscience is to precisely measure the activity of a large population of neurons with high spatiotemporal resolution. In our experiments we employed modern techniques such as patch clamp and calcium imaging to overcome the limitations of extracellular recording in sampling cortical neurons with various level of activity (Shoham et al. 2006). However, these methods present their own bias. Calcium imaging comes with a number of limitations such as neuropil contamination, out-of-focus fluorescent activity, non-homogeneous dye concentration in the imaged population and inadequate sensitivity in detection of single spikes (Göbel and Helmchen 2007; Peron et al. 2015a). Sensitivity and specificity of commonly used calcium indicators are tested in other studies. In the case of Oregon Green Bapta (OGB), false positive rate was shown to be much lower than false negative rate for single spike detection (11% vs. 45% respectively, Clancy et al. 2015). To improve our imaging, we used a recently described fluorescent indicator, Cal-520 which is shown to be more sensitive than the commonly used indicator, Oregon green or OGB (Tada et al. 2014). Higher sensitivity, however, may come with the cost of a high rate of false positive spikes due to pre-synaptic activity (Kerr et al. 2005).
A second limitation is inherent to using glass pipettes in patch clamp and cell-attached recordings. The size of the pipette can determine the size of recorded neurons and therefore

produce a systematic sampling bias towards neurons with size or morphology (Shoham et al. 2006). This however, is unlikely to affect our interpretation of the results since neuronal responsiveness is not linked with soma size in L2/3 of vS1 (Elstrott et al. 2014).

In our awake study, we were not able to describe the response properties for a number of neurons. For those neurons which we performed whisker imaging in parallel, still the full stimulation details are missing due to the lack of information about three dimensional movements of the whiskers. As such, our STA analysis only partially captures the relevant dynamics of the whisker movements. Our STA analysis is limited to curvature, since it was more reliable in reflecting whisker-object contacts. We also analyzed spike triggered average velocity. Even for the slip-tuned neurons (e.g. Figure 3.9G) STA velocity was too noisy to capture the effective feature due to whisker tracking errors which affected velocity measurements much more than curvature. Another challenge in naturalistic whisker stimulation is that the dynamics of the whole whisker array cannot be simultaneously measured and trimming of the whiskers to a single row is often necessary for whisker tracking (Clack et al. 2012). In our manual stimulation paradigm, the lack of precisely controlled stimulation was helpful in determining the responsiveness of many neurons but at the same time prevented us to fully quantify stimulus features and response properties of the recorded neurons. We propose that our manual probing method can be reutilized by future studies which would ideally use high-speed, 3-dimensional whisker imaging to quantify spatiotemporal mechanical properties of the intact whiskers and understand stimulus features which are effective in driving individual neurons.

4.5 Future directions

Regarding the stimulus features in the vibrissal sensory pathway, a number of key questions remain to be addressed; 1) is there a hierarchical processing in the vibrissal system underlying a Gestalt-like perception in rodents? 2) Assuming a hierarchical processing, at which stage of the sensory pathway do more complex/conditional features emerge? 3) How does intra-laminar or intra-cortical processing integrate elementary features into complex features? 4) Does sparse coding in supragranular vS1 enable multiple complex feature representations in this layer? 5) What is the role of cortical feedback in feature selectivity of L2/3 neurons? More sophisticated multi-dimensional stimulation paradigms, along with precise measurement of the whisker dynamics, behavioral state and neuronal activity is required to address these questions.

Another line of study could examine the laminar structure of the stimulus selectivity and feature representations in vS1. Laminar organization of the cortical area suggests distinct neuronal processing in each layer (Krupa et al. 2004; Petersen and Crochet 2013). For technical reasons, most of the recent studies using modern techniques have focused on supragranular layers. It is shown that the deep layers of the cortex may have a regulatory/feedback role in subcortical activity. However, deep layers also project to other cortical areas (Mao et al. 2011; Feldmeyer 2012) and may have a complementary role in sensory representation in vS1. A comparative study therefore is necessary to understand laminar structure of neuronal tuning and sparseness. At the level of behavior (Krupa et al. 2004), selective silencing/activation of each layer can be highly informative about the distinct role of each layer in sensory processing.

Mechanisms involved in spike generation in the cortical area have not been fully explored yet. Studying the dynamics of excitation-inhibition in response to different stimuli (Wilent and Contreras 2005a) may reveal the circuit mechanisms underlying narrow tuning of neurons in

superficial layers of vS1. For example, studying the various synaptic and neuromodulator inputs to supragranular vS1 can reveal what type of circuit computation can produce a neuron that is more sensitive to a gentle touch compared to strong movement. An open question regarding the role of anesthesia in sparse/dense observations is whether the strength of inhibition in vS1, or dynamics of excitatory-inhibitory inputs change by wakefulness similar to what seems to be the case in the visual cortex (Haider et al. 2013). Another interesting question is how the cellular mechanisms affect synaptic integration and the action potential threshold in vS1 (Crochet et al. 2011) and how they contribute to selective activation of neurons in response to different stimuli. Future studies can examine the relative strength of parallel whisker pathways projecting to L2/3 neurons and their role in feature selectivity (Jouhanneau et al. 2014). Finally, the role of cortical state, neuromodulators, cortical feedback and learning to feature selectivity and their contribution to sparseness needs to be further explored in future experiments.

In our study we proposed that a dense activation of neuronal ensembles in L2/3 may reflect the ecological relevance of rare, high-velocity events during whisker-object interactions. Behavioral studies have not yet quantified L2/3 sparseness in a task which would require fast whisker movements. For example, a discrimination task which involves tow stimuli with high-velocities would reveal the dynamics of sparseness in awake, behaving mice. It is necessary to sample neurons in specific tasks with variable stimulus contingencies to consider the effect of adaptation, habituation and reward expectation on the sparseness of the population response.

In the whisker system, it is not entirely clear which aspect of the stimulus is more ecologically relevant; intensity discrimination of a few features or discrimination of a large number of features. Behavioral relevance of slip events during texture discrimination has been examined, but the perceptual performance involving discrimination of features such as orientation it is yet

to be examined (Kwon et al. 2017). It is also necessary to investigate how a possibly gradual recruitment of neurons along one feature, affects the ability of the neurons to encode another feature. For example, it has been shown that increasing the frequency of whisker stimulation degrades directional selectivity of the neurons in vibrissal cortex (Puccini et al. 2006). Similar controlled experiments are required to address whether velocity coding degrades directional tuning of the neurons and to quantify the overlap between features when strong stimuli are presented.

Our second study showed that the majority of the L2/3 are responsive in awake condition, but they are not tuned to a single feature. Instead, a model of narrow sensory feature representation matches better with our awake data. In this context, dense activation in anesthetized condition can be an artifact of anesthesia and broadening of the feature coding may result from mechanisms which are dominant in this condition, such as propagating waves of synchronous activity and weaker/broader inhibition. More experiments are required to determine mechanisms behind the disparity of response to the sharp stimulus in awake versus anesthetized condition. In the future studies, it is important to investigate the effect of cortical state, motor control and inhibition in shaping the sensory response in the two conditions.

References

Adibi M, **Arabzadeh E**. A comparison of neuronal and behavioral detection and discrimination performances in rat whisker system. *J Neurophysiol* 105: 356–365, 2011.

Adibi M, **Diamond ME**, **Arabzadeh E**. Behavioral study of whisker-mediated vibration sensation in rats. *Proc Natl Acad Sci* 109: 971–976, 2012.

Ahissar E, **Kleinfeld D**. Closed-loop neuronal computations : focus on vibrissa somatosensation in rat. *Cereb Cortex* 13: 53–62, 2003.

Ahissar E, **Sosnik R**, **Bagdasarian K**, **Haidarliu S**. Temporal Frequency of Whisker Movement. II. Laminar Organization of Cortical Representations. *J Neurophysiol* 86: 354–367, 2001.

Andermann ML, **Moore CI**. A somatotopic map of vibrissa motion direction within a barrel column. *Nat Neurosci* 9: 543–551, 2006.

Anderson JS, **Carandini M**, **Ferster D**. Orientation tuning of input conductance, excitation, and inhibition in cat primary visual cortex. *J Neurophysiol* 84: 909–26, 2000a.

Anderson JS, **Lampl I**, **Gillespie DC**, **Ferster D**. The contribution of noise to contrast invariance of orientation tuning in cat visual cortex. *Science* 290: 1968–1972, 2000b.

Anjum F, **Turni H**, **Mulder PGH**, **van der Burg J**, **Brecht M**. Tactile guidance of prey capture in Etruscan shrews. *Proc Natl Acad Sci U S A* 103: 16544–16549, 2006.

Arabzadeh E, **Panzeri S**, **Diamond ME**. Whisker vibration information carried by rat barrel cortex neurons. *J Neurosci* 24: 6011–6020, 2004.

Arabzadeh E, **Panzeri S**, **Diamond ME**. Deciphering the spike train of a sensory neuron: counts and temporal patterns in the rat whisker pathway. *J Neurosci* 26: 9216–9226, 2006.

Arabzadeh E, **Petersen RS**, **Diamond ME**. Encoding of whisker vibration by rat barrel cortex

neurons: implications for texture discrimination. *J Neurosci* 23: 9146–9154, 2003.

Arabzadeh E, **Zorzin E**, **Diamond ME**. Neuronal encoding of texture in the whisker sensory pathway. *PLoS Biol* 3: e17, 2005.

Arieli A, **Sterkin A**, **Grinvald A**, **Aertsen A**. Dynamics of Ongoing Activity: Explanation of the Large Variability in Evoked Cortical Responses. *Science* 273: 1868–1871, 1996.

Arroyo S, **Bennett C**, **Aziz D**, **Brown SP**, **Hestrin S**. Prolonged Disynaptic Inhibition in the Cortex Mediated by Slow, Non-alpha7 Nicotinic Excitation of a Specific Subset of Cortical Interneurons. *J Neurosci* 32: 3859–3864, 2012.

Attwell D, **Laughlin SB**. An Energy Budget for Signaling in the Grey Matter of the Brain. *J Cereb Blood Flow Metab* 21: 1133–1145, 2001.

Averbeck BB, **Latham PE**, **Pouget A**. Neural correlations, population coding and computation. *Nat Rev Neurosci* 7: 358–66, 2006.

Avermann M, **Tomm C**, **Mateo C**, **Gerstner W**, **Petersen CCH**. Microcircuits of excitatory and inhibitory neurons in layer 2/3 of mouse barrel cortex. *J Neurophysiol* 107: 3116–3134, 2012.

Azouz R, **Gray CM**. Cellular mechanisms contributing to response variability of cortical neurons in vivo. *J Neurosci* 19: 2209–2223, 1999.

Azouz R, **Gray CM**. Dynamic spike threshold reveals a mechanism for synaptic coincidence detection in cortical neurons in vivo. *Proc Natl Acad Sci U S A* 97: 8110–8115, 2000.

Azouz R, **Gray CM**. Adaptive Coincidence Detection and Dynamic Gain Control in Visual Cortical Neurons In Vivo. *Neuron* 37: 513–523, 2003.

Babadi B, **Sompolinsky H**. Sparseness and Expansion in Sensory Representations. *Neuron* 83: 1213–1226, 2014.

Bagdasarian K, **Szwed M**, **Knutsen PM**, **Deutsch D**, **Derdikman D**, **Pietr M**, **Simony E**, **Ahissar E**. Pre-neuronal morphological processing of object location by individual whiskers. *Nat Neurosci* 16: 622–631, 2013.

Baker MA, **Tyner CF**, **Towe AL**. Observations on single neurons recorded in the sigmoid gyri of awake, nonparalyzed cats. *Exp Neurol* 32: 388–403, 1971.

Bale MR, **Campagner D**, **Erskine A**, **Petersen RS**. Microsecond-Scale Timing Precision in Rodent Trigeminal Primary Afferents. *J Neurosci* 35: 5935–5940, 2015.

Bale MR, **Davies K**, **Freeman OJ**, **Ince RAA**, **Petersen RS**. Low-Dimensional Sensory Feature Representation by Trigeminal Primary Afferents. *J Neurosci* 33: 12003–12012, 2013.

Bale MR, **Petersen RS**. Transformation in the neural code for whisker deflection direction along the lemniscal pathway. *J Neurophysiol* 102: 2771–80, 2009.

Barlow H. Single units and sensation: a neuron doctrine for perceptual psychology? *Perception* 1: 371–394, 1972.

Barth AL, **Poulet JFA**. Experimental evidence for sparse firing in the neocortex. *Trends Neurosci* 35: 345–355, 2012.

Bassant MH, **Baleyte JM**, **Lamour Y**. Effects of acetylcholine on single cortical somatosensory neurons in the unanesthetized rat. *Neuroscience* 39: 189–197, 1990.

Baudot P, **Levy M**, **Marre O**, **Monier C**, **Pananceau M**, **Frégnac Y**. Animation of natural scene by virtual eye-movements evokes high precision and low noise in V1 neurons. *Front Neural Circuits* 7: 206, 2013.

Bellavance M-A, **Takatoh J**, **Lu J**, **Demers M**, **Kleinfeld D**, **Wang F**, **Deschênes M**. Parallel Inhibitory and Excitatory Trigemino-Facial Feedback Circuitry for Reflexive Vibrissa Movements. *Neuron* 95: 673–682.e4, 2017.

Bodegård A, **Geyer S**, **Grefkes C**, **Zilles K**, **Roland PE**. Hierarchical processing of tactile shape in the human brain. *Neuron* 31: 317–328, 2001.

Boloori A-R, **Jenks RA**, **Desbordes G**, **Stanley GB**. Encoding and decoding cortical representations of tactile features in the vibrissa system. *J Neurosci* 30: 9990–10005, 2010.

Bortone DS, **Olsen SR**, **Scanziani M**. Translaminar Inhibitory Cells Recruited by Layer 6 Corticothalamic Neurons Suppress Visual Cortex. *Neuron* 82: 474–485, 2014.

Brecht M. Barrel cortex and whisker-mediated behaviors. *Curr Opin Neurobiol* 17: 408–416, 2007.

Brecht M, **Naumann R**, **Anjum F**, **Wolfe J**, **Munz M**, **Mende C**, **Roth-Alpermann C**. The neurobiology of Etruscan shrew active touch. *Phil Trans R Soc B* 366: 3026–36, 2011.

Brecht M, **Preilowski B**, **Merzenich MM**. Functional architecture of the mystacial vibrissae. *Behav Brain Res* 84: 81–97, 1997.

Brecht M, **Roth A**, **Sakmann B**. Dynamic Receptive Fields of Reconstructed Pyramidal Cells in Layers 3 and 2 of Rat Somatosensory Barrel Cortex. *J Physiol* 553: 243–265, 2003.

Brecht M, **Sakmann B**. Whisker maps of neuronal subclasses of the rat ventral posterior medial thalamus, identified by whole-cell voltage recording and morphological reconstruction. *J Physiol* 538: 495–515, 2002a.

Brecht M, **Sakmann B**. -Dynamic representation of whisker deflection by synaptic potentials in spiny stellate and pyramidal cells in the barrels and septa of layer 4 rat somatosensory cortex. *J Physiol* 543: 49–70, 2002b.

Brecht M, **Schneider M**, **Manns ID**. Silent Neurons in Sensorimotor Cortices: Implications for Cortical Plasticity. In: *Neural Plasticity in Adult Somatic Sensory-Motor Systems*. 2005, p. 1–19.

Briggs F. Organizing principles of cortical layer 6. *Front Neural Circuits* 4: 3, 2010.

Brombas A, **Fletcher LN**, **Williams SR**. Activity-dependent modulation of layer 1 inhibitory neocortical circuits by acetylcholine. *J Neurosci* 34: 1932–1941, 2014.

Brumberg JC, **Pinto DJ**, **Simons DJ**. Cortical Columnar Processing in the Rat Whisker-to-Barrel System. *J Neurophysiol* 82: 1808–1817, 1999.

Bruno RM. Synchrony in sensation. *Curr. Opin. Neurobiol.* 21: 701–708, 2011.

Bruno RM, **Sakmann B**. Cortex Is Driven by Weak but Synchronously Active Thalamocortical Synapses. *Science* 312: 1622–1627, 2006.

Buračas GT, **Zador AM**, **DeWeese MR**, **Albright TD**. Efficient Discrimination of Temporal Patterns by Motion-Sensitive Neurons in Primate Visual Cortex. *Neuron* 20: 959–969, 1998.

Bureau I, **Von Paul F Saint**, **Svoboda K**. Interdigitated paralemniscal and lemniscal pathways in the mouse barrel cortex. *PLoS Biol* 4: 2361–2371, 2006.

Bush NE, **Schroeder CL**, **Hobbs JA**, **Yang AE**, **Huet LA**, **Solla SA**, **Hartmann MJ**. Decoupling kinematics and mechanics reveals coding properties of trigeminal ganglion neurons in the rat vibrissal system. *Elife* 5, 2016.

Campagner D, **Evans MH**, **Bale MR**, **Erskine A**, **Petersen RS**. Prediction of primary somatosensory neuron activity during active tactile exploration. *Elife* 5, 2016.

Cao Y, **Roy S**, **Sachdev RNS**, **Heck DH**. Dynamic correlation between whisking and breathing rhythms in mice. *J Neurosci* 32: 1653–1659, 2012.

Carandini M, **Ferster D**. Membrane potential and firing rate in cat primary visual cortex. *J Neurosci* 20: 470–484, 2000.

Carvell GE, **Simons DJ**. Membrane potential changes in rat SmI cortical neurons evoked by controlled stimulation of mystacial vibrissae. *Brain Res* 448: 186–191, 1988.

Carvell GE, **Simons DJ**. Biometric analyses of vibrissal tactile discrimination in the rat. *J*

Neurosci 10: 2638–2648, 1990.

Castro-Alamancos MA. Absence of Rapid Sensory Adaptation in Neocortex during Information Processing States. *Neuron* 41: 455–464, 2004.

Cazakoff BN, **Lau BYB**, **Crump KL**, **Demmer HS**, **Shea SD**. Broadly tuned and respiration-independent inhibition in the olfactory bulb of awake mice. *Nat Neurosci* 17: 569–576, 2014.

Chadderton P, **Schaefer AT**, **Williams SR**, **Margrie TW**. Sensory-evoked synaptic integration in cerebellar and cerebral cortical neurons. *Nat Rev Neurosci* 15: 71–83, 2014.

Chagas AM, **Theis L**, **Sengupta B**, **Stüttgen MC**, **Bethge M**, **Schwarz C**. Functional analysis of ultra high information rates conveyed by rat vibrissal primary afferents. *Front Neural Circuits* 7: 190, 2013.

Chen JL, **Carta S**, **Soldado-Magraner J**, **Schneider BL**, **Helmchen F**. Behaviour-dependent recruitment of long-range projection neurons in somatosensory cortex. *Nature* 499: 336–340, 2013.

Chen JL, **Margolis DJ**, **Stankov A**, **Sumanovski LT**, **Schneider BL**, **Helmchen F**. Pathway-specific reorganization of projection neurons in somatosensory cortex during learning. *Nat Neurosci* 18: 1101–1108, 2015.

Chiaia NL, **Rhoades RW**, **Bennett Clarke CA**, **Fish SE**, **Killackey HP**. Thalamic processing of vibrissal information in the rat. I. Afferent input to the medial ventral posterior and posterior nuclei. *J Comp Neurol* 314: 201–216, 1991.

Clack NG, **O'Connor DH**, **Huber D**, **Petreanu L**, **Hires A**, **Peron S**, **Svoboda K**, **Myers EW**. Automated tracking of whiskers in videos of head fixed rodents. *PLoS Comput Biol* 8: e1002591, 2012.

Clancy KB, **Schnepel P**, **Rao a. T**, **Feldman DE**. Structure of a Single Whisker Representation

in Layer 2 of Mouse Somatosensory Cortex. *J Neurosci* 35: 3946–3958, 2015.

Cohen-Kashi Malina K, **Jubran M**, **Katz Y**, **Lampl I**. Imbalance between excitation and inhibition in the somatosensory cortex produces postadaptation facilitation. *J Neurosci* 33: 8463–8471, 2013.

Constantinople CM, **Bruno RM**. Effects and mechanisms of wakefulness on local cortical networks. *Neuron* 69: 1061–1068, 2011.

Constantinople CM, **Bruno RM**. Deep Cortical Layers Are Activated Directly by Thalamus. *Science* 340: 1591–1594, 2013.

Coombs JS, **Curtis DR**, **Eccles JC**. The generation of impulses in motoneurones. *J Physiol* 139: 232–2349, 1957.

Crochet S. Intracellular whole-cell patch-clamp recordings of cortical neurons in awake head-restrained mice. *Neuromethods* 67: 219–235, 2012.

Crochet S, **Petersen CCH**. Correlating whisker behavior with membrane potential in barrel cortex of awake mice. *Nat Neurosci* 9: 608–610, 2006.

Crochet S, **Poulet JFA**, **Kremer Y**, **Petersen CCH**. Synaptic mechanisms underlying sparse coding of active touch. *Neuron* 69: 1160–1175, 2011.

Curtis JC, **Kleinfeld D**. Phase-to-rate transformations encode touch in cortical neurons of a scanning sensorimotor system. *Nat Neurosci* 12: 492–501, 2009.

Dean AF. The variability of discharge of simple cells in the cat striate cortex. *Exp Brain Res* 44: 437–440, 1981.

DeCharms RC, **Zador A**. Neural Representation and the Cortical Code. *Annu Rev Neurosci* 23: 613–647, 2000.

Deschênes M, **Veinante P**, **Zhang ZW**. The organization of corticothalamic projections:

Reciprocity versus parity. *Brain Res. Rev.* 28: 286–308, 1998.

DeWeese MR, **Wehr MS**, **Zador AM**. Binary spiking in auditory cortex. *J Neurosci* 23: 7940–7949, 2003.

Diamond ME, **Arabzadeh E**. Whisker sensory system – From receptor to decision. *Prog Neurobiol* 103: 28–40, 2013.

Diamond ME, **Armstrong-James M**, **Budway MJ**, **Ebner FF**. Somatic sensory responses in the rostral sector of the posterior group (POm) and in the ventral posterior medial nucleus (VPM) of the rat thalamus: Dependence on the barrel field cortex. *J Comp Neurol* 318: 462–476, 1992.

Diamond ME, **von Heimendahl M**, **Arabzadeh E**. Whisker-Mediated Texture Discrimination. *PLoS Biol* 6: e220, 2008a.

Diamond ME, **von Heimendahl M**, **Knutsen PM**, **Kleinfeld D**, **Ahissar E**. "Where" and "what" in the whisker sensorimotor system. *Nat Rev Neurosci* 9: 601–612, 2008b.

DiCarlo JJ, **Zoccolan D**, **Rust NC**. How does the brain solve visual object recognition? *Neuron* 73: 415–434, 2012.

Durand S, **Iyer R**, **Mizuseki K**, **de Vries S**, **Mihalas S**, **Reid RC**. A Comparison of Visual Response Properties in the Lateral Geniculate Nucleus and Primary Visual Cortex of Awake and Anesthetized Mice. *J Neurosci* 36: 12144–12156, 2016.

Dykes R, **Lamour Y**. Neurons without demonstrable receptive fields outnumber neurons having receptive fields in samples from the somatosensory cortex of anesthetized or paralyzed cats and rats. *Brain Res* 440: 133–143, 1988a.

Dykes RW, **Lamour Y**. An electrophysiological study of single somatosensory neurons in rat granular cortex serving the limbs: a laminar analysis. *J Neurophysiol* 60: 703–724, 1988b.

Dykes RW, **Landry P**, **Metherate R**, **Hicks TP**. Functional role of GABA in cat primary

somatosensory cortex: shaping receptive fields of cortical neurons. *J Neurophysiol* 52: 1066–1093, 1984.

Ebara S, **Kumamoto K**, **Matsuura T**, **Mazurkiewicz JE**, **Rice FL**. Similarities and differences in the innervation of mystacial vibrissal follicle-sinus complexes in the rat and cat: A confocal microscopic study. *J Comp Neurol* 449: 103–119, 2002.

Eggermann E, **Kremer Y**, **Crochet S**, **Petersen CCH**. Cholinergic Signals in Mouse Barrel Cortex during Active Whisker Sensing. *Cell Rep* 9: 1654–1661, 2014.

Elstrott J, **Clancy KB**, **Jafri H**, **Akimenko I**, **Feldman DE**. Cellular mechanisms for response heterogeneity among L2/3 pyramidal cells in whisker somatosensory cortex. *J Neurophysiol* 112: 233–248, 2014.

Estebanez L, **Bertherat J**, **Shulz DE**, **Bourdieu L**, **Léger J-F**. A radial map of multi-whisker correlation selectivity in the rat barrel cortex. *Nat Commun* 7: 13528, 2016.

Estebanez L, **Boustani S El**, **Destexhe A**, **Shulz DE**. Correlated input reveals coexisting coding schemes in a sensory cortex. *Nat Neurosci* 15: 1691–1699, 2012.

Faisal AA, **Selen LPJ**, **Wolpert DM**. Noise in the nervous system. *Nat Rev Neurosci* 9: 292–303, 2008.

Fazlali Z, **Ranjbar-Slamloo Y**, **Adibi M**, **Arabzadeh E**. Correlation between Locus Coeruleus Activity and Cortical State : Implications for Sensory Coding in Rat Barrel Cortex. *Front Neural Circuits* 10: 14, 2016.

Feldmeyer D. Excitatory neuronal connectivity in the barrel cortex. *Front Neuroanat* 6: 24, 2012.

Feldmeyer D, **Brecht M**, **Helmchen F**, **Petersen CCH**, **Poulet JFA**, **Staiger JF**, **Luhmann HJ**, **Schwarz C**. Barrel cortex function. *Prog Neurobiol* 103: 3–27, 2013.

Ferezou I, **Bolea S**, **Petersen CCH**. Visualizing the cortical representation of whisker touch: voltage-sensitive dye imaging in freely moving mice. *Neuron* 50: 617–629, 2006.

Foldiak P. Sparse Coding In The Primate Cortex. In: *The Handbook of Brain Theory and Neural Networks*. 2002, p. 1–7.

Foldiak P, **Endres D**. Sparse coding. *Scholarpedia* 3: 2984, 2008.

Furuta T, **Urbain N**, **Kaneko T**, **Deschenes M**. Corticofugal Control of Vibrissa-Sensitive Neurons in the Interpolaris Nucleus of the Trigeminal Complex. *J Neurosci* 30: 1832–1838, 2010.

Gambino F, **Pagès S**, **Kehayas V**, **Baptista D**, **Tatti R**, **Carleton A**, **Holtmaat A**. Sensory-evoked LTP driven by dendritic plateau potentials in vivo. *Nature* 515: 116–119, 2014.

Garion L, **Dubin U**, **Rubin Y**, **Khateb M**, **Schiller Y**, **Azouz R**, **Schiller J**. Texture coarseness responsive neurons and their mapping in layer 2-3 of the rat barrel cortex in vivo. *Elife* 3: 3405, 2014.

Gdalyahu A, **Tring E**, **Polack PO**, **Gruver R**, **Golshani P**, **Fanselow MS**, **Silva AJ**, **Trachtenberg JT**. Associative fear learning enhances sparse network coding in primary sensory cortex. *Neuron* 75: 121–132, 2012.

Gentet LJ. Functional diversity of supragranular GABAergic neurons in the barrel cortex. *Front Neural Circuits* 6: 52, 2012.

Gentet LJ, **Avermann M**, **Matyas F**, **Staiger JF**, **Petersen CCH**. Membrane Potential Dynamics of GABAergic Neurons in the Barrel Cortex of Behaving Mice. *Neuron* 65: 422–35, 2010.

Gentet LJ, **Kremer Y**, **Taniguchi H**, **Huang ZJ**, **Staiger JF**, **Petersen CCH**. Unique functional properties of somatostatin-expressing GABAergic neurons in mouse barrel cortex. *Nat*

Neurosci 15: 607–612, 2012.

Gerdjikov T V, **Bergner CG**, **Stüttgen MC**, **Waiblinger C**, **Schwarz C**. Discrimination of vibrotactile stimuli in the rat whisker system: behavior and neurometrics. *Neuron* 65: 530–540, 2010.

Gibson JM. A quantitative comparison of stimulus-response relationships of vibrissa-activated neurons in subnuclei oralis and interpolaris of the rat's trigeminal sensory complex: receptive field properties and threshold distributions. *Somat Res* 5: 135–155, 1987.

Glazewski S, **Barth AL**. Stimulus intensity determines experience-dependent modifications in neocortical neuron firing rates. *Eur J Neurosci* 41: 410–419, 2015.

Goard M, **Dan Y**. Basal forebrain activation enhances cortical coding of natural scenes. *Nat Neurosci* 12: 1444–1449, 2009.

Göbel W, **Helmchen F**. In vivo calcium imaging of neural network function. *Physiology (Bethesda)* 22: 358–365, 2007.

Gollnick CA, **Millard DC**, **Ortiz AD**, **Bellamkonda R V**, **Stanley GB**. Response reliability observed with voltage-sensitive dye imaging of cortical later 2/3: The Probability of Activation Hypothesis. *J Neurophysiol* 115: 2456–2469, 2016.

Greenberg DS, **Houweling AR**, **Kerr JND**. Population imaging of ongoing neuronal activity in the visual cortex of awake rats. *Nat Neurosci* 11: 749–751, 2008.

Grinvald a, **Lieke E**, **Frostig RD**, **Gilbert CD**, **Wiesel TN**. Functional architecture of cortex revealed by optical imaging of intrinsic signals. *Nature* 324: 361–364, 1986.

Gur M, **Beylin A**, **Snodderly D**. Response variability of neurons in primary visual cortex (V1) of alert monkeys. *J Neurosci* 17: 2914–2920, 1997.

Haider B, **Duque A**, **Hasenstaub AR**, **Yu Y**, **McCormick DA**. Enhancement of Visual

Responsiveness by Spontaneous Local Network Activity In Vivo. *J. Neurophysiol.* 97: 4186–4202, 2007.

Haider B, **Häusser M**, **Carandini M**. Inhibition dominates sensory responses in the awake cortex. *Nature* 493: 97–100, 2013.

Harris KD, **Mrsic-Flogel TD**. Cortical connectivity and sensory coding. *Nature* 503: 51–58, 2013.

Hartings JA, **Simons DJ**. Inhibition suppresses transmission of tonic vibrissa-evoked activity in the rat ventrobasal thalamus. *J Neurosci* 20: RC100, 2000.

Von Heimendahl M, **Itskov PM**, **Arabzadeh E**, **Diamond ME**. Neuronal activity in rat barrel cortex underlying texture discrimination. *PLoS Biol* 5: 305, 2007.

Helmstaedter M, **Staiger JF**, **Sakmann B**, **Feldmeyer D**. Efficient Recruitment of Layer 2/3 Interneurons by Layer 4 Input in Single Columns of Rat Somatosensory Cortex. *J Neurosci* 28: 8273–8284, 2008.

Henze DA, **Buzsáki G**. Action potential threshold of hippocampal pyramidal cells in vivo is increased by recent spiking activity. *Neuroscience* 105: 121–130, 2001.

Hernández-Pérez R, **Cuaya L V.**, **Rojas-Hortelano E**, **Reyes-Aguilar A**, **Concha L**, **de Lafuente V**. Tactile object categories can be decoded from the parietal and lateral-occipital cortices. *Neuroscience* 352: 226–235, 2017.

Hicks TP, **Dykes RW**. Receptive field size for certain neurons in primary somatosensory cortex is determined by GABA-mediated intracortical inhibition. *Brain Res* 274: 160–164, 1983.

Higley MJ, **Contreras D**. Balanced Excitation and Inhibition Determine Spike Timing during Frequency Adaptation. *J Neurosci* 26: 448–457, 2006.

Hires SA, **Gutnisky D a**, **Yu J**, **O'Connor DH**, **Svoboda K**. Low-noise encoding of active

touch by layer 4 in the somatosensory cortex. *Elife* 4: 6619, 2015.

House DRC, **Elstrott J**, **Koh E**, **Chung J**, **Feldman DE**. Parallel regulation of feedforward inhibition and excitation during whisker map plasticity. *Neuron* 72: 819–831, 2011.

Hubel DH, **Wiesel TN**. Receptive fields of single neurones in the cat's striate cortex. *J Physiol* 148: 574–591, 1959.

Isaacson JS, **Scanziani M**. How inhibition shapes cortical activity. *Neuron* 72: 231–243, 2011.

Ito M. Some quantitative aspects of vibrissa-driven neuronal responses in rat neocortex. *J Neurophysiol* 46: 705–715, 1981.

Ito M. Processing of vibrissa sensory information within the rat neocortex. *J Neurophysiol* 54: 479–490, 1985.

Jacob V, **Le Cam J**, **Ego-Stengel V**, **Shulz DE**. Emergent Properties of Tactile Scenes Selectively Activate Barrel Cortex Neurons. *Neuron* 60: 1112–1125, 2008.

Jadhav SP, **Feldman DE**. Texture coding in the whisker system. *Curr Opin Neurobiol* 20: 313–318, 2010.

Jadhav SP, **Wolfe J**, **Feldman DE**. Sparse temporal coding of elementary tactile features during active whisker sensation. *Nat Neurosci* 12: 792–800, 2009.

Jouhanneau J-S, **Ferrarese L**, **Estebanez L**, **Audette NJ**, **Brecht M**, **Barth AL**, **Poulet JFA**. Cortical fosGFP Expression Reveals Broad Receptive Field Excitatory Neurons Targeted by POm. *Neuron* 84: 1065–1078, 2014.

Kandel ER, **Schwarts, James H**, **Jessell TM**, **Siegelbaum SA**, **Hudspeth AJ**. *Principles Of Neural Science*. McGraw-Hill, Health Professions Division, 2000.

Kara P, **Reinagel P**, **Reid RC**. Low Response Variability in Simultaneously Recorded Retinal, Thalamic, and Cortical Neurons. *Neuron* 27: 635–646, 2000.

Kato HK, **Gillet SN**, **Isaacson JS**. Flexible Sensory Representations in Auditory Cortex Driven by Behavioral Relevance. *Neuron* 88: 1027–1039, 2015.

Kerr JJND, **Greenberg D**, **Helmchen F**. Imaging input and output of neocortical networks in vivo. *Proc Natl Acad Sci U S A* 102: 14063–14068, 2005.

Kerr JND, **de Kock CPJ**, **Greenberg DS**, **Bruno RM**, **Sakmann B**, **Helmchen F**. Spatial organization of neuronal population responses in layer 2/3 of rat barrel cortex. *J Neurosci* 27: 13316–13328, 2007.

Kleinfeld D, **Deschênes M**. Neuronal basis for object location in the vibrissa scanning sensorimotor system. *Neuron* 72: 455–468, 2011.

Knutsen PM, **Ahissar E**. Orthogonal coding of object location. *Trends Neurosci* 32: 101–109, 2009.

de Kock CPJ, **Bruno RM**, **Spors H**, **Sakmann B**. Layer- and cell-type-specific suprathreshold stimulus representation in rat primary somatosensory cortex. *J Physiol* 581: 139–154, 2007.

de Kock CPJ, **Sakmann B**. Spiking in primary somatosensory cortex during natural whisking in awake head-restrained rats is cell-type specific. *Proc Natl Acad Sci U S A* 106: 16446–16450, 2009.

Kole MHP, **Stuart GJ**. Is action potential threshold lowest in the axon? *Nat Neurosci* 11: 1253–1255, 2008.

Kremer Y, **Léger J-F**, **Goodman D**, **Brette R**, **Bourdieu L**. Late emergence of the vibrissa direction selectivity map in the rat barrel cortex. *J Neurosci* 31: 10689–10700, 2011.

Krupa DJ, **Wiest MC**, **Shuler MG**, **Laubach M**, **Nicolelis MAL**. Layer-specific somatosensory cortical activation during active tactile discrimination. *Science* 304: 1989–1992, 2004.

Kwon SE, **Tsytsarev V**, **Erzurumlu RS**, **O'Connor DH**. Organization of orientation-specific whisker deflection responses in layer 2/3 of mouse somatosensory cortex. *Neuroscience* 368: 46–56, 2018.

Kwon SE, **Yang H**, **Minamisawa G**, **O'Connor DH**. Sensory and decision-related activity propagate in a cortical feedback loop during touch perception. *Nat Neurosci* 19: 1243–1249, 2016.

Larkum ME, **Nevian T**. Synaptic clustering by dendritic signalling mechanisms. *Curr Opin Neurobiol* 18: 321–331, 2008.

Lavallee P, **Urbain N**, **Dufresne C**, **Bokor H**, **Acsady L**, **Deschenes M**. Feedforward Inhibitory Control of Sensory Information in Higher-Order Thalamic Nuclei. *J Neurosci* 25: 7489–7498, 2005.

Lee CCY, **Diamond ME**, **Arabzadeh E**. Sensory Prioritization in Rats: Behavioral Performance and Neuronal Correlates. *J Neurosci* 36: 3243–3253, 2016.

Lee S-H, **Simons DJ**. Angular tuning and velocity sensitivity in different neuron classes within layer 4 of rat barrel cortex. *J Neurophysiol* 91: 223–229, 2004.

Lee SM, **Friedberg MH**, **Ebner FF**. The role of GABA-mediated inhibition in the rat ventral posterior medial thalamus. II. Differential effects of GABAA and GABAB receptor antagonists on responses of VPM neurons. *J Neurophysiol* 71: 1716–1726, 1994.

Lefort S, **Tomm C**, **Floyd Sarria J-C**, **Petersen CCH**. The excitatory neuronal network of the C2 barrel column in mouse primary somatosensory cortex. *Neuron* 61: 301–316, 2009.

Lennie P. The cost of cortical computation. *Curr Biol* 13: 493–497, 2003.

Letzkus JJ, **Wolff SBE**, **Meyer EMM**, **Tovote P**, **Courtin J**, **Herry C**, **Lüthi A**. A disinhibitory microcircuit for associative fear learning in the auditory cortex. *Nature* 480: 331–

335, 2011.

Levy WB, **Baxter RA**. Energy efficient neural codes. *Neural Comput* 8: 531–543, 1996.

Lichtenstein SH, **Carvell GE**, **Simons DJ**. Responses of rat trigeminal ganglion neurons to movements of vibrissae in different directions. *Somat Mot Res* 7: 47–65, 1990.

Lin I-C, **Okun M**, **Carandini M**, **Harris KD**. The Nature of Shared Cortical Variability. *Neuron* 87: 644–656, 2015.

Lottem E, **Azouz R**. Mechanisms of Tactile Information Transmission through Whisker Vibrations. *J Neurosci* 29: 11686–11697, 2009.

Manita S, **Miyakawa H**, **Kitamura K**, **Murayama M**. Dendritic Spikes in Sensory Perception. *Front Cell Neurosci* 11: 29, 2017.

Mao T, **Kusefoglu D**, **Hooks BM**, **Huber D**, **Petreanu L**, **Svoboda K**. Long-Range Neuronal Circuits Underlying the Interaction between Sensory and Motor Cortex. *Neuron* 72: 111–123, 2011.

Maravall M, **Diamond ME**. Algorithms of whisker-mediated touch perception. *Curr Opin Neurobiol* 25: 176–186, 2014.

Martini FJ, **Molano-Mazón M**, **Maravall M**. Interspersed Distribution of Selectivity to Kinematic Stimulus Features in Supragranular Layers of Mouse Barrel Cortex. *Cereb Cortex* 27: 1–8, 2017.

Minnery BS, **Bruno RM**, **Simons DJ**. Response transformation and receptive-field synthesis in the lemniscal trigeminothalamic circuit. *J Neurophysiol* 90: 1556–1570, 2003.

Minnery BS, **Simons DJ**. Response Properties of Whisker-Associated Trigeminothalamic Neurons in Rat Nucleus Principalis. *J Neurophysiol* 89: 40–56, 2003.

Mitchinson B, **Martin CJ**, **Grant RA**, **Prescott TJ**. Feedback control in active sensing: rat

exploratory whisking is modulated by environmental contact. *Proc Biol Sci* 274: 1035–1041, 2007.

Miyashita T, **Feldman DE**. Behavioral Detection of Passive Whisker Stimuli Requires Somatosensory Cortex. *Cereb Cortex* 23: 1655–1662, 2013.

Moore CI, **Nelson SB**. Spatio-Temporal Subthreshold Receptive Fields in the Vibrissa Representation of Rat Primary Somatosensory Cortex. *J Neurophysiol* 80: 2882–2892, 1998.

Moore JD, **Mercer Lindsay N**, **Deschênes M**, **Kleinfeld D**. Vibrissa Self-Motion and Touch Are Reliably Encoded along the Same Somatosensory Pathway from Brainstem through Thalamus. *PLoS Biol* 13: 1–28, 2015.

Morgenstern NA, **Bourg J**, **Petreanu L**. Multilaminar networks of cortical neurons integrate common inputs from sensory thalamus. *Nat Neurosci* 19: 1034–1040, 2016.

Morita T, **Kang H**, **Wolfe J**, **Jadhav SP**, **Feldman DE**. Psychometric curve and behavioral strategies for whisker-based texture discrimination in rats. *PLoS One* 6: 20437, 2011.

Muñoz W, **Tremblay R**, **Levenstein D**, **Rudy B**. Layer-specific modulation of neocortical dendritic inhibition during active wakefulness. *Science* 355: 954–959, 2017.

Muralidhar S, **Wang Y**, **Markram H**. Synaptic and cellular organization of layer 1 of the developing rat somatosensory cortex. *Front Neuroanat* 7: 52, 2014.

Niell CM, **Stryker MP**. Modulation of visual responses by behavioral state in mouse visual cortex. *Neuron* 65: 472–479, 2010.

Nimmerjahn A, **Kirchhoff F**, **Kerr JND**, **Helmchen F**. Sulforhodamine 101 as a specific marker of astroglia in the neocortex in vivo. *Nat Methods* 1: 31–37, 2004.

O'Connor D, **Hires S**, **Guo Z**, **Li N**. Neural coding during active somatosensation revealed using illusory touch. *Nat Neurosci* 16: 958–965, 2013.

O'Connor DH, **Clack NG**, **Huber D**, **Komiyama T**, **Myers EW**, **Svoboda K**. Vibrissa-based object localization in head-fixed mice. *J Neurosci* 30: 1947–1967, 2010a.

O'Connor DH, **Peron SP**, **Huber D**, **Svoboda K**. Neural activity in barrel cortex underlying vibrissa-based object localization in mice. *Neuron* 67: 1048–1061, 2010b.

Oberlaender M, **de Kock CPJ**, **Bruno RM**, **Ramirez A**, **Meyer HS**, **Dercksen VJ**, **Helmstaedter M**, **Sakmann B**. Cell type-specific three-dimensional structure of thalamocortical circuits in a column of rat vibrissal cortex. *Cereb Cortex* 22: 2375–2391, 2012.

Ohki K, **Chung S**, **Ch'ng YH**, **Kara P**, **Reid RC**. Functional imaging with cellular resolution reveals precise micro-architecture in visual cortex. *Nature* 433: 597–603, 2005.

Okun M, **Lampl I**. Instantaneous correlation of excitation and inhibition during ongoing and sensory-evoked activities. *Nat Neurosci* 11: 535–537, 2008.

Ollerenshaw DR, **Bari B a**, **Millard DC**, **Orr LE**, **Wang Q**, **Stanley GB**. Detection of tactile inputs in the rat vibrissa pathway. *J Neurophysiol* 108: 479–490, 2012.

Ollerenshaw DR, **Zheng HJ V**, **Millard DC**, **Wang Q**, **Stanley GB**. The adaptive trade-off between detection and discrimination in cortical representations and behavior. *Neuron* 81: 1152–1164, 2014.

Olshausen BA, **Field DJ**. Sparse coding of sensory inputs. *Curr Opin Neurobiol* 14: 481–487, 2004.

Oram MW, **Wiener MC**, **Lestienne R**, **Richmond BJ**. Stochastic nature of precisely timed spike patterns in visual system neuronal responses. *J Neurophysiol* 81: 3021–3033, 1999.

Palmer LM, **Shai AS**, **Reeve JE**, **Anderson HL**, **Paulsen O**, **Larkum ME**. NMDA spikes enhance action potential generation during sensory input. *Nat Neurosci* 17: 383–390, 2014.

Pammer L, **O'Connor DH**, **Hires SA**, **Clack NG**, **Huber D**, **Myers EW**, **Svoboda K**. The

mechanical variables underlying object localization along the axis of the whisker. *J Neurosci* 33: 6726–6741, 2013.

Panzeri S, **Macke JH**, **Gross J**, **Kayser C**. Neural population coding: combining insights from microscopic and mass signals. *Trends Cogn Sci* 19: 162–172, 2015.

Pei Y-C, **Hsiao SS**, **Craig JC**, **Bensmaia SJ**. Shape Invariant Coding of Motion Direction in Somatosensory Cortex. *PLoS Biol* 8: 1000305, 2010.

Peron S, **Chen T-W**, **Svoboda K**. Comprehensive imaging of cortical networks. *Curr Opin Neurobiol* 32: 115–123, 2015a.

Peron SP, **Freeman J**, **Iyer V**, **Guo C**, **Svoboda K**. A Cellular Resolution Map of Barrel Cortex Activity during Tactile Behavior. *Neuron* 86: 783–799, 2015b.

Petersen CCH, **Crochet S**. Synaptic computation and sensory processing in neocortical layer 2/3. *Neuron* 78: 28–48, 2013.

Petersen CCH, **Hahn TTG**, **Mehta M**, **Grinvald A**, **Sakmann B**. Interaction of sensory responses with spontaneous depolarization in layer 2/3 barrel cortex. *Proc Natl Acad Sci U S A* 100: 13638–13643, 2003.

Petilla T, **Nomenclature I**, **Ascoli G a**, **Alonso-Nanclares L**, **Anderson S a**, **Barrionuevo G**, **Benavides-Piccione R**, **Burkhalter A**, **Buzsáki G**, **Cauli B**, **Defelipe J**, **Fairén A**, **Feldmeyer D**, **Fishell G**, **Fregnac Y**, **Freund TF**, **Gardner D**, **Gardner EP**, **Goldberg JH**, **Helmstaedter M**, **Hestrin S**, **Karube F**, **Kisvárday ZF**, **Lambolez B**, **Lewis D a**, **Marin O**, **Markram H**, **Muñoz A**, **Packer A**, **Petersen CCH**, **Rockland KS**, **Rossier J**, **Rudy B**, **Somogyi P**, **Staiger JF**, **Tamas G**, **Thomson AM**, **Toledo-Rodriguez M**, **Wang Y**, **West DC**, **Yuste R**. Petilla terminology: nomenclature of features of GABAergic interneurons of the cerebral cortex. *Nat Rev Neurosci* 9: 557–568, 2008.

Petreanu L, **Huber D**, **Sobczyk A**, **Svoboda K**. Channelrhodopsin-2-assisted circuit mapping of long-range callosal projections. *Nat Neurosci* 10: 663–668, 2007.

Pinto DJ, **Hartings JA**, **Brumberg JC**, **Simons DJ**. Cortical Damping: Analysis of Thalamocortical Response Transformations in Rodent Barrel Cortex. *Cereb Cortex* 13: 33–44, 2003.

Pinto DJD, **Brumberg JCJ**, **Simons DJ**. Circuit dynamics and coding strategies in rodent somatosensory cortex. *J Neurophysiol* 83: 1158–1166, 2000.

Pitkow X, **Liu S**, **Angelaki DE**, **DeAngelis GC**, **Pouget A**. How Can Single Sensory Neurons Predict Behavior? *Neuron* 87: 411–423, 2015.

Pluta SR, **Lyall EH**, **Telian GI**, **Ryapolova-Webb E**, **Adesnik H**. Surround Integration Organizes a Spatial Map during Active Sensation. *Neuron* 94: 1220–1233, 2016.

Pouille F, **Marin-Burgin A**, **Adesnik H**, **Atallah B V**, **Scanziani M**. Input normalization by global feedforward inhibition expands cortical dynamic range. *Nat Neurosci* 12: 1577–1585, 2009.

Poulet JFA, **Petersen CCH**. Internal brain state regulates membrane potential synchrony in barrel cortex of behaving mice. *Nature* 454: 881–885, 2008.

Puccini GD, **Compte A**, **Maravall M**. Stimulus dependence of barrel cortex directional selectivity. *PLoS One* 1: 137, 2006.

Quian Quiroga R, **Kraskov A**, **Koch C**, **Fried I**. Explicit Encoding of Multimodal Percepts by Single Neurons in the Human Brain. *Curr Biol* 19: 1308–1313, 2009.

Quian Quiroga R, **Kreiman G**, **Koch C**, **Fried I**. Sparse but not "Grandmother-cell" coding in the medial temporal lobe. *Trends Cogn Sci* 12: 87–91, 2008.

Ramirez A, **Pnevmatikakis E a**, **Merel J**, **Paninski L**, **Miller KD**, **Bruno RM**. Spatiotemporal

receptive fields of barrel cortex revealed by reverse correlation of synaptic input. *Nat Neurosci* 17: 866–875, 2014.

Ranjbar-Slamloo Y, **Arabzadeh E**. High-velocity stimulation evokes "dense" population response in layer 2/3 vibrissal cortex. *J Neurophysiol* 117: 1218–1228, 2017.

Riesenhuber M, **Poggio T**. Hierarchical models of object recognition in cortex. *Nat Neurosci* 2: 1019–1025, 1999.

Rinberg D, **Koulakov A**, **Gelperin A**. Sparse Odor Coding in Awake Behaving Mice. *J Neurosci* 26: 8857–8865, 2006.

Ritt JT, **Andermann ML**, **Moore CI**. Embodied Information Processing: Vibrissa Mechanics and Texture Features Shape Micromotions in Actively Sensing Rats. *Neuron* 57: 599–613, 2008.

Robinson DA. The electrical properties of metal microelectrodes. *Proc IEEE* 56: 1065–1071, 1968.

Rolls ET, **Tovee MJ**. Sparseness of the neuronal representation of stimuli in the primate temporal visual cortex. *J Neurophysiol* 73: 713–726, 1995.

Rudy B, **Fishell G**, **Lee S**, **Hjerling-Leffler J**. Three groups of interneurons account for nearly 100% of neocortical GABAergic neurons. *Dev Neurobiol* 71: 45–61, 2011.

Sabri MM, **Arabzadeh E**. Information processing across behavioral states: Modes of operation and population dynamics in rodent sensory cortex. *Neuroscience* 368: 214–228, 2018.

Sachdev RNS, **Ebner FF**, **Wilson CJ**. Effect of subthreshold up and down states on the whisker-evoked response in somatosensory cortex. *J Neurophysiol* 92: 3511–3521, 2004.

Sachidhanandam S, **Sreenivasan V**, **Kyriakatos A**, **Kremer Y**, **Petersen CCH**. Membrane potential correlates of sensory perception in mouse barrel cortex. *Nat Neurosci* 16: 1671–1677, 2013.

Sakata S, **Harris KD**. Laminar-dependent effects of cortical state on auditory cortical spontaneous activity. *Front Neural Circuits* 6: 109, 2012.

Sato TR, **Gray NW**, **Mainen ZF**, **Svoboda K**. The functional microarchitecture of the mouse barrel cortex. *PLoS Biol* 5: 189, 2007.

Schwarz C. The Slip Hypothesis: Tactile Perception and its Neuronal Bases. *Trends Neurosci* 39: 449–462, 2016.

Severson KS, **Xu D**, **Van de Loo M**, **Bai L**, **Ginty DD**, **O'Connor DH**. Active Touch and Self-Motion Encoding by Merkel Cell-Associated Afferents. *Neuron* 94: 666–676, 2017.

Shadlen MN, **Newsome WT**. The variable discharge of cortical neurons: implications for connectivity, computation, and information coding. *J Neurosci* 18: 3870–3896, 1998.

Shepherd GMG, **Svoboda K**. Laminar and Columnar Organization of Ascending Excitatory Projections to Layer 2/3 Pyramidal Neurons in Rat Barrel Cortex. *J Neurosci* 25: 5670–5679, 2005.

Shoham S, **O'Connor DH**, **Segev R**. How silent is the brain: is there a "dark matter" problem in neuroscience? *J Comp Physiol* 192: 777–784, 2006.

Shoykhet M, **Doherty D**, **Simons DJ**. Coding of deflection velocity and amplitude by whisker primary afferent neurons: implications for higher level processing. *Somatosens Mot Res* 17: 171–180, 2000.

Simons DJ. Response properties of vibrissa units in rat SI somatosensory neocortex. *J Neurophysiol* 41: 798–820, 1978.

Simons DJ. Temporal and spatial integration in the rat SI vibrissa cortex. *J Neurophysiol* 54: 615–635, 1985.

Simons DJ, **Carvell GE**. Thalamocortical response transformation in the rat vibrissa/barrel

system. *J Neurophysiol* 61: 311–330, 1989.

Sosnik R, **Haidarliu S**, **Ahissar E**. Temporal frequency of whisker movement. I. Representations in brain stem and thalamus. *J Neurophysiol* 86: 339–353, 2001.

Spanne A, **Jörntell H**. Questioning the role of sparse coding in the brain. *Trends Neurosci* 38: 417–427, 2015.

Sreenivasan V, **Esmaeili V**, **Kiritani T**, **Galan K**, **Crochet S**, **Petersen CCH**. Movement Initiation Signals in Mouse Whisker Motor Cortex. *Neuron* 92: 1368–1382, 2016.

Stuart G, **Schiller J**, **Sakmann B**. Action potential initiation and propagation in rat neocortical pyramidal neurons. *J Physiol* 505: 617–632, 1997.

Stuart GJ, **Spruston N**. Dendritic integration: 60 years of progress. *Nat Neurosci* 18: 1713–1721, 2015.

Stüttgen MC, **Kullmann S**, **Schwarz C**. Responses of rat trigeminal ganglion neurons to longitudinal whisker stimulation. *J Neurophysiol* 100: 1879–1884, 2008.

Swadlow HA. Efferent neurons and suspected interneurons in motor cortex of the awake rabbit: axonal properties, sensory receptive fields, and subthreshold synaptic inputs. *J Neurophysiol* 71: 437–53, 1994.

Szwed M, **Bagdasarian K**, **Ahissar E**. Encoding of vibrissal active touch. *Neuron* 40: 621–630, 2003.

Tada M, **Takeuchi A**, **Hashizume M**, **Kitamura K**, **Kano M**. A highly sensitive fluorescent indicator dye for calcium imaging of neural activity in vitro and in vivo. *Eur J Neurosci* 39: 1720–1728, 2014.

Taub AH, **Katz Y**, **Lampl I**. Cortical balance of excitation and inhibition is regulated by the rate of synaptic activity. *J Neurosci* 33: 14359–14368, 2013.

Teich MC, **Johnson DH**, **Kumar AR**, **Turcott RG**. Rate fluctuations and fractional power-law noise recorded from cells in the lower auditory pathway of the cat. *Hear Res* 46: 41–52, 1990.

Theunissen FE. From synchrony to sparseness. *Trends Neurosci* 26: 61–64, 2003.

Thévenaz P, **Ruttimann UE**, **Unser M**. A pyramid approach to subpixel registration based on intensity. *IEEE Trans Image Process* 7: 27–41, 1998.

Towe AL, **Harding GW**. Extracellular microelectrode sampling bias. *Exp Neurol* 29: 366–381, 1970.

Tremblay N, **Warren RA**, **Dykes RW**, **Warren A**. Electrophysiological studies of acetylcholine and the role of the basal forebrain in the somatosensory cortex of the cat. I. Cortical neurons excited by glutamate. *J Neurophysiol* 64: 1199–1211, 1990.

Tremblay R, **Lee S**, **Rudy B**. GABAergic Interneurons in the Neocortex: From Cellular Properties to Circuits. *Neuron* 91: 260–292, 2016.

Veinante P, **Deschênes M**. Single- and multi-whisker channels in the ascending projections from the principal trigeminal nucleus in the rat. *J Neurosci* 19: 5085–5095, 1999.

Veinante P, **Jacquin MF**, **Deschênes M**. Thalamic projections from the whisker-sensitive regions of the spinal trigeminal complex in the rat. *J Comp Neurol* 420: 233–243, 2000.

Vincis R, **Gschwend O**, **Bhaukaurally K**, **Beroud J**, **Carleton A**. Dense representation of natural odorants in the mouse olfactory bulb. *Nat Neurosci* 15: 537–539, 2012.

Vinje WE, **Gallant JL**. Natural Vision Sparse Coding and Decorrelation in Primary Visual Cortex During Sparse Coding and Decorrelation in Primary Visual Cortex During Natural Vision. *Science* 287: 1273–1276, 2000.

Waiblinger C, **Brugger D**, **Whitmire CJ**, **Stanley GB**, **Schwarz C**. Support for the slip hypothesis from whisker-related tactile perception of rats in a noisy environment. *Front Integr*

Neurosci 9: 53, 2015.

Wallach A, **Ebara S**, **Ahissar E**. What Do Sensory Organs Tell the Brain? *Neuron* 94: 423–425, 2017.

Wang C-L, **Zhang L**, **Zhou Y**, **Zhou J**, **Yang X-J**, **Duan S -m.**, **Xiong Z-Q**, **Ding Y-Q**. Activity-Dependent Development of Callosal Projections in the Somatosensory Cortex. *J Neurosci* 27: 11334–11342, 2007.

Wang Q, **Webber RM**, **Stanley GB**. Thalamic synchrony and the adaptive gating of information flow to cortex. *Nat Neurosci* 13: 1534–1541, 2010.

Warren RA, **Dykes RW**. Population Analysis of Single Neurons in Cat Somatosensory Cortex. *Somatosens Mot Res* 9: 297–312, 1992.

Wilent WB, **Contreras D**. Synaptic responses to whisker deflections in rat barrel cortex as a function of cortical layer and stimulus intensity. *J Neurosci* 24: 3985–3998, 2004.

Wilent WB, **Contreras D**. Dynamics of excitation and inhibition underlying stimulus selectivity in rat somatosensory cortex. *Nat Neurosci* 8: 1364–1370, 2005a.

Wilent WB, **Contreras D**. Stimulus-dependent changes in spike threshold enhance feature selectivity in rat barrel cortex neurons. *J Neurosci* 25: 2983–2991, 2005b.

Williams SR, **Stuart GJ**. Dependence of EPSP efficacy on synapse location in neocortical pyramidal neurons. *Science* 295: 1907–1910, 2002.

Wolfe J, **Hill DN**, **Pahlavan S**, **Drew PJ**, **Kleinfeld D**, **Feldman DE**. Texture coding in the rat whisker system: slip-stick versus differential resonance. *PLoS Biol* 6: 215, 2008.

Wolfe J, **Houweling AR**, **Brecht M**. Sparse and powerful cortical spikes. *Curr Opin Neurobiol* 20: 306–312, 2010.

Woolsey TA, **Van der Loos H**. The structural organization of layer IV in the somatosensory

region (S I) of mouse cerebral cortex. The description of a cortical field composed of discrete cytoarchitectonic units. *Brain Res* 17: 205–242, 1970.

Wu GK, **Li P**, **Tao HW**, **Zhang LI**. Nonmonotonic Synaptic Excitation and Imbalanced Inhibition Underlying Cortical Intensity Tuning. *Neuron* 52: 705–715, 2006.

Wurtz RH. Recounting the impact of Hubel and Wiesel. *J Physiol* 587: 2817–2823, 2009.

Xu N, **Harnett MT**, **Williams SR**, **Huber D**, **O'Connor DH**, **Svoboda K**, **Magee JC**. Nonlinear dendritic integration of sensory and motor input during an active sensing task. *Nature* 492: 247–251, 2012.

Xu X, **Callaway EM**. Laminar specificity of functional input to distinct types of inhibitory cortical neurons. *J Neurosci* 29: 70–85, 2009.

Xu X, **Roby KD**, **Callaway EM**. Immunochemical characterization of inhibitory mouse cortical neurons: Three chemically distinct classes of inhibitory cells. *J Comp Neurol* 518: 389–404, 2010.

Xue M, **Atallah B V.**, **Scanziani M**. Equalizing excitation–inhibition ratios across visual cortical neurons. *Nature* 511: 596–600, 2014.

Yang H, **Kwon SE**, **Severson KS**, **O'Connor DH**. Origins of choice-related activity in mouse somatosensory cortex. *Nat Neurosci* 19: 127–134, 2015.

Yu C, **Derdikman D**, **Haidarliu S**, **Ahissar E**. Parallel Thalamic Pathways for Whisking and Touch Signals in the Rat. *PLoS Biol* 4: 124, 2006.

Yu J, **Gutnisky DA**, **Hires SA**, **Svoboda K**. Layer 4 fast-spiking interneurons filter thalamocortical signals during active somatosensation. *Nat Neurosci* 19: 1647–1657, 2016.

Yu Y, **Shu Y**, **McCormick DA**. Cellular/Molecular Cortical Action Potential Backpropagation Explains Spike Threshold Variability and Rapid-Onset Kinetics. *J Neurosci* 28: 7260–7272,

2008.

Zhu JJ, **Connors BW**. Intrinsic firing patterns and whisker-evoked synaptic responses of neurons in the rat barrel cortex. *J Neurophysiol* 81: 1171–1183, 1999.

Zucker E, **Welker WI**. Coding of somatic sensory input by vibrissae neurons in the rat's trigeminal ganglion. *Brain Res* 12: 138–156, 1969.

Appendix: mechanical parameters of the piezo stimuli and spiking response in L2/3

The paradigms described in this appendix were performed in parallel with the main paradigm in Chapter 2 (standard stimuli plus a sharp stimulus). Thus, the experimental procedure is the same except for the stimulus characteristics. Briefly, blind whole-cell and cell-attached recordings were performed in urethane anesthetized mice and the stimuli were delivered to multiple whiskers via a calibrated piezo-electric device. Two paradigms for stimulation were used here: (1) a "variable duration" paradigm and (2) a "sharp stimulus set" paradigm. In variable duration paradigm 6 deflections (plus a catch stimulus, Figure A.2*A*) were delivered 25 times each, with a pseudorandom order and 1.5-2.5 s inter-stimulus intervals. The rising edge of the input voltage to the piezo (Figure A.1) consisted of a half Gaussian function starting from 2 standard deviation followed by a piecewise cubic interpolation using "pchip" function in MATLAB, as the dropping edge. The duration of the stimulus was systematically reduced by changing the standard deviation of the Gaussian function (0.5-3 ms with 0.5ms steps, Figure A.1). In the case of the sharp stimulus (SD = 0.5 ms), the rising edge was replaced by a step function (Figure A.1)

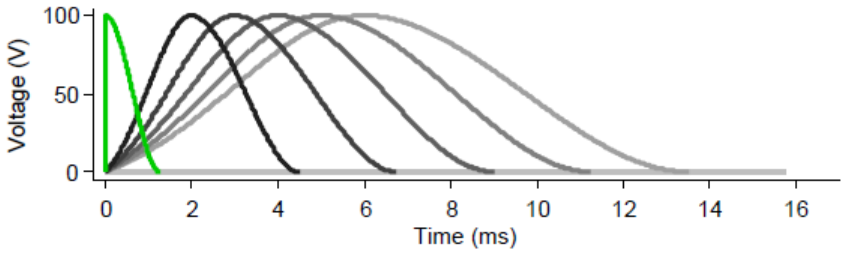

Figure A.1*: Voltage inputs which drive piezo-electric actuator in variable duration paradigm.*

The shape of the input voltage determines the mechanical properties of whisker deflection by the piezoelectric device. Majority of experiments classically utilize these devices to deliver controlled stimuli to the whiskers. A drawback of these devices is the emergence of an intense ringing due to the fast rate of the input voltage (Figure A.2*A*). Therefore, majority of the studies

use a filtered input voltage to prevent piezo from ringing. Alternatively, one can determine a function that smoothly drives piezo and keep the deflection brief and minimize the ringing. Based on previous results (Ranjbar-Slamloo and Arabzadeh 2017), we assumed that constraining piezo mechanics by keeping a smooth and slow voltage input can diminish the effectiveness of stimulus velocity/acceleration. The question here is that if we systematically reduce the duration of the stimulus by decreasing the standard deviation of the Gaussian voltage fed to the piezo; (1) how do the mechanical properties of the piezo in terms of resonation, velocity and acceleration change? (2) Which of these parameters could determine the spiking response in L2/3 of vS1?

We obtained the movement profile of the piezo by using a calibrated optic sensor as described in Chapter 2. As depicted in the Figure A.2*A*, the piezo position does not faithfully follow the voltage input. Note that the amplitude of the movement is increased as the duration of the voltage input is decreased (gray stimuli) and then decrease substantially for the sharp stimulus. The resonation followed by the initial deflection did not systematically increase by shortening of the duration but was prominent for the briefest stimulus as well as the sharp stimulus (Figure A.2*A*). We obtained the moment-to-moment velocity of the stimuli by taking the first derivative of the position profile. The velocity monotonically increased by decreasing the standard deviation of the Gaussian voltage input. As Figure A.2*B* shows, the angular velocity of the piezo vigorously oscillates for the fastest gray stimulus and the sharp stimulus due their high amplitude resonations. As such, the peak velocities for these stimuli are at least 1 degree/ms higher than the rest of the stimuli. The maximum velocity achieved by the fastest gray stimulus is 0.95 degree/ms faster than that of the sharp stimulus but happened 3.4 ms later; the sharp stimulus achieved two peaks of velocity at 0.17 and 0.67 ms from the stimulus onset (2.38 and 3.16 degree/ms respectively) and another peak of comparable speed (3.15 degree/ms) on the opposite

direction at 2.5 ms from the stimulus onset. On the other hand, the gray stimulus owning the highest peak velocity achieved the first peak of velocity at 1.86 ms from the onset (2.4 degree/ms). Therefore, the kinetic energy of the fastest gray stimulus is higher than the sharp stimulus but is delayed relative to the stimulus onset. We used the second derivative of the position as representative of the stimulus acceleration. Despite lower velocity, the sharp stimulus achieves very high peaks of acceleration within the first millisecond from the stimulus onset. The highest peak acceleration of the sharp stimulus is more than 3 times higher than that of fastest gray stimulus (Figure A.2*C*&*E*). Therefore, in this paradigm velocity and acceleration are not perfectly correlated.

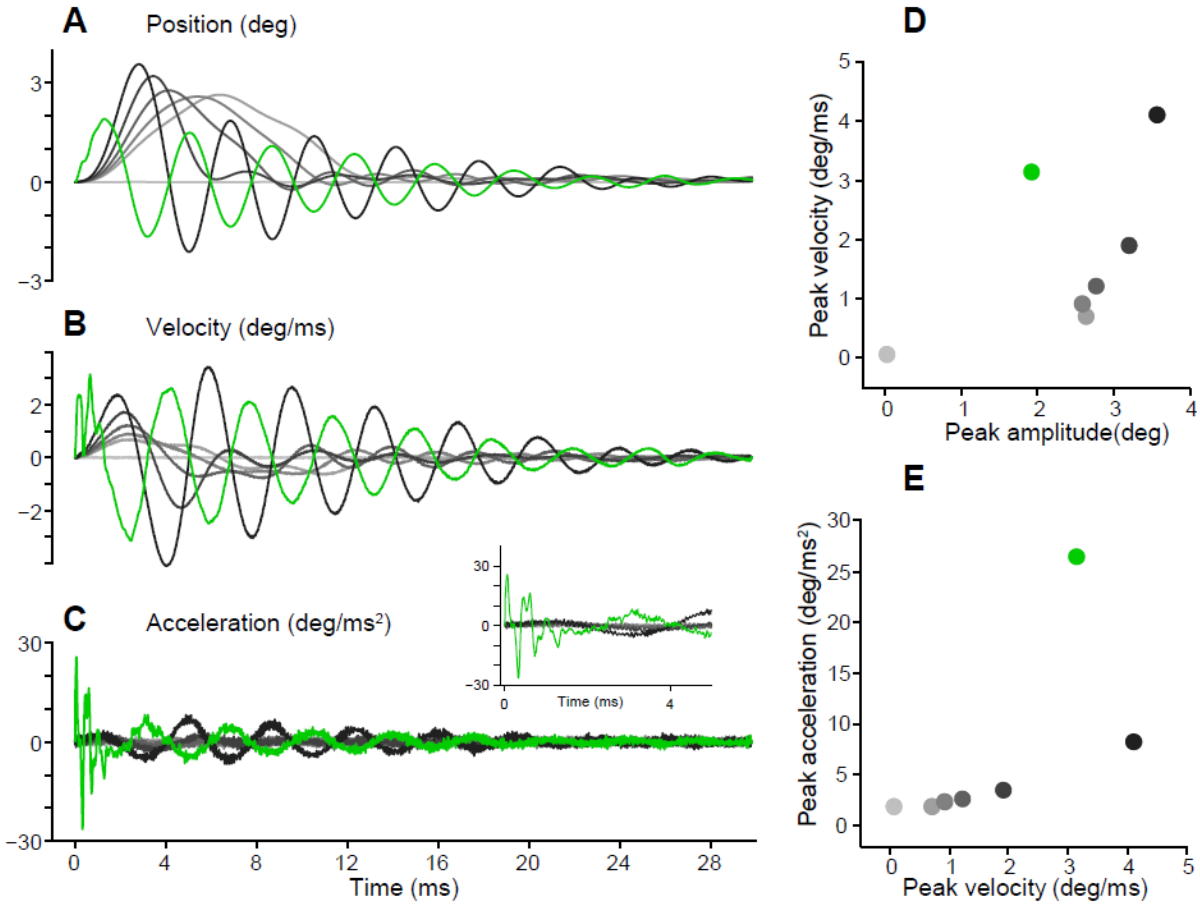

Figure A.2*: Whisker stimulation paradigm based on the duration of the stimulus*

***A**: Radial position of the 7 deflections (including stimulus zero) is plotted as a function of time. **B**: First derivative of the stimulus movement representing the velocity. **C**: Second derivative of the movement representing acceleration. Note the early peaks in acceleration profile in the case of the sharp stimulus (green). The inset is an expansion of the acceleration profile. **D**: Absolute peak velocity of each stimulus is plotted against the absolute peak position (amplitude). **E**: Absolute peak velocity is plotted against the absolute peak acceleration.*

We found that the sharp stimulus, despite a lower peak velocity is two times more effective in evoking spiking activity in L2/3. Here, we show that the velocity is not monotonically encoded by vS1 neurons (Figure A.3*A*&*C*). We obtained a similar result in the awake mice (Figure A.3*B*). Instead, when we plotted the neuronal response versus stimulus acceleration, we found an almost linear relationship. Therefore, unlike the stimulus velocity, the acceleration is monotonically represented by the L2/3 of vS1 neurons.

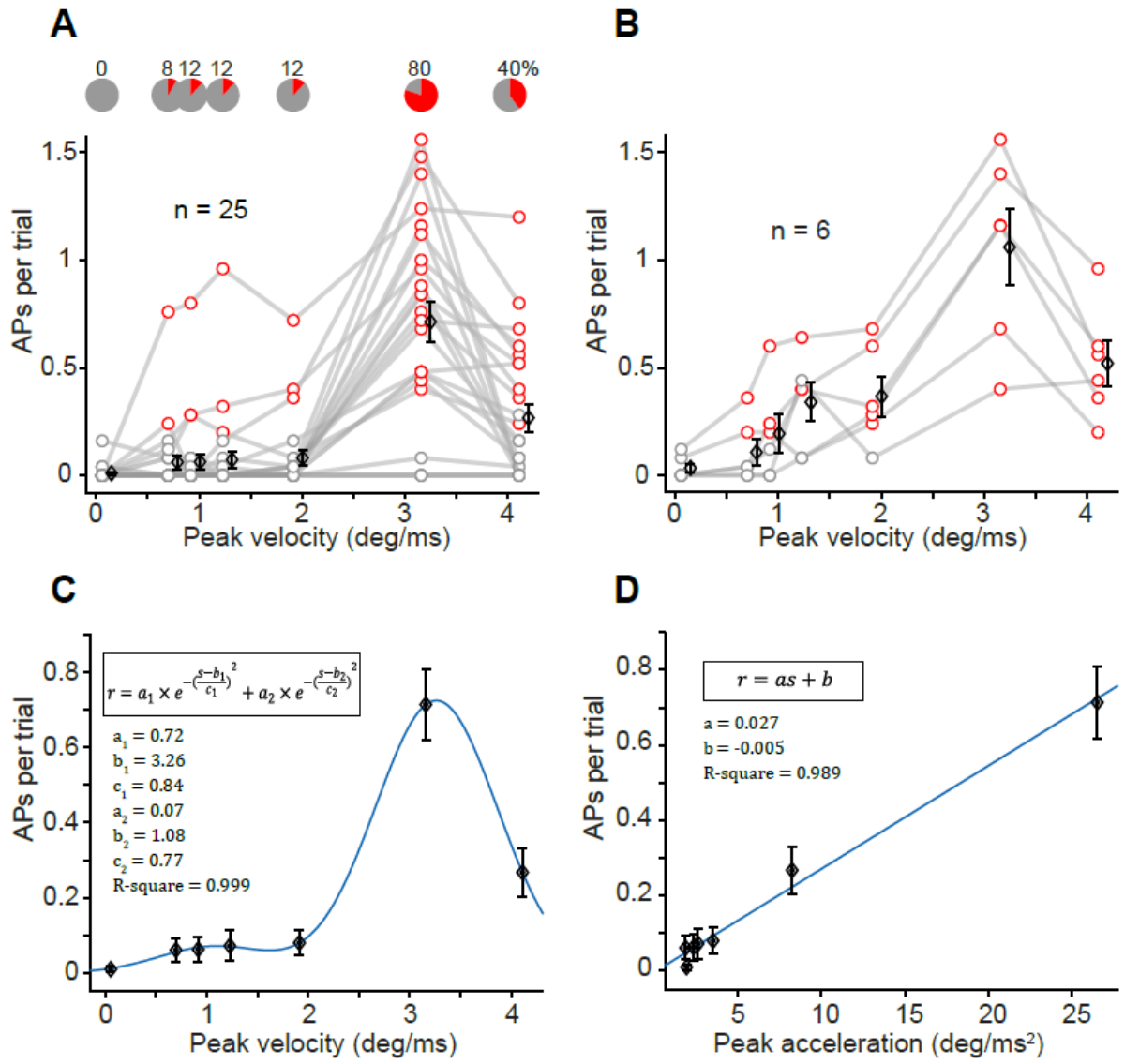

Figure A.3*: Response profile of L2/3 neurons in the variable duration paradigm*

A*: Average number of evoked spikes is plotted against the peak velocity of the stimuli. Red circles represent significant responses based on ROC analysis (see the methods chapter). Pie charts on top represent the percentage of significantly responsive neurons for each stimulus.* ***B****: Average number of evoked spikes versus peak velocity in awake condition.* ***C****: A Gaussian function with two terms (inset equation) fitted on the averaged response versus the peak velocity.* ***D****: A linear function fitted on the average response as in* ***A*** *versus peak acceleration.*

In the second paradigm we employed a classic approach to increase the intensity of the stimulus by using a series of sharp deflections with a range of amplitudes. Here, 11 sharp stimuli were presented with 1.5-2.5 inter-stimulus intervals and a pseudorandom order, as of the earlier paradigms. The analyses of the stimulus parameters showed that the velocity is linearly increased by the amplitude (Figure A.4*G*). Likewise, the stimulus acceleration monotonically (almost linearly) increased by the velocity (Figure A.4*H*). Note that for both velocity and acceleration, the intensity gap between the smallest and the largest stimuli is gradually filled (Figure A.4*G&H*), as in the case of standard stimuli in Chapter 2.

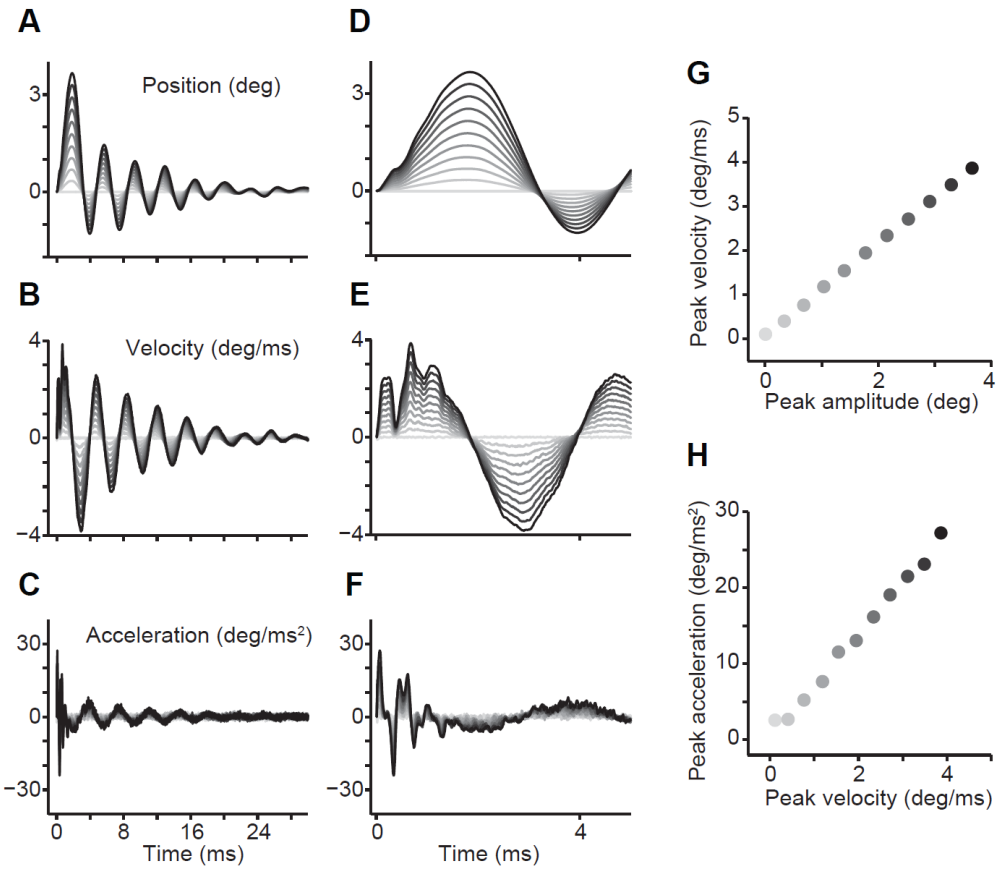

Figure A.4*: Stimulus set consisting of sharp stimuli*

***A**-C: Position (**A**), velocity (**B**) and acceleration (**C**) profiles of the stimulus set. **D-F**: Expanded views of the panels on the right-side. **G**: Absolute peak velocity of each stimulus is plotted against the absolute peak position (amplitude). **H**: Absolute peak velocity is plotted against the absolute peak acceleration.*

The activity of 9 regular spiking neurons in L2/3 of vS1 was probed by this stimulus set. As a result of a close association between the velocity and acceleration, the two features were similarly represented by the neuronal activity. This is reflected in similar parameters when a sigmoidal function was fitted on the average response versus velocity or acceleration (Figure A.5*B*&*C*)

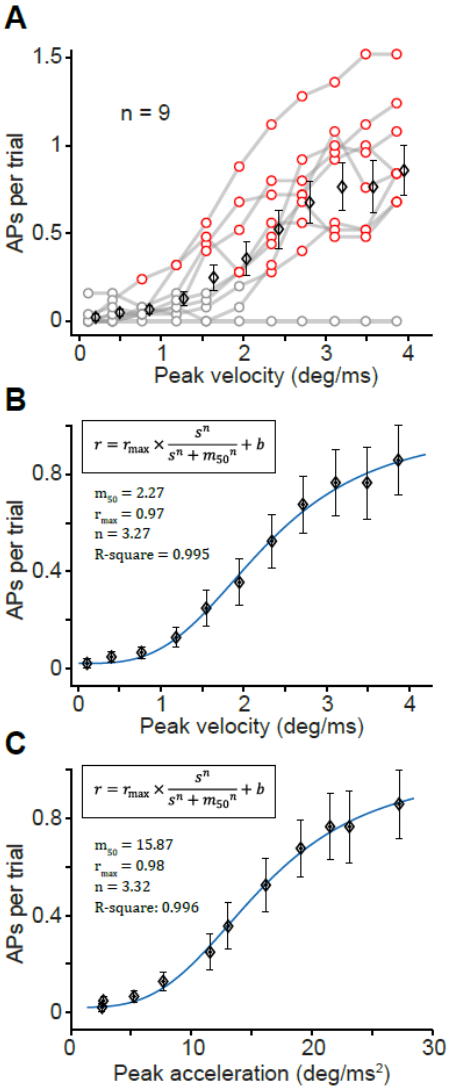

***Figure A.5**: Responses to sharp stimuli*

***A**: Response profile of neurons recorded from L2/3 being presented by sharp stimuli with gradually increasing velocity/acceleration. **B&C**: Average response is plotted versus velocity (**B**) or acceleration (**C**) which is similarly encoded by L2/3 spiking responses. Blue curves show Naka-Rushton functions (insets) fitted on the average response*